GEOCHEMICAL VARIABILITY & IMPLICATIONS FOR MAGMA TRANSPORT AT 14°N ON THE MID-ATLANTIC RIDGE

by

Emma Elizabeth McCully

A thesis

submitted in partial fulfillment

of the requirements for the degree of

Master of Science in Geosciences

Boise State University

August 2020

© 2020

Emma Elizabeth McCully

ALL RIGHTS RESERVED

BOISE STATE UNIVERSITY GRADUATE COLLEGE

DEFENSE COMMITTEE AND FINAL READING APPROVALS

of the thesis submitted by

Emma Elizabeth McCully

Thesis Title: Geochemical Variability & Implications for Magma Transport at 14°N on the Mid-Atlantic Ridge

Date of Final Oral Examination: 03 June 2020

The following individuals read and discussed the thesis submitted by student Emma Elizabeth McCully, and they evaluated their presentation and response to questions during the final oral examination. They found that the student passed the final oral examination.

V. Dorsey Wanless, Ph.D.	Chair, Supervisory Committee
Mark Schmitz, Ph.D.	Member, Supervisory Committee
Brittany D. Brand, Ph.D.	Member, Supervisory Committee

The final reading approval of the thesis was granted by V. Dorsey Wanless, Ph.D., Chair of the Supervisory Committee. The thesis was approved by the Graduate College.

DEDICATION

60 years ago, it would have been impossible for me to collect this data, as women were not allowed to participate in seagoing expeditions. This work is dedicated to the women who risked everything to give future generation of female scientists a wider path.

"I was so busy making maps, I let them argue"- Marie Tharp, Oceanographer

ACKNOWLEDGEMENTS

I would like to acknowledge the village that created this work. Firstly, to my advisor and mentor, Dorsey Wanless, you have my immense gratitude for your guidance, patience, and belief in my abilities even when I did not believe in them myself. Thank you for taking a chance on me! Brittany Brand and Mark Schmitz, thank you both for your guidance and support throughout the last two years. Thanks to Karen Viskupic for her support and guidance, as well as instilling in me a passion for Geoscience education. This research would be impossible without the tireless efforts of the crews of the *R/V Atlantis, AUV Sentry, DSV Alvin,* and the science parties of AT33-03 and AT40-02. Both research expeditions were funded by NSF.

All of my fellow graduate students have been an immense support, thank you to you all. I would especially like to thank all the Igneous Petrology and Volcanology Lab members, present and past, for cultivating a supportive environment for us to all grow. This work would not be possible without the guidance and support of Darin Schwartz who has inspired me to reach further, dig deeper, and coffee walk often.

I have an incredible community of people, and I would like to thank my friends across the globe for their encouragement, camaraderie, and love over the last two years. My family has been the most solid rock throughout my life, and I am so grateful to my parents and brother for their unconditional love and support. There are no adequate words I have to thank my extended family, and especially my grandparents who made it

possible for me to pursue higher education without fear of crippling debt. I never thought this was in the cards for me and I emphatically thank my mentors: Jim Hunter, Jennifer Cholnoky, Meg Estapa, Amy Frappier, the Skidmore Geoladies, Dan Fornari, Bridgit Boulahanis, and Meghan Jones. I thank you all for fostering in me the belief that I am capable of being here.

ABSTRACT

Observations of seafloor bathymetry and gravity surveys indicate that magma focuses in the center of slow spreading Mid-Ocean Ridge (MOR) segments, however; it is not well constrained how magma is generated, stored, and transported to the segment ends. There are two end-member models for magma transport: 1) a focused magma model wherein the magma upwells beneath the entire ridge axis, is focused and pools beneath the center of the segment, and is then transported towards the segment ends via lateral diking in the shallow crust and 2) a distributed magma model wherein magma vertically upwells and is erupted on the seafloor along the entire segment, but there is enhanced focusing in the segment center. (Figure 1). Both models are supported by the bathymetric and geophysical observations but have different implications for the chemistry of lavas erupted along the segment.

To test how lava chemistries vary along a slow-spreading MOR, we systematically sampled a segment of the Mid-Atlantic Ridge. The segment (~14°N) (Figure 2) is known to host Popping Rocks, gas-rich basalts which, upon reaching surface pressures, explode. Two expeditions to this region in 2016 and 2018 collected both ship-based bathymetry (75 m gridded resolution) aboard the R/V *Atlantis* and high-resolution bathymetry (1 m) from the Autonomous Underwater Vehicle (AUV) *Sentry*. 27 dives from the Human Occupied Vehicle (HOV) *Alvin* collected 382 lavas all of which have been analyzed for major element contents, and 162 have been analyzed for trace element

contents. During these expeditions, samples were collected both along and across axis from the magmatically robust segment center, through a transition region, to a sparsely magmatic region.

Analytical results show that there is significant chemical variability along this segment. For example, there is less variability at the segment center (K/Ti ratios from 0.24 to 0.46 and La/Sm from 2.58 to 3.59) compared to the sparsely magmatic region (K/Ti values from 0.06 to 0.42 and La/Sm). This suggests that magmas erupted at the segment center are more homogeneous compared to lavas erupting in the sparsely magmatic region. Major element contents in each region vary, but on average, become more mafic moving southward away from the magmatically robust segment center towards the sparsely magmatic region. Petrologic modeling of fractional crystallization and trace element contents show that fractional crystallization dominates the chemical variability in the sparsely magmatic region, while either extent of melting or differing mantle sources dominates the variability in the transition regions and the sparsely magmatic region. Reconciling these data with both physical and geophysical observations of a slow spreading ridge, we present a model of magma generation, storage, and transport that is a hybrid of the two proposed models.

TABLE OF CONTENTS

DEDICATION iv

ACKNOWLEDGEMENTS v

ABSTRACT vii

LIST OF TABLES xi

LIST OF FIGURES xii

LIST OF ABBREVIATIONS xv

INTRODUCTION 1

Geologic Setting 5

SAMPLE COLLECTION 10

Popping Rocks Cruises 10

METHODS 13

Major Element Analysis 13

Trace Element Analysis 13

RESULTS 15

Chemical Variability Along-Axis 15

Trace Element variability Along-Axis 19

DISCUSSION 22

Magma Storage Depths and Crystallization along-axis 23

Trace Element Variability Along-Axis 30

Model for Magma Generation and Transport on a Slow Spreading Segment.....31

Comparison to other MAR Segments.....35

CONCLUSIONS.....39

FUTURE WORK.....41

Extent of Melting Along-Axis.....41

REFERENCES.....46

APPENDIX A.....52

LIST OF TABLES

Table A.1. Major Element Contents of the 14°N Segment. Collected on a Cameca SX Five Electron Microprobe at Boise State University. 53

Table A.2 Trace Element Contents of the 14°N Segment. These data were measured on the LA-ICP-MS at Boise State University. Trace Element concentrations are given in ppm. 58

LIST OF FIGURES

Figure 1. Cartoon schematic of two end member models of magma generation, storage, and transport at slow-spreading MORs. Cartoon schematic of two end member models of magma generation, storage, and transport at slow-spreading MORs. The colors representing differing extents of melting. The warmer colors represent and greater extent of melting and grade down to lower extents of melting towards the cooler colors. (A) Focused magmatism model where melts are generated along the entire axis. The melts are focused at the center of the segment and transported towards the segment ends in the shallow crust. (B) Distributed magmatism model where melts are produced along the entire ridge segment and ascend vertically to the seafloor..... 5

Figure 2. (A).Bathymetric map of the segment in its entirety, bound by the 15°20’ N Fracture Zone and Marathon Fracture Zone. Chaotic bathymetry along-axis characteristic of typical slow-spreading MOR morphologies. (B). High resolution bathymetric map of the study region between 13°36’ and 14°08’N. Each region and subregion are labeled. Lines represent DSV (Deep Submergence Vehicle) *Alvin* navigation path. 8

Figure 3. Simplified schematic of a cross section of an MOR’s melting regime, adapted from Plank & Langmuir (1992). The upwelling mantle undergoes decompression melting and will buoyantly rise (represented by black arrows) until intersecting with the lithosphere, where melt will truncate. The lithosphere thickening both along and across the ridge can truncate the melting columns in three-dimension, creating a pyramid-like melting regime. 8

Figure 4. “Bulls-eye effect” wherein MBA gravity low focused at the center of at the 14°N segment of the MAR (Smith et al., 2008). The lower MBA at the segment center is interpreted as an area of greater upwelling. Increased upwelling is subsequently interpreted as an area of greater magma supply. 9

Figure 5. Major element contents (A) MgO (B) CaO, and (C) FeOT weight percent for each region by latitude. 18

Figure 6. (A) K/Ti ratio. Trace element ratios (B) La/Sm and (C) La/Yb by latitude. 18

Figure 7. La/Sm vs Sm/Yb for the entire segment. Generally, the compositions fall in a linear trend, but several samples from the OCC transect do not, due to the presence of the extinct OCC. 19

Figure 8a-h. REE plots for all transects of the segment from north to south. 21

Figures 9. Histogram diagrams of each transect along the segment for Al_2O_3, MgO, CaO, and FeOT. Figure is organized from north to source. Average values for each region are shown by the black bar, and the standard deviation is represented by the surrounding grey region and terminated with the dotted lines. 24

Figure 10. Histogram diagrams of each region moving down segment for K/Ti, La/Sm, and La/Yb ratios. Average values for each region are shown by the black bar, and the standard deviation is represented by the surrounding grey region and terminated with the dotted lines. 25

Figure 11. Major element variation diagrams showing the compositions of lavas collected from all regions. Top row shows Al2O3 and MgO (wt %) contents at each location with modeled fractional crystallization trend. Bottom row shows CaO/Al2O3 and MgO (wt %) contents at each location with modeled fraction crystallization trends. The details of the model can be found within the text. Labeled on each modeled fractional crystallization trend are the percent of crystallization along the liquid line of decent. The major element contents from the magmatic center and northern transition region fit the model trends well around 1.5-2kbar but moving away from the warm magmatic center either multiple depths of crystallization or multiple parents are required to account for the range in chemistry. From the magmatic center to the southernmost region, the amount of fractional crystallization required to reach the least mafic samples decreases by ~30%. 28

Figure 12. Proposed "hybrid model" of magma generation, storage, and transport at a slow spreading MOR based upon the geochemical findings of this study. Close up view of the proposed model includes labeled transects from this study. 34

Figure 13. Sm/Yb vs La/Sm values from Gale et al (2011) combined with our regional data. Their extremely enriched samples are explained via low extents of melting from the Azores platform. 37

Figure 14. K/Ti and MgO data from Niu and Batiza (1994) combined with our regional data. The samples from 26°S are categorically more depleted than the NMORB samples from 14°N. 38

Figure 15. REE plot of average compositions of chemically distinct groups within the sparsely magmatic transect. 42

Figure 16. (A) REE plot of average composition of the popping rocks and chemically homogenous lavas (green line) and the average composition of a subset of non-popping rocks that are chemically homogenous. These two subsets of data were both collected in the Popping Rocks Region. (B) Average composition of the southern region sits between two averaged subsets of data from the popping rocks region (same two groups as figure 16a)..... 44

LIST OF ABBREVIATIONS

AUV	Autonomous Underwater Vehicle
EMORB	Enriched Mid-Ocean Ridge Basalt
HOV	Human Operated Vehicle
HREE	Heavy Rare Earth Elements
LREE	Light Rare Earth Elements
MAR	Mid-Atlantic Ridge
MBA	Mantle Bouger Anomaly
MOR	Mid-Ocean Ridge
MORB	Mid-Ocean Ridge Basalt
MREE	Middle Rare Earth Elements
NMORB	Normal Mid-Ocean Ridge Basalt
OCC	Oceanic Core Complex
PPM	Parts Per Million
R/V	Research Vessel
REE	Rare Earth Element
SIMS	Secondary Ion Mass Spectrometry

INTRODUCTION

Mid-Ocean Ridges (MORs) are the longest volcanic system on Earth, extending ~65,000 km on the ocean floor (Searle, 2013). These tectonic boundaries serve as a critical flux of heat and mass from Earth's interior to exterior. They are responsible for the generation of the oceanic crust, which covers ~70% of the Earth's surface. Thus, quantifying magma generation, storage, and transport at MORs is necessary to constrain Earth's thermal budget and is fundamental to our understanding of plate tectonics.

As tectonic plates diverge at MORs, the mantle upwells and undergoes decompression melting, generating magma (Plank & Langmuir, 1992). Melt generation stops when the upwelling mantle intersects the lithospheric boundary and thus, the thickness of the lithosphere is a critical control on the total extent of melting (Langmuir et al., 1992). At MORs, the lithosphere thickens away from the ridge axis as the oceanic plate cools. This truncates the melting column, resulting in lower extents of melting with distance from the ridge (Figure 3). The thickness of the lithosphere can also vary along a ridge axis, which may further influence the extents of melting within individual ridge segments. Thus, lithosphere thickening both along and across the ridge can truncate the melting columns in three-dimension, creating a pyramid-like melting regime.

MORs spread at various rates ranging from ultra-slow Gakkel Ridge (<20 km Ma^{-1}) (Grindlay et al., 1998) to super-fast spreading East Pacific Rise (>130-150 km Ma^{-1}) (Sinton et al., 1991). Previous studies of MORs have shown that changes in spreading rate correlate with differences in magma flux, ridge crest morphology, lava composition

(e.g., Macdonald, 1982; Parmentier & Forsyth, 1985; Hooft et al., 2000), depths of fractional crystallization (Wanless & Behn, 2017), crustal thickness, axial depth and the presence or absence of an axial magma chamber (Langmuir et al., 1992; Sinton & Detrick, 1992). In general, faster spreading ridges have higher rates of magma generation, which results in elevated ridge crests and steady-state axial magma chambers. This relatively constant supply of magma results in nearly uniform crustal and lithospheric thicknesses along axis and therefore, similar extents of melting (e.g., Plank & Langmuir, 1992; Sinton & Detrick, 1992; Sinton et al., 1991).Thus, at fast-spreading ridges, magmas are produced beneath the entire length of a ridge segment and these melts are supplied vertically from the mantle to the overlying crust (Perfit & Chadwick, 1998).

In contrast, at slow-spreading ridges, like the Mid-Atlantic Ridge (MAR), magma supply is lower and more variable along individual segments, resulting in increased variability in many of these parameters. For example, bathymetric and gravity surveys of the MAR suggests that mantle upwelling is focused at the center of a spreading segment and diminish towards the transform faults that bound each segment (e.g., Lin et al., 1990; Detrick et al., 1995) (Figure 4). Enhanced mantle upwelling and melt focusing towards the segment center results in higher magma supply and thicker crust compared to the segment ends, which are more tectonized and often have extensive faulting that can form oceanic core complexes (OCCs) (Detrick et al., 1995). Variations in magma supply also results in relatively thin basaltic crust and thicker lithosphere at the magmatically poor segment ends (e.g., Cannat, 1996; Dusunur et al., 2009). This suggests that the magma supply to the segment center is robust, with diminished supply towards the segment ends.

Despite these observations, there is no consensus on how magmas are actually transported to the ridge axis at slow-spreading centers, particularly to the sparsely magmatic regions towards the segment ends. This has resulted in two end-member models for how magma is distributed along a slow-spreading ridge: **(1)** Focused magmatism and **(2)** Distributed magmatism. In the focused magmatism model, magmas generated in the mantle beneath the entire ridge axis are focused towards the segment center along the base of a sloping lithosphere (Figure 1). Melts then ascend into the crust and erupt on the seafloor at the segment center or are distributed laterally down the ridge axis towards the segment ends in the shallow crust (e.g, Whitehead et al., 1984, Schouten et al., 1985; Lin & Morgan, 1992; Fialko & Rubin, 1998) (Figure 1a). Thus, in this model all magmas erupted along the segment pass through the segment center. In contrast, in models of distributed magmatism, magmas are generated in the mantle and ascend vertically into the overlying crust along the entirety of the ridge, but with diminished supply towards the segment ends compared to the segment center due to a thickening lithospheric lid (e.g., Langmuir et al., 1977; Bender et al., 1984; Niu & Batiza, 1994; Reynolds & Langmuir, 1997) (Figure 1b). Thus, magmas generated beneath the segment ends do not pass through the segment center prior to eruption. Both models can account for changes in the ridge axis morphology and geophysical observations; however, they may produce distinct lava chemistries with distance from the segment center because melting a homogenous mantle source to different extents will produce different trace element content and ratios due to different compatibilities during melting. Trace elements that are the most incompatible in solids are the first to enter into the melt phase (i.e. La or Ba). Therefore, lower extent of melting will produce magmas that are enriched

compositions, while higher extents of melting results in lower incompatible trace element ratios. In addition to changes in melting systematics, there are variations in thermal regimes and crustal architecture along slow-spreading ridge segments. Higher magma supply results in warmer lithosphere and crust at the segment centers, which promotes storage and crystallization in the shallow crust, while lower magma supply at the segment ends results in more mafic magmas (Rubin & Sinton, 2007). Thus, models of focused versus distributed magmatism predict distinct variations in major and trace element ratios along a ridge segment, which can be tested using the geochemistry of erupted lavas.

This study investigates how magma generation and transport varies along a single segment of the slow-spreading Mid-Atlantic Ridge from the magmatically robust segment center towards a segment end. To test these two models of magma distribution, we systematically mapped and sampled basaltic lavas along half of a segment of the MAR (~14° N), from the magmatic segment center through a more sparsely magmatic region at a non-transform offset and into a second nodal basin (Figure 2b). At several locations, samples were collected along transects across the ridge axis, allowing for both across-axis and along-axis investigations. Major and trace element contents are used to address the question of how lava chemistry varies along a single segment of a slow-spreading MOR. The geochemical results are incorporated into petrologic models to quantify the extents and depths of fractional crystallization along-axis and to determine changes in the extent of melting. These results are used to investigate magma generation and subsequent transport along axis and create a simplified physical model for the distribution of magma along a slow-spreading MOR segment.

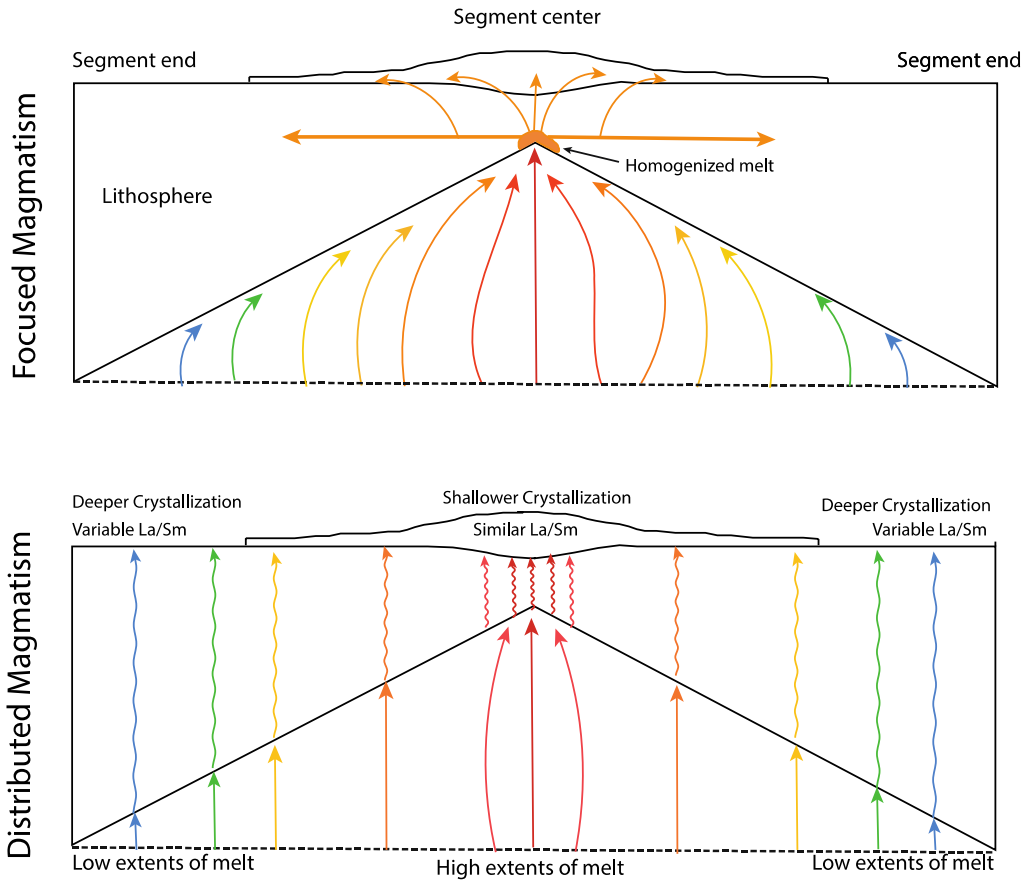

Figure 1. Cartoon schematic of two end member models of magma generation, storage, and transport at slow-spreading MORs. Cartoon schematic of two end member models of magma generation, storage, and transport at slow-spreading MORs. The colors representing differing extents of melting. The warmer colors represent and greater extent of melting and grade down to lower extents of melting towards the cooler colors. (A) Focused magmatism model where melts are generated along the entire axis. The melts are focused at the center of the segment and transported towards the segment ends in the shallow crust. (B) Distributed magmatism model where melts are produced along the entire ridge segment and ascend vertically to the seafloor.

Geologic Setting

This research focuses on a single segment of the slow spreading Mid-Atlantic Ridge (MAR) at ~14°N, bound by the 15°20’ N Fracture Zone to the North and the Marathon Fracture Zone to the south (Figure 2). The segment is ~270 km long and has a classic slow spreading ridge morphology (Figures 2) (e.g., Tolstoy et al., 1993; Hooft et

al., 2000). It consists of a magmatically robust segment center (~14°05' N) that is shallower than the segment ends, has well defined axial valley walls, and is dominated by volcanic accretion. Moving from the center of the ridge towards the ends, the ridge axis deepens, the axial valley walls become less defined, and there are higher extents of tectonism (i.e., increased faulting). This region, referred to as the transition zone, eventually grades into a sparsely magmatic region that extends to the ridge segment ends (Figure 2b). The sparsely magmatic region contains numerous Oceanic Core Complexes (OCCs), extensive tectonism, deeper axial valley, and the absence of clear axial valley walls.

OCCs are formed at slow spreading centers from a low-angle detachment fault that exposes mantle rocks at the surface, which scrape against the asymmetrically diverging axis, creating a corrugated surface atop the OCC (i.e., Blackman et al., 1998; John & Cheadle, 2010). These detachment faults are associated with varying rates of diking in the lithosphere, and OCC topography and composition have been linked to cyclical magmatic and amagmatic periods in a relatively low magma supply region (Olive et al., 2010). Both active and extinct OCCs are abundant in this region of the MAR. There are 44 OCCs identified within a ~300 km range of the ridge axis (Smith et al., 2008), but only one OCC falls within the study site at 13°50 N and it is extinct. The presence of this extinct OCC is important to the study, as part of our systematic sampling included a transect across-axis adjacent to this OCC, including a dive atop the OCC.

Just southwest of the OCC, there is a 4000 m deep nodal basin which trends NW-SE along-axis and begins to offset the ridge axis to the east. Nodal basin formation is still up for debate, but it is thought to form from asthenospheric heat loss compounded with

the cold, dense lithosphere (Sleep & Biehler, 1970). This nodal basin contains numerous faults, in addition to this nodal basin are many volcanic constructs. One of particular importance to this study is a series of pillow mounds, trending generally north-south and is referred to as “Popping Rock Ridge” (Jones et al., 2019). This name is derived from the unique gas-rich highly vesicular basalts which, upon reaching surface pressures, degas and “pop” on deck, subsequently releasing the volatiles trapped within the rock (Sarda & Graham, 1989). The first popping rock was described in 1985, and the goal of better understanding the spatial extent of the popping rocks as well as better understanding their implications for mantle dynamics was the major motivation for the research expeditions to this region. Despite intense sampling along this segment, this is the only region in which popping rocks were found.

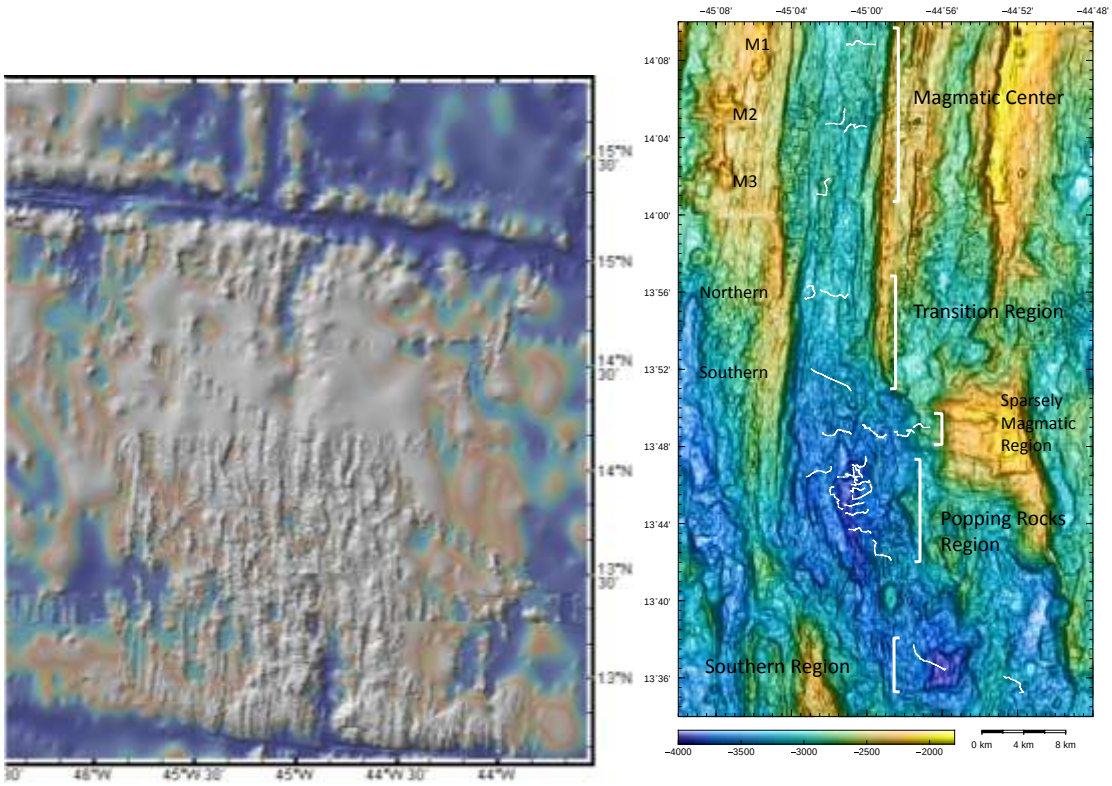

Figure 2. (A).Bathymetric map of the segment in its entirety, bound by the 15°20' N Fracture Zone and Marathon Fracture Zone. Chaotic bathymetry along-axis characteristic of typical slow-spreading MOR morphologies. (B). High resolution bathymetric map of the study region between 13°36' and 14°08'N. Each region and subregion are labeled. Lines represent DSV (Deep Submergence Vehicle) *Alvin* navigation path.

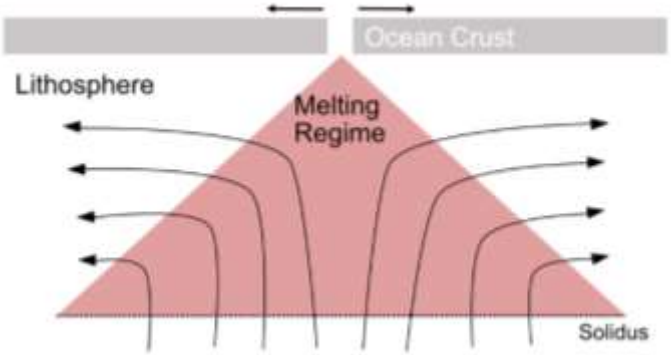

Figure 3. Simplified schematic of a cross section of an MOR's melting regime, adapted from Plank & Langmuir (1992). The upwelling mantle undergoes decompression melting and will buoyantly rise (represented by black arrows) until intersecting with the lithosphere, where melt will truncate. The lithosphere thickening both along and across the ridge can truncate the melting columns in three-dimension, creating a pyramid-like melting regime.

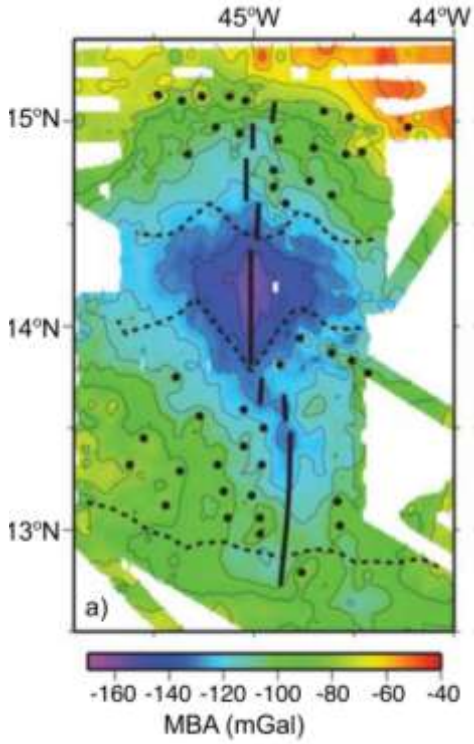

Figure 4. "Bulls-eye effect" wherein MBA gravity low focused at the center of at the 14°N segment of the MAR (Smith et al., 2008). The lower MBA at the segment center is interpreted as an area of greater upwelling. Increased upwelling is subsequently interpreted as an area of greater magma supply.

SAMPLE COLLECTION

Popping Rocks Cruises

Data used in this research were collected during two research expeditions in 2016 (AT 33-03) and 2018 (AT 40-02) both aboard the *R/V Atlantis*. During these research expeditions, lava samples and bathymetric data were collected from ~70 km of the ridge from the segment center at ~14°10'N to the south of the non-transform offset ~13°50' N, resulting in a detailed investigation of nearly half of a ridge segment (Figure 2a). This segment was previously mapped at ~75 meter resolution using ship-based SeaBeam 2100 multibeam (Smith et al., 2006) (Figure 2b); however, high-resolution (1 m) bathymetric maps were also produced using AUV *Sentry* at several locations.

During these research expeditions, 421 basaltic lavas were collected during twenty-seven dives using the *Alvin* human occupied submersible. Lavas were collected from five primary regions: (1) Magmatic Region, (2) Transition Regions, (3) OCC transect, (4) Popping Rocks Region, and (5) Southern Region (Figure 2b). To analyze patterns of chemical variability along axis, we have divided the segment into distinct subregions. The magmatically robust segment center is broken down into three sections: M1, M2, and M3, each of which are approximately 0.5 degrees apart. Sixty-one samples were collected from this region on four *Alvin* dives. This region is dominated by volcanic eruptions and has well defined axial valley walls. Moving south, the axial valley walls are wider and volcanic constructs are present, but the valley is deeper and more faulting is evident in the bathymetry (Figure 2b). This suggests a transition towards lower magma

supply and thus, we have termed these regions the Transition region (Northern and Southern Transition zones). We note, that the large faults cutting through this region connect back to the segment center, which may support models for down-axis diking. Thus, this region may not truly be transitional. The Northern Transition zone, where two *Alvin* dives were conducted, is about half a degree away from the Southern Transition zone, where one *Alvin* dive was conducted. In total, 45 lavas were collected from the Transition region. South of the transition region, the axial valley deepens, the seafloor fabric has higher extents of faulting, and the eastern rift valley wall disappears into an extinct OCC. All of these observations suggest lower magma supply and a shift towards the sparsely magmatic region of the ridge segment. Thirty-nine lavas were collected on four *Alvin* dives from this region, that we term the OCC transect due to the presence of an extinct OCC that bounds the transect to the east; however, most lavas were not collected on the OCC. This is the longest transect spanning from the top of the OCC to the western wall. Just south of this transect there is a nodal basin forming a non-transform offset. Within the nodal basin there are numerous volcanic constructs and curvilinear faults. Many (but not all) of the lavas collected from this region are highly vesicular and gas-rich popping rocks, giving rise to the name the Popping Rocks Region. In total, 207 lavas were collected from this region during 14 *Alvin* dives. While this is the only region in which popping rocks were recovered along the entire segment, not all the samples collected here “pop”. Two Alvin dives were conducted in the Southern Region, which is offset to the east from the magmatic center via a non-transform offset. 30 lavas were collected during two Alvin dives in this region. Lavas collected from region provide an important geochemical comparison to lavas from the magmatic center, the transition

zone, and popping rocks region, as there is no obvious surficial connection to the magmatic center and it is well within the sparsely magmatic portion the segment.

METHODS

Major Element Analysis

Major elements were collected on basaltic glasses from 382 lavas. Basaltic glass was chipped from the outer rind of the basalts and mounted in epoxy for geochemical analyses. The epoxy mounts were polished using polycrystalline diamond suspension fluid with 6, 3, and 1 μm grit. Major element contents were collected using SXFive Electron Microprobe at Boise State University. Internal standards VG-2 and A-99 were run after every three unknown samples to correct for instrumental drift. The microprobe had an accelerating voltage of 15kV, a beam width of 20 μm, and the current was 40 nA. Six spots were analyzed on each sample and averaged to determine the final composition. Outliers were removed prior to averaging. Na, which was the first element analyzed to prevent volitization, was analyzed for 20 seconds on-peak and 10 seconds off-peak. The other major elements were analyzed for 30 seconds on-peak and 15 seconds off-peak.

Trace Element Analysis

Basaltic glass was chipped from each sample and sonicated using MQ water and 1% hydrogen peroxide followed by milliQ water to remove alteration. This process was repeated at least three times and continued until clean. Fifty milligrams of glass was then hand-picked, using a binocular microscope, avoiding microphenocrysts and any remaining alteration that the sonication process was unable to remove. Glass chips were then dissolved in a series of acids following methods outlined in Schwartz et al. (2018).

The dissolved samples were analyzed for trace element contents using the Thermo Electron X-Series II Quadrupole Inductively Coupled Plasma Mass Spectrometer with an ESI SC-FAST autosampler at Boise State University. Analyses were corrected for drift using JB-3 (measured after every 5 unknowns), an internal standard from the Geological Survey of Japan. Calibration curves were created using standards BHVO-2, BIR-1, DNC-1, W-2 (US Geological Survey), and 2392-9 (University of Florida internal standard, (Goss et al., 2010)). Each basalt sample was measured three times and averaged; the uptake time is 10s, and the analysis time is 30s. In total, 197 lavas were analyzed for trace element contents.

RESULTS

Chemical Variability Along-Axis

There is considerable variability in both major and trace element contents in the lavas erupted along this segment. For example, MgO values range from 4.99 to 9.44 wt %, K/Ti values range from 0.06 to 0.51, and La/Sm values ranges from 1.06 to 4.14. MOR basalts (MORB) are commonly divided into geochemical groups based on incompatible element ratios (K/Ti or La/Sm). Using the definitions of Gale et al. (2011) we define Enriched MORB (E-MORB) as having a K/Ti >0.2 or $La/Sm_N > 2$ and Normal MORB (N-MORB) as having a K/Ti ≤ 0.11 or $La/Sm_N < 1$. Based on this, the vast majority of the of the samples collected along this segment are E-MORB (~97%). Only 11 NMORB samples were collected. Below, we describe the specific chemical results of each region (from north to south).

M1 is the northernmost region sampled and is located just north of the segment center. Ten samples were collected from one Alvin dive, four of which were analyzed for trace element contents. The most evolved lavas observed along the entire ridge axis were collected at this location. MgO contents in the region vary from 4.99 to 8.20 wt %, FeOT varies from 7.86 to 11.10 wt %, and CaO varies from 9.65 to 13.27 wt % (Figure 5). K/Ti values range from 0.26 to 0.47. Ca/Al values range from 0.66 to 0.82. La/Sm values range from 3.31 to 3.69. Sm/Yb values range from 1.80 to 1.90 (Figure 6).

M2 is the most central of all sections examined. Samples were collected on two *Alvin* dives (4824 and 4925) that transect the axial valley. Thirty-three samples were

collected from the region, 9 of which were analyzed for trace element contents. MgO contents in the region vary from 5.65 to 8.25, FeOT varies from 8.33 to 12.18 wt %, and CaO varies from 9.89 to 12. wt % (Figure 5). K/Ti values range from 0.31 to 0.40. Ca/Al ranges from 0.68 to 0.80. La/Sm values range from 3.06 to 3.30. Sm/Yb values range from 1.67 to 1.76 (Figure 6).

M3 is the southernmost magmatic center transect. Eighteen samples were collected from this transect, 5 of which were analyzed for trace element contents. MgO contents in the region vary from 5.52 to 8.24 wt %, FeOT varies from 8.67 to 11.39 wt %, and CaO varies from 9.68 to 12.52 wt % (Figure 5). K/Ti values range from 0.24 to 0.43. Ca/Al values range from 0.68 to 0.82. La/Sm values range from 2.58 to 3.60 and Sm/Yb values range from 1.60 to 1.87 (Figure 6).

The **northern transition** region included two *Alvin* dives (4952 and 4958) with 34 samples, 5 of which were analyzed for trace element contents. In this region, MgO contents vary from 5.65 to 8.75 wt %, FeOT from 9.05 to 11.19 wt %, and CaO from 10.35 to 13.43 wt % (Figure 5). K/Ti values range from 0.1 to 0.44. Ca/Al value range from 0.72 to 0.89. La/Sm values range from 1.26 to 3.47 and Sm/Yb values range from 0.71 to 1.69 (Figure 6).

12 samples were collected from one Alvin dive that crossed the axial valley in the **southern transition** region. All 12 samples were analyzed for trace element contents. MgO contents in the region vary from 6.71 to 8.67 wt %, FeOT from 8.50 to 9.85 wt %, and CaO from 10.96 to 12.96 wt % (Figure 5). K/Ti values range from 0.32 to 0.40. Ca/Al values range from 0.72 to 0.84. La/Sm values range from 2.90 to 3.48 and Sm/Yb values range from 1.48 to 1.93 (Figure 6).

Thirty-nine samples were collected along the **OCC transect** during four *Alvin* dives (4822, 4948, 4950, and 4959) which span across the axial valley and on top of the extinct OCC. 35 of these samples were analyzed for trace element contents. MgO contents in the region vary from 6.05 to 8.65 wt %, FeO from 8.79 to 11.22 wt %, and CaO from 9.71 to 12.91 wt % (Figure 5). K/Ti values range from 0.06 to 0.42, and Ca/Al values range from 0.63 to 0.82. La/Sm values range from 1.06 to 3.70 and Sm/Yb values range from 0.83 to 1.82 (Figure 6). Nine of the samples collected from this transect are NMORB, making it the region with the most NMORB along the entire segment.

The **popping rocks region** is the most sampled region, with 207 basaltic lavas, 108 of which were analyzed for trace element contents. MgO contents varies from 6.08 to 9.44 wt %, FeOT from 8.74 to 10.47, and CaO from 10.54 to 13.14 (Figure 5). K/Ti values range from 0.18 to 0.51 and Ca/Al values range from 0.71 to 0.88. La/Sm ranges from 1.99 to 4.14 and Sm/Yb ranges from 1.03 to 2.15 (Figure 6). In general, the popping rocks have relatively limited compositions compared to other lavas sampled in the region.

The **southern region** is comprised of two *Alvin* dives, 4954 which traversed a small basin, and dive 4955 which traversed a number of small seamounts. 30 samples were collected in this region and 19 of them were analyzed for trace element contents. MgO contents vary from 6.91 to 8.27 wt %, FeOT from 9.07 to 10.51 wt %, and CaO from 10.81 to 11.77 wt % (Figure 5). K/Ti values range from 0.11 to 0.32. Ca/Al values range from 0.72 to 0.77. La/Sm values range from 1.32 to 3.21, and Sm/Yb values range from 0.98 to 1.87 (Figure 6). This region has the most limited range of major element contents, but a relatively wide range of trace element ratios.

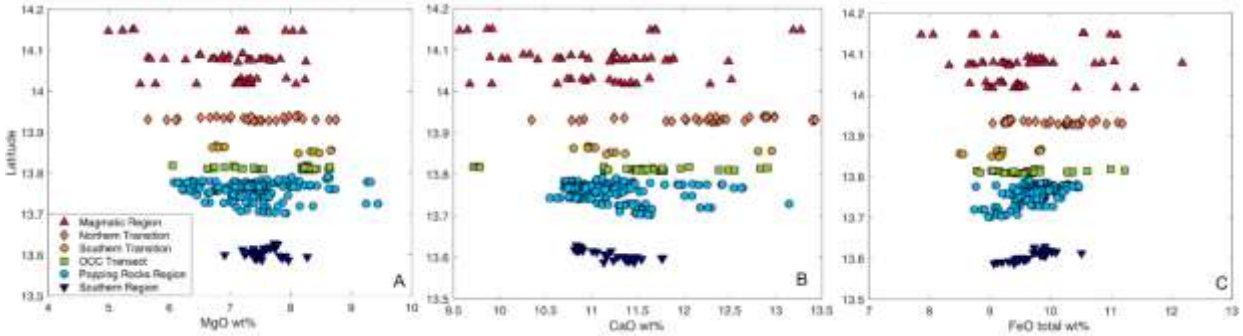

Figure 5. Major element contents (A) MgO (B) CaO, and (C) FeOT weight percent for each region by latitude.

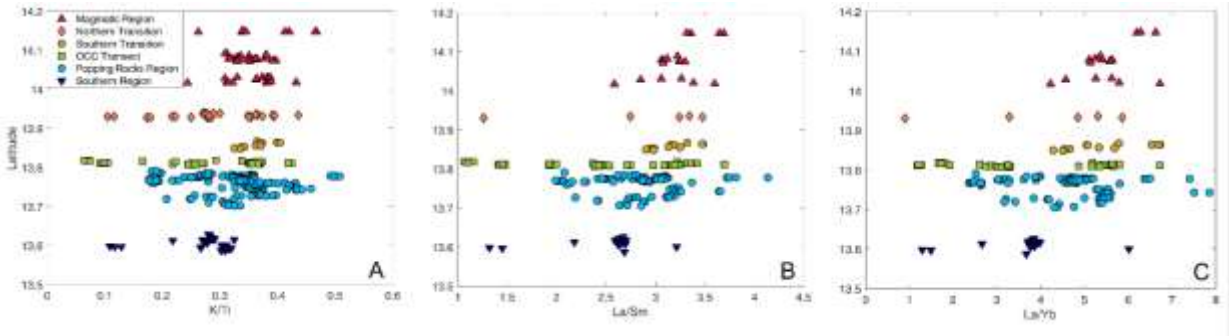

Figure 6. (A) K/Ti ratio. Trace element ratios (B) La/Sm and (C) La/Yb by latitude.

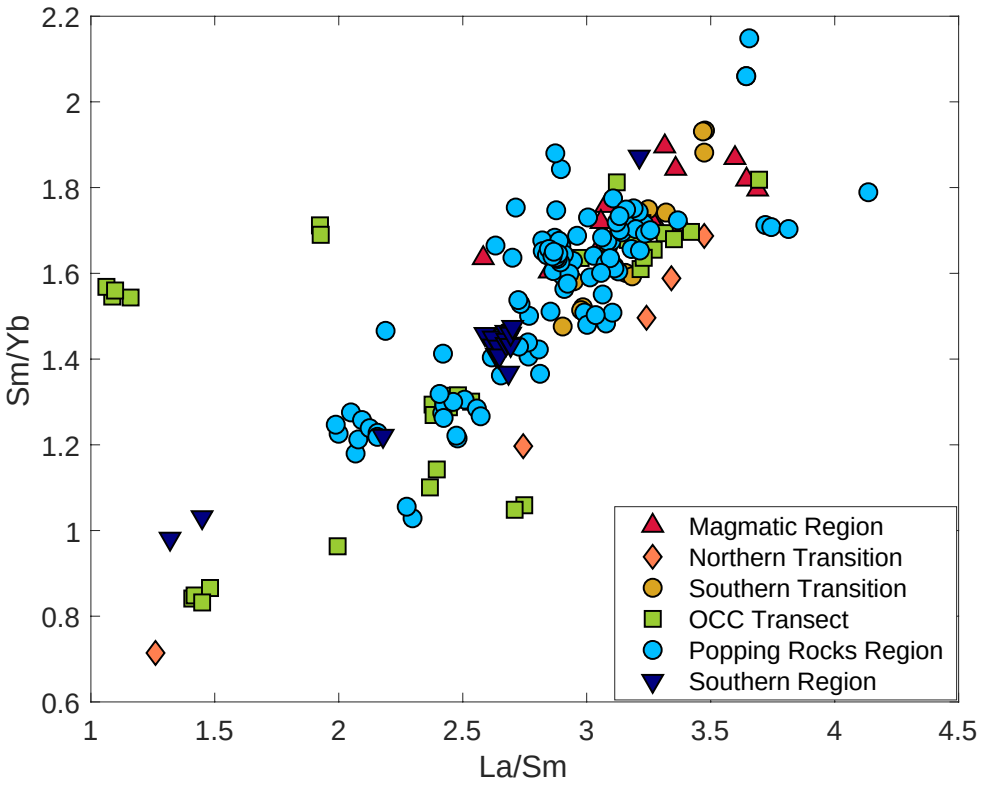

Figure 7. La/Sm vs Sm/Yb for the entire segment. Generally, the compositions fall in a linear trend, but several samples from the OCC transect do not, due to the presence of the extinct OCC.

Trace Element variability Along-Axis

The basalts erupted in the magmatic region all have relatively similar slopes in REE diagrams (Figures 8a-c), suggesting similar mantle sources and extents of melting. The spread in the individual trace element patterns can be predominately be accounted for by increasing extents of fractional crystallization. This is consistent with a limited range of REE ratios (Figure 8) major element contents (Figure 5). The trace element variability in lavas erupted in magmatic region 3, which may indicate small variations in the extents of melting or mantle source. However, in general, the range of basaltic

compositions erupted in the magmatic center can be explained predominantly by fractional crystallization.

The greatest variability in REE patterns is observed in the OCC transect region, where both depleted N-MORB patterns and enriched E-MORB patterns are observed. This is consistent with trace element ratios (Figures 6&7) that show a wide range of values. This variability may be related to either melting of a heterogeneous mantle source or changes in the extent melting; however, isotopic analyses are required to discriminate between the two.

Lavas erupted in the popping rocks region also shows significant spread in trace element patterns. In this region, the actual popping rocks are some of the most enriched rocks and all have remarkably similar REE patterns. This suggests that the popping rocks have undergone similar extents of crystallization and extents of melting of a similar mantle source. Other lavas within the region show a range of REE patterns, suggesting both variations in extent of crystallization and changes in melting or mantle source.

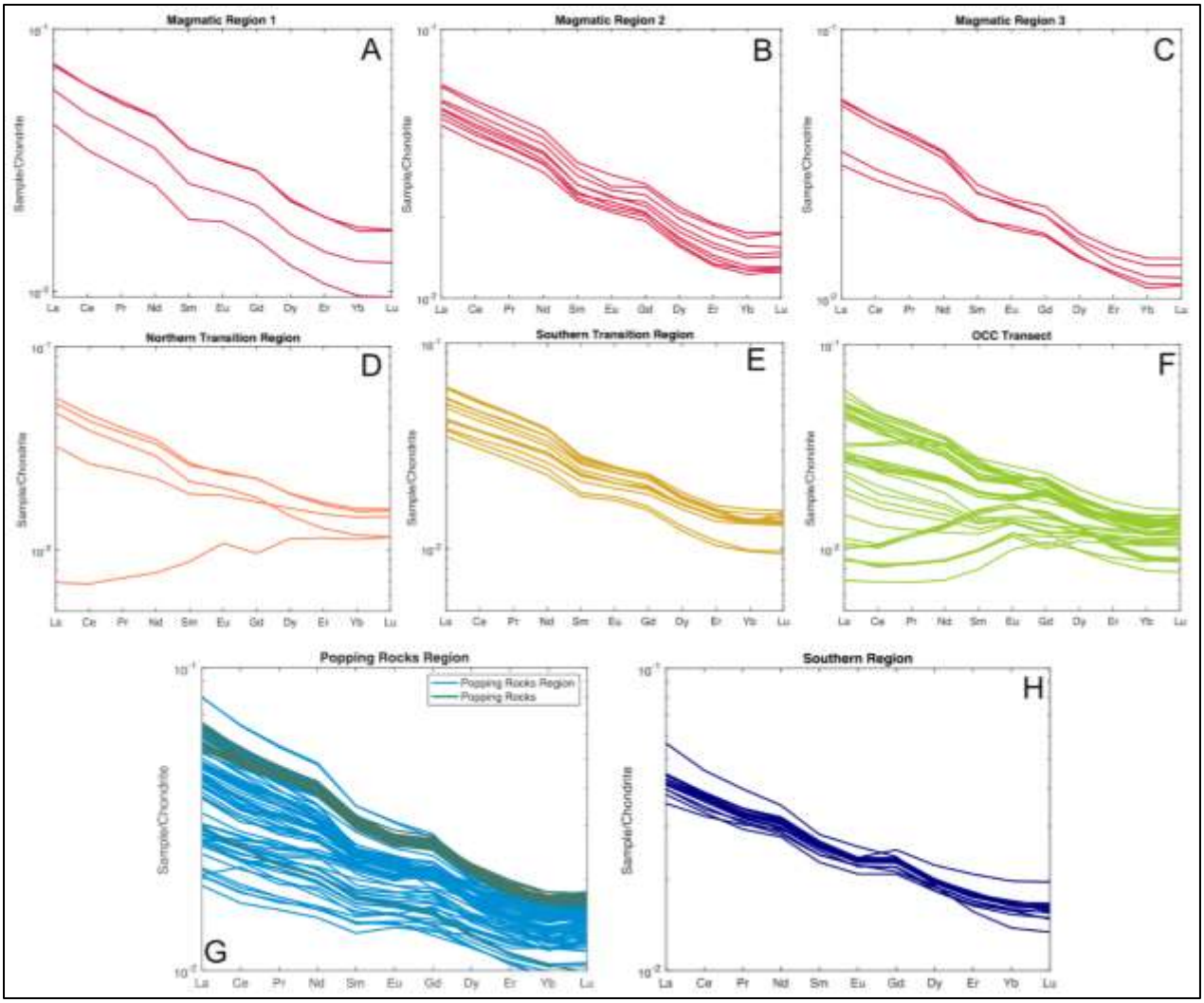

Figure 8a-h. REE plots for all transects of the segment from north to south.

DISCUSSION

Observations of seafloor bathymetry and geophysical surveys provide evidence for a higher magma supply at the segment center that diminishes towards the segment ends. For example, Mantle Bouger Anomalies (MBAs), which are proxies for density, suggest that that mantle upwelling is focused at the centers of slow spreading ridge segments (e.g., Kuo & Forsyth, 1988; Lin et al., 1990; Blackman & Forsyth, 1991; Tolstoy et al., 1993). Furthermore, seismic surveys suggest that the lithosphere thickens from ~6.5 km at the segment center to ~10 km near the ridge offset (e.g, Cannat, 1996; Dusunur et al., 2009), while there is a decrease in crustal thicknesses near ridge segment ends (White et al., 1984). Combined, these observations suggest a diminishing magma supply with distance from the segment center. While extensive geophysical surveys have not been conducted along the 14°N segment, a gravity survey of the region (Figure 4) shows a significant MBA low at the center of the segment, which increases in a bulls-eye fashion moving away from the segment center (Smith et al., 2008). Further, bathymetric data of this region show a chaotic bathymetry along-axis, typical of a slow-spreading MOR. There is a bathymetric high in the segment center, which diminishes moving towards the segment ends (Figure 2a). Thus, the morphology and gravity data along this ridge segment support models for a decreasing magma supply from the center of the segment towards the segment ends.

Magma Storage Depths and Crystallization along-axis

Previous geochemical studies of the global MOR system have shown that major element compositions in erupted lavas can vary with spreading rate, which is generally attributed to changes in magma flux and storage within the system (e.g., Grove et al., 1992; Rubin & Sinton, 2007; Rubin et al., 2011). Faster spreading ridges erupt lavas with a wide range of major element contents, reflecting significant storage and crystallization within a warmer, shallow crust (Perfit & Chadwick, 1998; Perfit, 2001; Sinton & Detrick, 1992; Rubin & Sinton, 2007). In contrast, slower spreading ridges, where the flux is lower, tend to erupt basalts with more limited and more mafic major element contents, suggesting less storage and crystallization prior to eruption (Rubin & Sinton, 2007). This shift is commonly attributed to cooler thermal regimes, thicker lithosphere, and the absence of steady state magmatic systems at slower spreading rates (Sinton & Detrick, 1992). However, geophysical observations also suggest that magma flux and thus, thermal regimes, varies along individual slow spreading ridge segments (Detrick et al., 1995), which may influence the major element and trace element contents of erupted lavas.

At the 14°N segment, there is a relatively wide range of major element compositions erupted along segment; however, a systematic decrease in variability is observed from north to south (Figures 5&9). In the magmatic region, major element contents have the greatest variability and largest standard deviations compared to other regions (Figure 9). For example, the magmatic region's standard deviation of MgO is 0.78, while the southern region's is 0.33. This variability generally decreases towards the south and is particularly evident in the southern most region, where the least major

element variability and smallest standard deviation is observed (Figure 5). Average compositions of the southern lavas are more mafic, with higher MgO (9.68) and lower CaO (11.2) and Al_2O_3 (15.17) contents (Figures 5&9). Combined, these observations suggest that magmas within the magmatic center can undergo higher extents of crystallization prior to eruption on the seafloor compared to lavas erupted in the lower magma supply regions. This is consistent with geophysical studies suggesting warmer, thinner lithosphere and thicker crust in the more magmatically robust segment center (Tolstoy et al., 1993, Detrick et al., 1995).

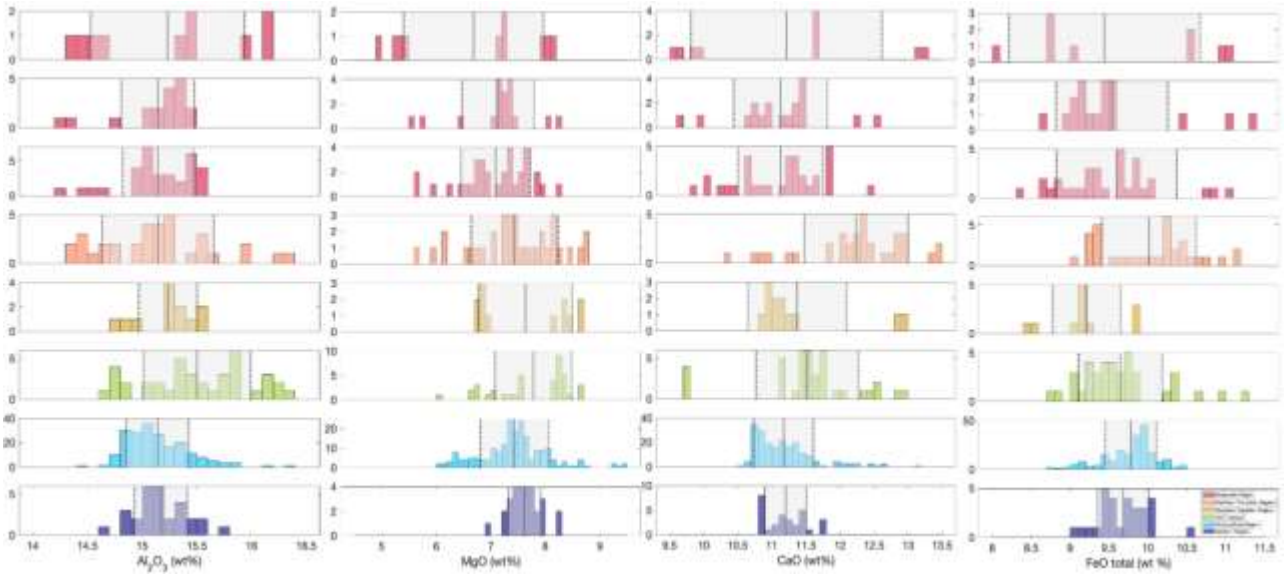

Figures 9. Histogram diagrams of each transect along the segment for Al_2O_3, MgO, CaO, and FeOT. Figure is organized from north to source. Average values for each region are shown by the black bar, and the standard deviation is represented by the surrounding grey region and terminated with the dotted lines.

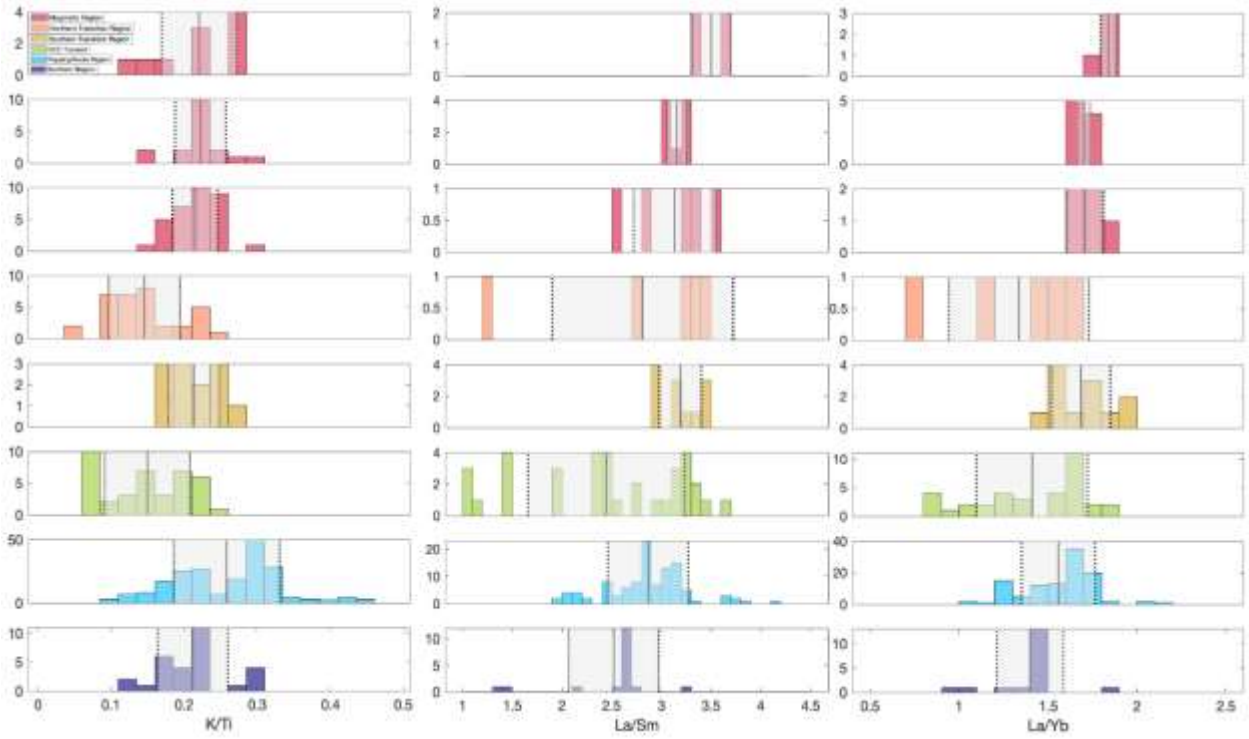

Figure 10. Histogram diagrams of each region moving down segment for K/Ti, La/Sm, and La/Yb ratios. Average values for each region are shown by the black bar, and the standard deviation is represented by the surrounding grey region and terminated with the dotted lines.

Quantifying the depths over which fractional crystallization occurs along axis is important for constraining the mechanics of magma generation, storage, and transport along-axis and can help discriminate between the two models for magmatism on a slow spreading ridge. In the model of focused magmatism, where melts are transported down axis in the shallow crust, fractional crystallization depths may be similar and shallow at all locations (Figure 1a). For distributed magmatism, the depths of fractional crystallization may be more variable and perhaps deeper away from the segment center due to a thicker, cooler lithosphere that allows for the onset of crystallization at greater depths (Figure 1b). Thus, quantifying the depths of crystallization can provide insights into magma transport and storage on a slow spreading ridge.

To quantify the extents and depths of crystallization observed along the ridge segment, we calculated liquid lines of descent at each location using the petrologic modelling software Petrolog (Danyushevsky & Plechov, 2011). Fractional crystallization trends were calculated at a variety of pressures and starting compositions from each region. Initial water contents for the models are from analyses of basalts that were collected in the area using Secondary Ion Mass Spectrometry (SIMS) and are reported in Jones et al. (2018). Oxygen fugacity was buffered at QFM for all runs. Pressures were varied from 0.5 to 5 kbar for each starting composition. The best fit modeled crystallization trend was chosen based upon qualitative best fit to the regional basalt compositions and is shown in Figure 10; chemistry for each location are provided in appendix A. We note that because samples were collected from numerous volcanic constructs at each location, we do not expect a single fractional crystallization trend to account for all variability in a given region. This is supported by the range in K/Ti ratios within each region, which suggests that multiple parent magmas are required. However, examining general trends in the depths and extents of crystallization along axis can provide insights into magma storage along axis.

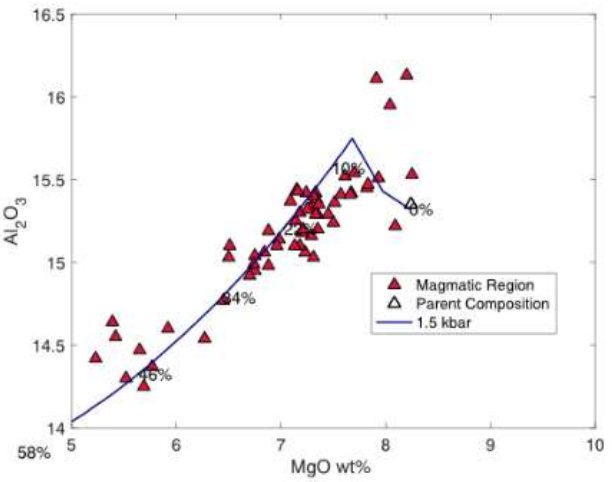
Magmatic Region
Parent Composition
1.5 kbar
Al2O3
MgO wt%
0%
10%
22%
34%
46%
58%

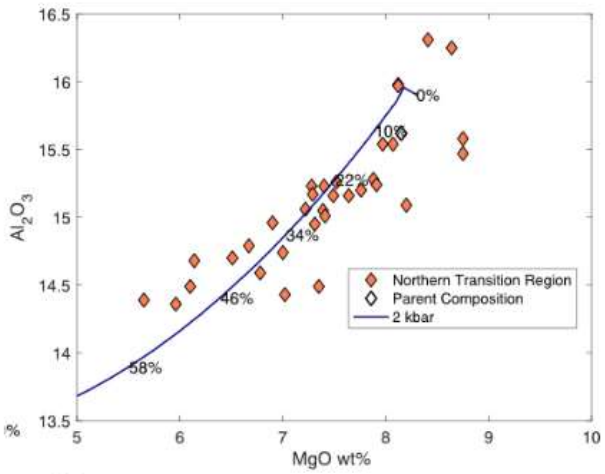
Northern Transition Region
Parent Composition
2 kbar
Al2O3
MgO wt%
0%
10%
22%
34%
46%
58%

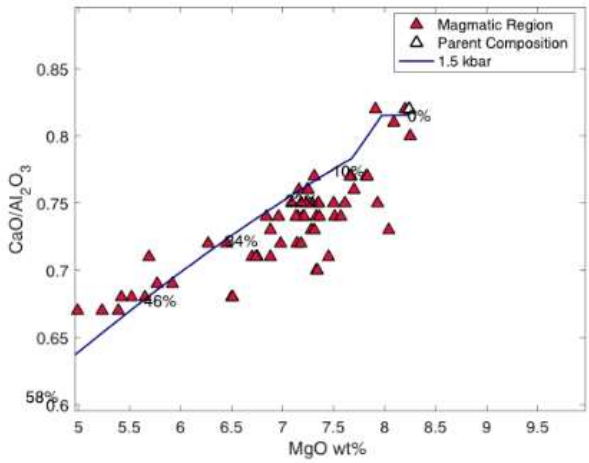
Magmatic Region
Parent Composition
1.5 kbar
CaO/Al2O3
MgO wt%
0%
10%
22%
34%
46%
58%

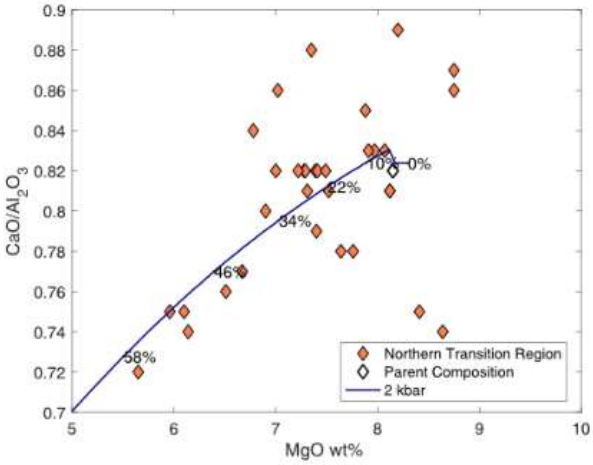
Northern Transition Region
Parent Composition
2 kbar
CaO/Al2O3
MgO wt%
0%
10%
22%
34%
46%
58%

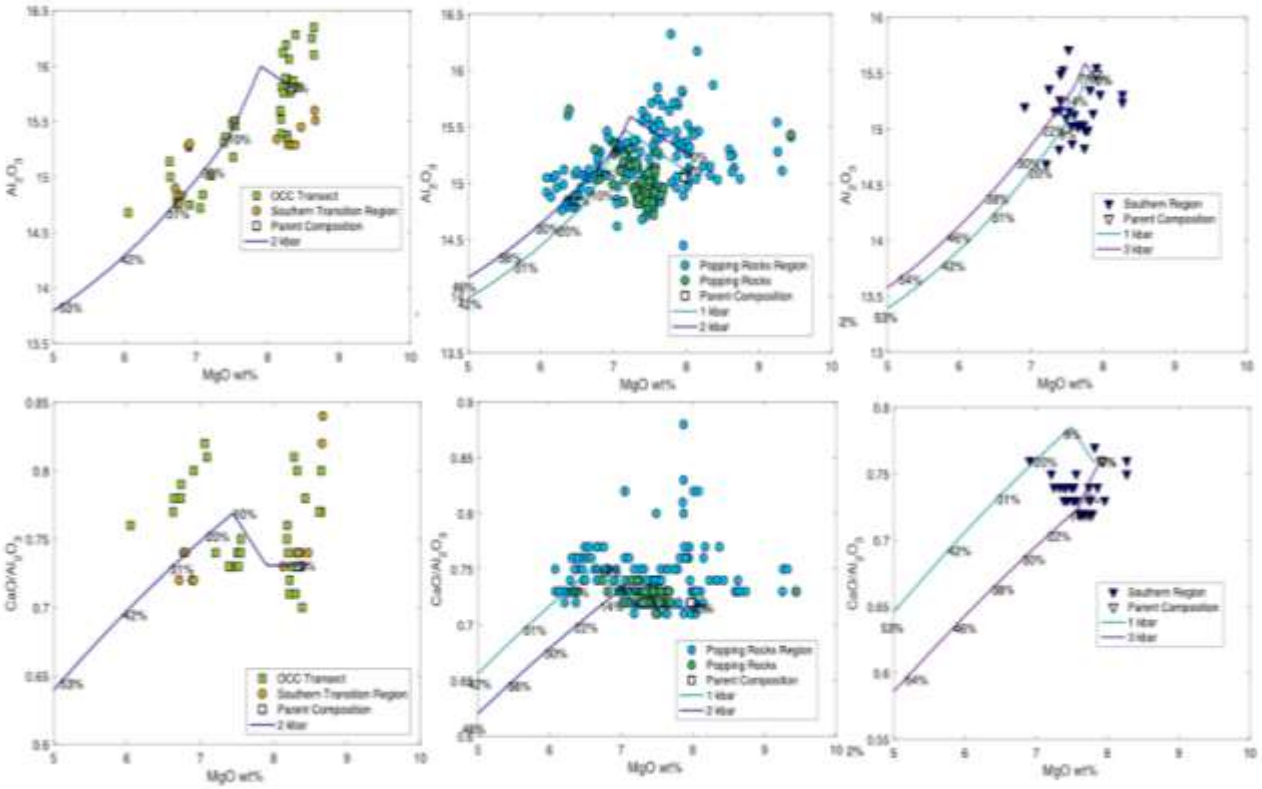

Figure 11. Major element variation diagrams showing the compositions of lavas collected from all regions. Top row shows Al2O3 and MgO (wt %) contents at each location with modeled fractional crystallization trend. Bottom row shows CaO/Al2O3 and MgO (wt %) contents at each location with modeled fraction crystallization trends. The details of the model can be found within the text. Labeled on each modeled fractional crystallization trend are the percent of crystallization along the liquid line of decent. The major element contents from the magmatic center and northern transition region fit the model trends well around 1.5-2kbar but moving away from the warm magmatic center either multiple depths of crystallization or multiple parents are required to account for the range in chemistry. From the magmatic center to the southernmost region, the amount of fractional crystallization required to reach the least mafic samples decreases by ~30%.

In the warm magmatic center and the nearby northern transition region, major element contents can be reproduced relatively well by fractional crystallization of a single parent magma at 1.5 to 2 kbar. These models suggest ~50% crystallization of Olivine, Plagioclase, and Clinopyroxene to produce the entire suite of lavas. Moving south, the

best-fit fractional crystallization trends require variable pressures and/or parent magmas to account for the range of major element contents observed. These models require a lower extent of fractional crystallization to account for the range of compositions, suggesting less storage prior to eruption. For example, in the southern most section where MgO contents are relatively limited and generally more mafic (average MgO is 9.68), only 10-15% crystallization of Olivine, Plagioclase, and Clinopyroxene is required.

The shift in major element variability, average MgO content, extents of crystallization, and perhaps depths of crystallization suggest that magma storage varies along the segment. In general, the magmatic center has more variable and evolved compositions that are consistent with greater extents of crystallization and storage in warmer, shallow crust. Lavas erupted in the southern region are on average more mafic and less variable, suggesting limited crystallization prior to eruption. The range of major element contents at a given MgO in the transition, OCC and popping rocks regions suggests a range of parent compositions, variable crystallization and perhaps a range of depths of crystallization. This is particularly evident at the OCC transect. Combined, these results suggest a focused model for magmatism within the magmatic center, with increasing complexity with distance from the segment center, perhaps suggesting a hybrid model of both horizontal and vertical melt transport in the transition, OCC transect and popping rocks regions. In contrast, the southern region, which is offset from the magmatic center, has limited and more mafic major element contents that support a vertical melt supply consistent with distributed model of magmatism.

Trace Element Variability Along-Axis

Rare Earth Elements (REEs) can provide important insights into magmatic processes due to slight differences in their compatibilities during mantle melting. For example, highly incompatible elements (i.e., La and Ce) enter the melt phase more readily then less incompatible REEs (i.e., Dy and Yb), and thus REE patterns and ratios of these elements can be used to investigate changes in the extents of melting. REE contents can also provide constraints on extents of fractional crystallization in basaltic magmas, as most REEs are incompatible in the primary crystallizing mineral phases (olivine, plagioclase and clinopyroxene). Thus, while crystallization should not change trace element ratios, it will cause an increase in REE contents in the melt.

At 14°N, there is an increase in variability in trace element contents and ratios with distance from the segment center. In regions that are dominated by volcanism, like the magmatic center (M1, M2, and M3), there is a relatively limited range of trace element ratios (Figure 6) and patterns (Figure 6), despite clearly sampling multiple eruptive units. The limited range of trace element ratios (Figure 6&7), may be attributed to melt homogenization during focusing at the segment center. To the south, as the seafloor fabric indicates a transition towards tectonically dominated accretion, trace element variability increases (Figure 6). For example, the Northern Transect has La/Sm values ranging from 1.26 to 3.47 and the OCC transect has lavas with La/Sm value ranging from 1.06 to 3.70 and Sm/Yb values range from 0.83 to 1.82. This suggests variable extents of melting and/or mantle sources and less homogenization of melts prior to eruption. Trace element ratios are variable in the southern region (Figure 6), consistent with lower magma supply in the region. While the REE patterns appear similar (Figure

8h), the range of La/Sm values is similar to other sparsely magmatic regions (Figures 6B&10). Combined, these results again suggest increasing complexity for melt generation and transport in the transition and sparsely magmatic regions, with less variability in the magmatically robust portion of the segment.

Model for Magma Generation and Transport on a Slow Spreading Segment

The systematic sampling of lavas from the magmatically robust segment center to the sparsely magmatic region along the 14°N segment of the MAR allows us to evaluate the two models for melt generation and transport along slow-spreading MORs in detail. Major element contents, fractional crystallization models, and REE patterns suggest that there are changes in the extent and possibly depth of crystallization along the ridge axis. In the magmatically robust segment center lavas have the highest variability in major element contents that can generally be explained by shallow (1 kbar) crystallization of similar parental magmas. Furthermore, the relatively limited trace element patterns and ratios in lavas erupted in this region suggest a similar mantle source, extent of melting or efficient homogenization process. These observations are consistent with focused magmatism at the segment center. In the transition and sparsely magmatic regions, variability in trace element contents and ratios increases significantly, while average major element contents become more mafic. In these regions, fractional crystallization of a single parent magma at a single pressure is unable to explain all chemical variability. Furthermore, the range of trace element patterns and ratios suggests a range of melts can be preserved and erupted in these regions. Combined, these data suggest that all lavas erupted the OCC transect, popping rocks and transition zones are not efficiently homogenized prior to eruption and instead require multiple parent magmas produced by

variable extents melting or mantle sources. This range of variability and the absence of a systematic shift in trace element ratios with distance along axis are inconsistent with either model of magma supply and instead suggest that melts can take a variety of pathways to reach the seafloor in these regions. Both the Petrolog model results (Figure 11) and the REE patterns of the southern region (Figure 8h) suggest limited fractional crystallization prior to eruption in this colder region. This region is offset to the east from the magmatic center via a non-transform offset and thus, there is no surficial or geochemical evidence that magmas pass through the segment center and are transported laterally in the shallow crust. Thus, these melts appear to bypass the segment center entirely. Combined, these results are consistent with a model where warmer conditions in the segment center allow for greater storage, homogenization, and increased crystallization, while in the cooler sparsely magmatic region there is less storage, homogenization, and crystallization; however, the regions in between may require numerous melt pathways.

To reconcile physical and chemical observations at the 14°N segment, we suggest a hybrid model of magma generation and transport along a slow spreading MOR (Figure 12). Our model is most consistent with models for distributed magmatism, where melts to the sparsely magmatic southern region, offset from the magmatic center, are supplied vertically from the mantle to the seafloor. In contrast, lavas erupted in the magmatically robust segment center are likely produced by melt focusing and homogenization along the base of a sloping lithosphere over relatively short distances in the mantle, which then undergo variable extents of crystallization in the shallow crust prior to eruption. This model is consistent with geophysical observations of a shallower axis and lower MBA at

the segment center wherein magma is generated along the entirety of the ridge segment, but only a portion is focused towards the segment center via the sloping lithosphere. These focused magmas may then be distributed laterally down axis via diking in the shallow crust, perhaps as far as the transition region (Figure 12). However, the increased variability in trace element ratios observed in the OCC transect and the popping rocks region suggest that not all magmas erupted here pass through the segment center. Instead, we suggest that magmas feeding volcanism the colder, more tectonized regions, may either be transported down axis from the magmatic center or ascend vertically from the mantle, preserving variable chemistries due to differing extents of melting. These melts undergo variable extents of crystallization at a range of depths due to the colder lithosphere. In this hybrid model, we suggest that the transition in ridge morphology from magmatically robust to sparsely magmatic results in a complex magmatic system where melts can ascend both vertically from the mantel and horizontally along axis, allow for a wide range of erupted compositions.

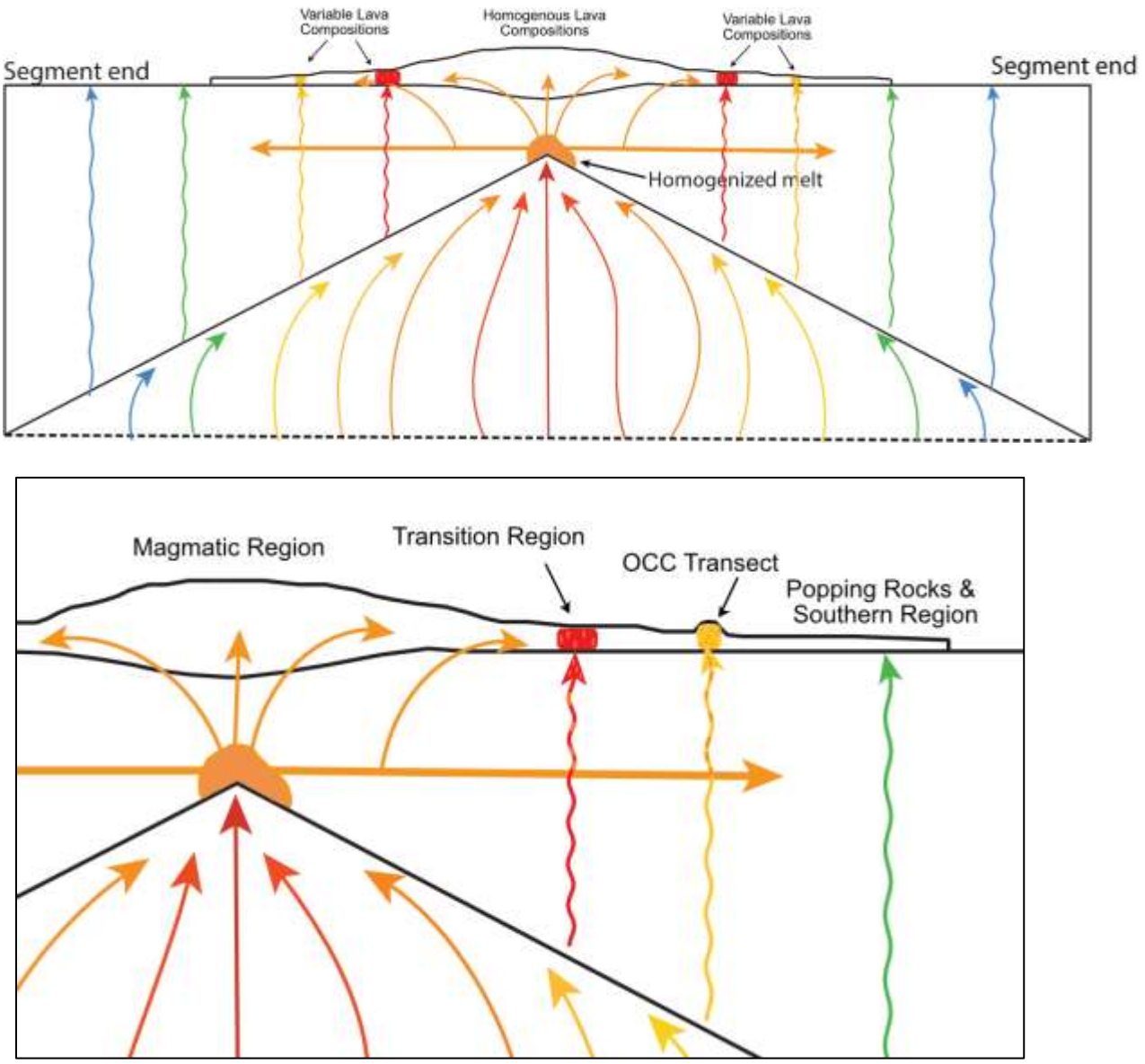

Figure 12. Proposed "hybrid model" of magma generation, storage, and transport at a slow spreading MOR based upon the geochemical findings of this study. Close up view of the proposed model includes labeled transects from this study.

Comparison to other MAR Segments

This study is not the first to investigate magma transport, storage, and generation at slow spreading MORs. Two notable studies (Niu and Batiza 1994), and Gale et al. (2011) have sampled basalts along-axis of the MAR but had different sampling intervals that led to different conclusions. One study focused on lavas erupted from several different short segments, but predominantly focused on sampling segment centers and not sparsely magmatic regions (Gale), while the second study focused on a single segment of the MAR, but the dredges were spaced out along the entirety of the segment (Niu and Batiza, 1994).

Gale et al. (2011) investigated 9 segments the North Atlantic near the Azores platform, including the Lucky Strike segment, which is one of the only locations along the MAR to have a seismically imaged magma chamber (Singh et al., 2006). The presence of the magma chamber at the center of the Lucky Strike Segment suggests focused magmatism; however, the geochemical results did not support this model due to the wide range of trace element contents erupted (Figures 13). This geochemical study included lavas from the segment centers to the transition regions, but did not include lavas from the sparsely magmatic regions (Gale et al., 2011). Generally, the Lucky Strike segment is more enriched than other MAR segments (including the 14°N segment; Figure 13), which they attributed to low extents of melting from the Azores platform source (Gale et al., 2011). The wide range of compositions erupted does not favor a model for melt focusing or homogenization. The authors could not justify an exclusively homogenized model because the variability and enrichment at the segment centers does not extend to the transitional regions. This makes it hard to justify the idea that the only

mechanism of magma transport along axis is through batches of magma laterally diking from a central source along the entirety of the axis (Gale et al., 2011).

The second study sampled over a 100 km ridge axis at 26°S via dredging (Niu & Batiza, 1994). Major element contents of basaltic glasses show no clear chemical gradient or trend along axis. Because the samples were collected via dredge, it is not possible to determine if any across-axis trends exist along the segment. Unlike the Lucky Strike segment and 14°N segment, lavas were all relatively depleted N-MORB (K/Ti > 0.11) (Figure 14). Based upon these two end-member along-axis MAR case studies, the 14°N segment is more depleted than Lucky Strike and more enriched and variable than 26°S.

At 14°N, we have systematically sampled ~50 km along and across axis of a ridge segment and have captured the geochemical complexity that can be found along a single ridge axis. Despite the lack of plume influence at 14°N, the chemical variability is similar to that observed in the 9 segments sampled near the Azores (Gale et al., 2011). Like Gale et al. (2011), lavas from 14°N are more enriched at the segment center compared to segment ends, but there is a wide range of compositions erupted at the OCC transect and Popping Rocks Region, as evidenced by our trace element ratios (Figure 7). Perhaps it is the lack of detailed sampling both along and across axis that has produced the extremely enriched Lucky Strike and extremely depleted 26°S datasets. Furthermore, unlike the Lucky Strike Segment, there is no nearby hot spot or shallow magma chamber to influence the basalt chemistry. Despite this lack of plume influence, our dataset more closely resembles the Lucky Strike (Figure 13). Thus, this range of chemical variability can be produced in the absence of a plume and along a single segment. This may result

from the systematic, high-resolution sampling down a ridge segment, and may indicate that the 14°N segment is more representative of a typical MAR segment's variability.

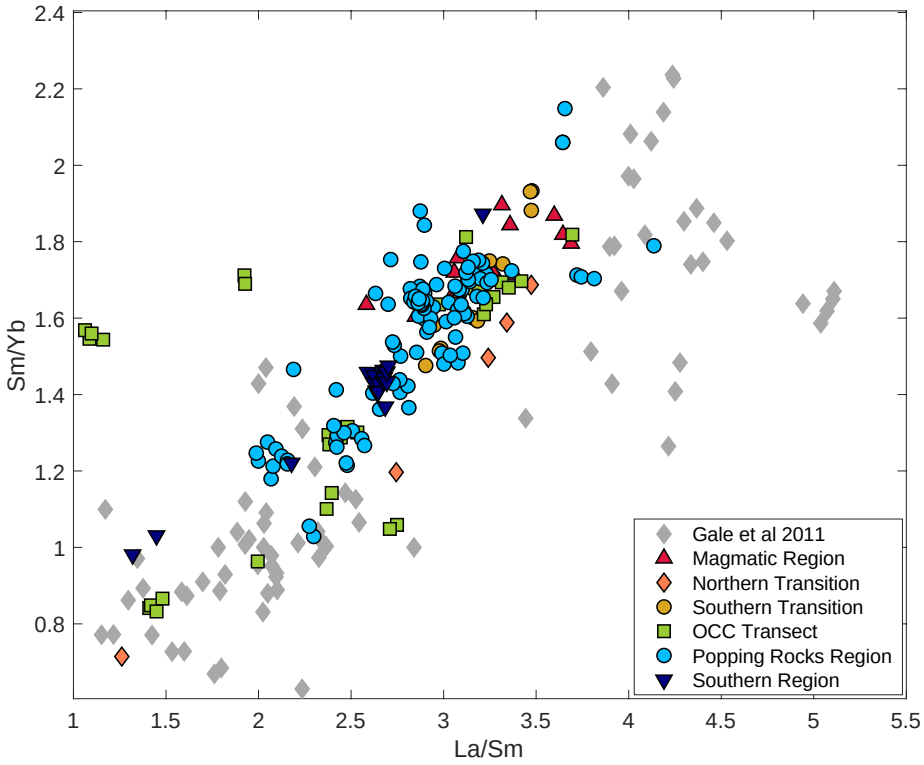

Figure 13. Sm/Yb vs La/Sm values from Gale et al (2011) combined with our regional data. Their extremely enriched samples are explained via low extents of melting from the Azores platform.

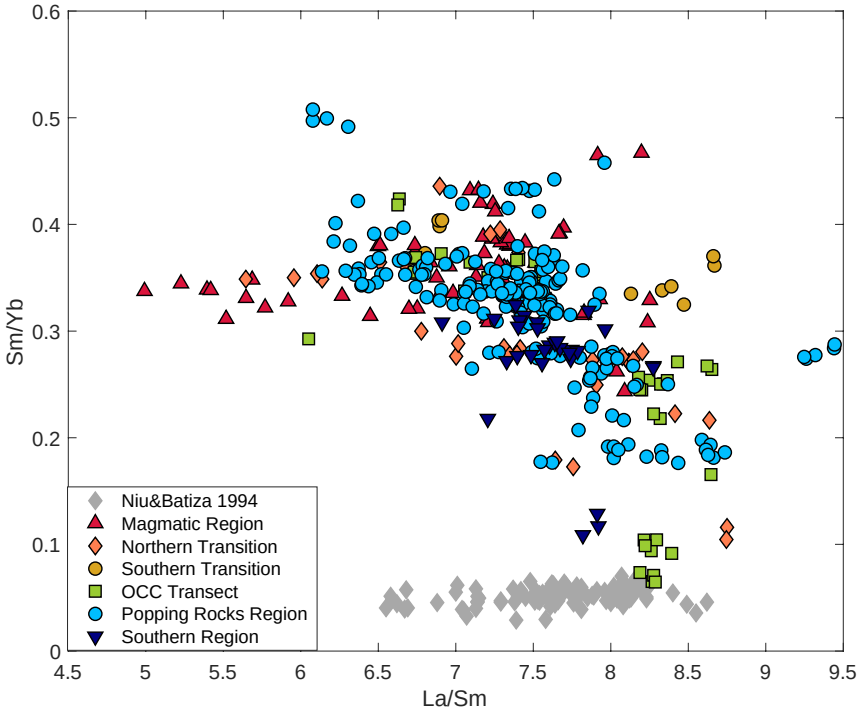

Figure 14. K/Ti and MgO data from Niu and Batiza (1994) combined with our regional data. The samples from 26°S are categorically more depleted than the NMORB samples from 14°N.

CONCLUSIONS

Systematically sampling along axis at a slow-spreading MOR has provided a unique opportunity to examine magma generation, storage, and transport along-axis. This large suite of data provides its own set of challenges and opportunities in sorting through patterns in the chemistry. In revisiting the overarching questions of this project, we can use the work presented here to address several of these outstanding questions.

There is a wide range of major and trace element contents in lavas erupted along this ridge segment; however, the variability is more complex than the simple melt transport models may imply. Major element contents vary in each region, but with a general trend of decreasing variability moving away from the magmatic center. The greatest major element variability is observed in the magmatic center, suggesting that significant fractional crystallization occurs in this region. Petrologic models indicate that crystallization is occurring between 1 and 2 kbar. Trace element ratios and patterns in lavas erupted in the magmatic center are relatively limited, suggesting melts are focused and homogenized prior to eruption. This is consistent with geophysical models for melt focusing. However, moving down axis, average major element contents become more mafic, less crystallization is required, and crystallization depths are slightly greater. This is consistent with less storage and crystallization in the shallow crust prior to eruption. Furthermore, trace element ratios become highly variable, consistent with the preservation of a wide range of melt compositions. Combined, this suggests that not all lavas erupted in these regions are being fed through the shallow magmatic plumbing

system at the segment center. Instead, melts within the transition, OCC and popping rocks regions may either ascend directly from the underlying mantle and erupt on the seafloor or they may be transported down axis via diking. This may also suggest that there is a limited distance over which melts entering the crust at the segment center can be transported down the ridge axis. Thus, a hybrid model is needed to sufficiently explain the varying chemistry, fractional crystallization depths, as well as various extents of melting observed along this segment.

Figure 12 is cartoon schematic of one possible hybrid model. The majority of magma is focused in the segment center, in agreement with the MBA low we see from the gravity surveys. Some homogenized melt may be transported laterally down axis via shallow dikes. This likely extends through the magmatic region and into the transition region and the OCC transect. However, other eruptions in the region may require vertical ascent of melts directly from the mantle to account for the variability in trace element ratios (i.e. the northern transition and sparsely magmatic regions). This hybrid model could also account for the varying depths of fractional crystallization occurring along-axis. Finally, we do not see a simple gradient in the extent of melting along axis, suggesting that melting and melt transport may be more complex at slow-spreading ridges. Future work on melting systematics and sources is required to sort out these complexities.

FUTURE WORK

Extent of Melting Along-Axis

The range of trace element ratios and patterns observed may be related to changes in mantle source or changes in the extents of melting. Future work will require new isotopic analyses and numerical modeling to constrain how these parameters vary down the ridge axis. Isotopic analyses will be used to determine the role of source variability. Trace element patterns and ratios can be used to evaluate melting systematics once the source is constrained. Despite the absence of isotopes, I have begun to evaluate melting systematics using trace element patterns. For example, assuming a similar source, the trace element patterns from individual regions suggest variable extents of melting (northern transition region, the sparsely magmatic region, and the popping rocks region). These three regions are also the most chemically variable with respect to all trace element ratios and K/Ti values (Figure 6). To quantify this variability and to determine the extents of melting, I will first determine the range of mantle sources by measuring radiogenic isotopes and then model mantle melting using numerical equations. Below, I outline a few preliminary cases for variability in melting based on trace element ratios.

One case study of differing extents of melting is the OCC transect. When distinct chemical groups are averaged in REE space, we see a trend across-axis (Figure 15). The average compositions of the western axial valley are the most enriched, suggesting lower extents of melting while the Eastern Axial valley is less enriched. These two regions have similar HREE (Yb and Lu), but variable LREE and MREE (La, Ce, and Sm), perhaps

suggesting that they were formed by variable extents of melting of the same mantle source. Lavas collected from the western base of the OCC (labeled OCC Slope in Figure 15) have nearly parallel patterns to the Eastern Axial Valley, which may suggest similar extents of melting from a similar mantle source, but lower extents of fractional crystallization. The four basalts collected from the top of the OCC have distinctly depleted LREE, suggesting either a different source or higher extents of melting. The complexity in magmatic processes of a single across-axis transect exemplifies how challenging it is to make broad generalizations about the processes occurring along-axis and demonstrate the need for further analyses and petrologic modeling. In this case study, the presence of the extinct OCC clearly plays an important role in the magmatic upwelling and very well may be an important control on the chemistry.

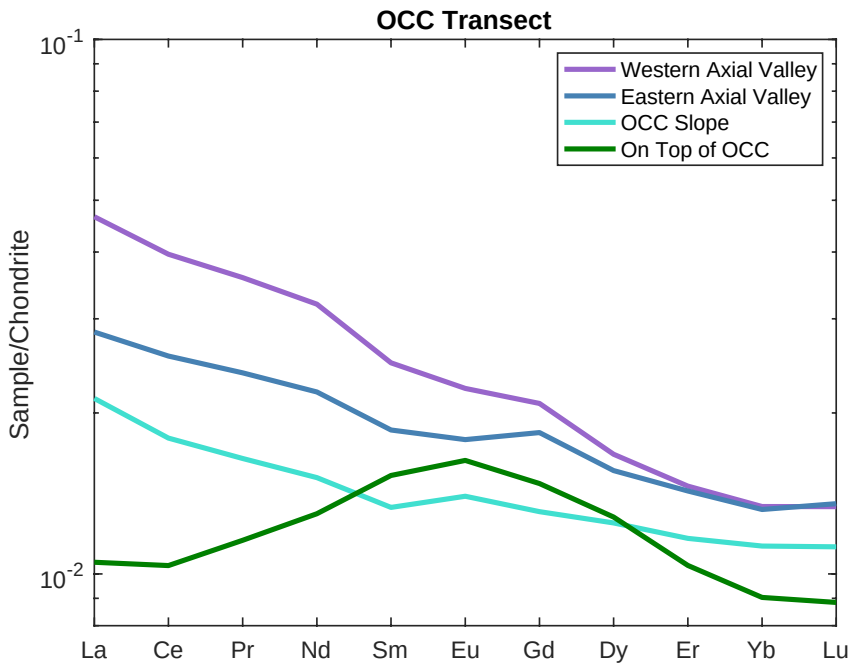

Figure 15. REE plot of average compositions of chemically distinct groups within the sparsely magmatic transect.

Another example of variable extents of melting within a single region is in the Popping Rocks Region. Figure 16 shows the average trace element pattern of the popping rocks and a subset of lavas from the region which have similar REE pattern but did not pop upon recovery. These two patterns suggest that the more enriched popping rock composition may have undergone a greater extent of melting of a similar source compared to other lavas in the region; however, the mantle source and extent of melting has not yet been constrained. Further, the average composition of the Southern Region falls between the two averaged subsets of lavas from the Popping Rocks Region (Figure 16b). This suggests that the lavas erupted in the Southern Region could have undergone a greater extent of melting of a similar source to the popping rocks composition, but perhaps a lower extent of melting than the non-popping subset.

These examples suggest that there is significant variability in the extent of melting along this segment of the MAR. However, more analyses and petrologic modeling is necessary to investigate the role of source variations and extents of melting. An outstanding piece of this work that must be continued is differentiating between differing extents of melting and different source. Future work would involve systematically analyzing radiogenic isotope values along axis to determine if the extensive variability we see in the transition and sparsely magmatic regions are due to differing extents of melting or source. I will then use melting equations to model the extents of melting in different subpopulations of lavas erupted along the 14°N segment.

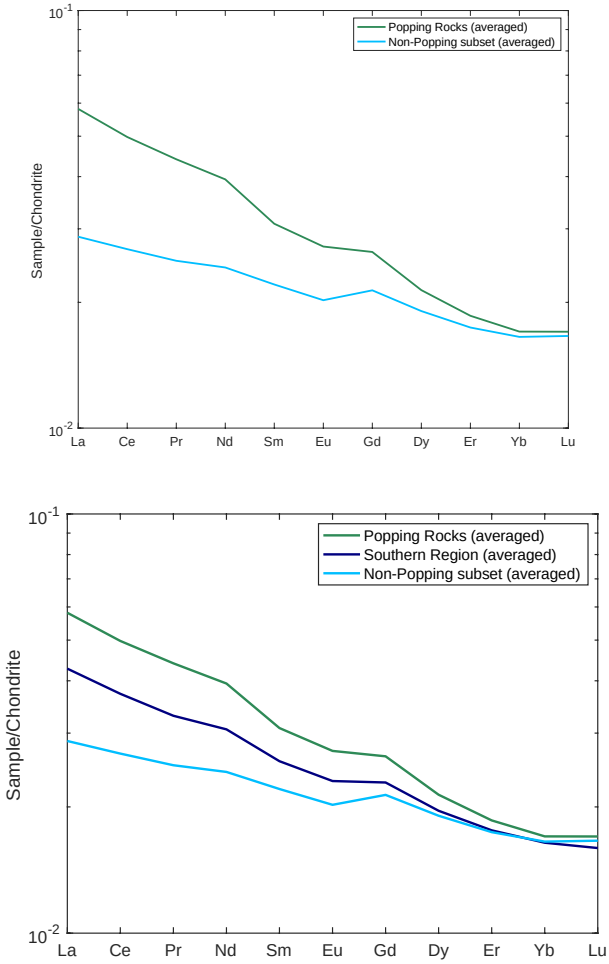

Figure 16. (A) REE plot of average composition of the popping rocks and chemically homogenous lavas (green line) and the average composition of a subset of non-popping rocks that are chemically homogenous. These two subsets of data were both collected in the Popping Rocks Region. (B) Average composition of the southern region sits between two averaged subsets of data from the popping rocks region (same two groups as figure 16a).

Because of the enormity of this region's data set, these case studies barely scratch the surface of what we can learn looking at different mantle melting in this region. There is an obvious need to explore in greater detail how extent of mantle melting varies along-axis, and to quantify that variability. Further, without radiogenic isotopes, we will have trouble distinguishing whether differencing extents of melt or different sources create some of the chemical variability along axis. In the future, it is our hope to incorporate

radiogenic isotope analysis to further our understanding of this region's magma generation, storage, and transport and to refine our proposed hybrid model of melt distribution along slow-spreading MORs.

REFERENCES

Bender, J. F., Langmuir, C. H., & Hanson, G. N. (1984). Petrogenesis of Basalt Glasses from the Tamayo Region, East Pacific Rise. *Journal of Petrology*, *25*(1), 213–254. https://doi.org/10.1093/petrology/25.1.213

Blackman, D. K., & Forsyth, D. W. (1991). Isostatic compensation of tectonic features of the Mid-Atlantic Ridge: 25–27°30′S. *Journal of Geophysical Research*, *96*(B7), 11741. https://doi.org/10.1029/91jb00602

Blackman, D. K., Cann, J. R., Janssen, B., & Smith, D. K. (1998). Origin of extensional core complexes: Evidence from the Mid-Atlantic Ridge at Atlantis Fracture Zone. *Journal of Geophysical Research: Solid Earth*, *103*(B9), 21315–21333. https://doi.org/10.1029/98jb01756

Cannat, M. (1996). How thick is the magmatic crust at slow spreading oceanic ridges? Melt migration in the axial lithosphere of slow spreading ridges: Constraints from ultramafic and gabbroic samples. *Journal of Geophysical Research*, *101*, 2847–2857. https://doi.org/10.1029/95JB03116

Danyushevsky, L. V., & Plechov, P. (2011). Petrolog3: Integrated software for modeling crystallization processes. *Geochemistry, Geophysics, Geosystems*, *12*(7). https://doi.org/10.1029/2011GC003516

Detrick, R. S., Needham, H. D., & Renard, V. (1995). Gravity anomalies and crustal thickness variations along the Mid- Atlantic Ridge between 33°N and 40°N. *Journal of Geophysical Research*, *100*(B3), 3767–3787. https://doi.org/10.1029/94JB02649

Detrick, Robert S, Needham, H. D., & Renard, V. (1995). Gravity anomalies and crustal thickness variations along the Mid-Atlantic Ridge between 33øN and 40øN. *Journal of Geophysical Research*, *100*, 3767–3787.

Dusunur, D., Escartín, J., Combier, V., Seher, T., Crawford, W., Cannat, M., et al.

(2009). Seismological constraints on the thermal structure along the Lucky Strike segment (Mid-Atlantic Ridge) and interaction of tectonic and magmatic processes around the magma chamber. *Marine Geophysical Research*, *30*(2), 105–120. https://doi.org/10.1007/s11001-009-9071-3

Fialko, Y. A., & Rubin, A. M. (1998). Thermodynamics of lateral dike propagation: Implications for crustal accretion at slow spreading mid-ocean ridges. *Journal of Geophysical Research: Solid Earth*, *103*(B2), 2501–2514. https://doi.org/10.1029/97jb03105

Gale, A., Escrig, S., Gier, E. J., & Goldstein, S. L. (2011). Enriched basalts at segment centers: The Lucky Strike (37°17 ′ N) and Menez Gwen (37°50 ′ N) segments of the Mid - Atlantic Ridge, *12*(6), 1–26. https://doi.org/10.1029/2010GC003446

Goss, A. R., Perfit, M. R., Ridley, W. I., Rubin, K. H., Kamenov, G. D., Soule, S. A., et al. (2010). Geochemistry of lavas from the 2005-2006 eruption at the East Pacific Rise, 9°46'N-9°56N: Implications for ridge crest plumbing and decadal changes in magma chamber compositions. *Geochemistry, Geophysics, Geosystems*, *11*(5), 1–35. https://doi.org/10.1029/2009GC002977

Grindlay, N. R., Madsen, J. A., Rommevaux-Jestin, C., & Sclater, J. (1998). A different pattern of ridge segmentation and mantle Bouguer gravity anomalies along the ultra-slow spreading Southwest Indian Ridge (15°30′E to 25°E). *Earth and Planetary Science Letters*, *161*(1–4), 243–253. https://doi.org/10.1016/s0012-821x(98)00154-x

Grove, T. L., Kinzler, R. J., & Bryan, W. B. (1992, January 1). Fractionation of Mid-Ocean Ridge Basalt (MORB). *Mantle Flow and Melt Generation at Mid - Ocean Ridges*. https://doi.org/doi:10.1029/GM071p0281

Hooft, E. E. E., Detrick, R. S., Toomey, D. R., Collins, J. A., & Lin, J. (2000). Crustal thickness and structure along three contrasting spreading segments of the Mid-Atlantic Ridge, 33.5°-35°N. *Journal of Geophysical Research: Solid Earth*, *105*(B4), 8205–8226. https://doi.org/10.1029/1999jb900442

John, B. E., & Cheadle, M. J. (2010). Deformation and Alteration Associated With Oceanic and Continental.pdf. *University of Wyoming*, 175–205.

Jones, M. R., Schwartz, D. M., Brodsky, H., Wanless, V. D., Soule, S. A., Curtice, J., et al. (2019). New constraints on mantle carbon from Mid-Atlantic Ridge popping rocks. *Earth and Planetary Science Letters*, *511*(April), 67–75. https://doi.org/10.1016/j.epsl.2019.01.019

Kuo, B. Y., & Forsyth, D. W. (1988). Gravity anomalies of the ridge-transform system in the South Atlantic between 31 and 34.5° S: Upwelling centers and variations in crustal thickness. *Marine Geophysical Researches*, *10*(3–4), 205–232. https://doi.org/10.1007/BF00310065

Langmuir, C. H., Bender, J. F., Bence, A. E., Hanson, G. N., & Taylor, S. R. (1977). Petrogenesis of basalts from the FAMOUS area: Mid-Atlantic Ridge. *Earth and Planetary Science Letters*, *36*(1), 133–156. https://doi.org/10.1016/0012-821X(77)90194-7

Langmuir, Charles H., Klein, E. M., & Plank, T. (1992). Petrological Systematics of Mid-Ocean Ridge Basalts: Constraints on Melt Generation Beneath Ocean Ridges (pp. 183–280). https://doi.org/10.1029/gm071p0183

Lin, J, Purdy, G. M., Schouten, H., Sempere, J. C., & Zervas, C. (1990). Evidence from gravity data for focused magmatic accretion along the Mid-Atlantic Ridge. *Nature*, *344*(6267).

Lin, Jiarl, & Phipps Morgan, J. (1992). *TI-IE SPREADING RATE DEPENDENCE OF THREE-DIMENSIONAL MID-OCEAN RIDGE GRAVITY STRUCTURE* (Vol. 19).

Macdonald, K. C. (1982). MID-OCEAN RIDGES : Fine Scale Tectonic , Volcanic and Plate Boundary Zone. *Annual Review of Earth and Planetary Sciences*.

Niu, Y., & Batiza, R. (1994a). Magmatic processes at a slow spreading ridge segment: 26°S Mid- Atlantic Ridge. *Journal of Geophysical Research*, *99*(B10). https://doi.org/10.1029/94jb01663

Niu, Y., & Batiza, R. (1994b). Magmatic processes at a slow spreading ridge segment: 26S Mid-Atlantic Ridge. *Journal of Geophysical Research*, *99*(94).

Olive, J. A., Behn, M. D., & Tucholke, B. E. (2010). The structure of oceanic core complexes controlled by the depth distribution of magmaemplacement. *Nature*

Geoscience, *3*(7), 491–495. https://doi.org/10.1038/ngeo888

Parmentier, E. M., & Forsyth, D. W. (1985). Three dimensional flow beneath a slow spreading ridge axis: A dynamic origin of the deepening of the median valley toward fracture zones, J. Geophys. Res., 90, 678-684, *90*, 678–684.

Perfit, M.R. (2001). Mid-ocean Ridge Geochemistry And Petrology. In *Encyclopedia of Ocean Sciences* (pp. 1778–1788). Elsevier. https://doi.org/10.1006/rwos.2001.0096

Perfit, Michael R., & Chadwick, W. W. (1998). Magmatism at mid-ocean ridges: Constraints from volcanological and geochemical investigations. In *Geophysical Monograph Series* (Vol. 106, pp. 59–115). Blackwell Publishing Ltd. https://doi.org/10.1029/GM106p0059

Plank, T., & Langmuir, H. (1992). Effects of the Melting Regime on the Composition of the Oceanic Crust, *97*.

Reynolds, J. R., & Langmuir, C. H. (1997). Petrological systematics of the Mid-Atlantic Ridge south of Kane: Implications for ocean crust formation. *Journal of Geophysical Research: Solid Earth*, *102*(B7), 14915–14946. https://doi.org/10.1029/97jb00391

Rubin, K. H., & Sinton, J. M. (2007). Inferences on mid-ocean ridge thermal and magmatic structure from MORB compositions. *Earth and Planetary Science Letters*, *260*(1–2), 257–276. https://doi.org/10.1016/j.epsl.2007.05.035

Rubin, K. H., Smith, M. C., Bergmanis, E. C., Perfit, M. R., Sinton, J., & Batiza, R. (2011). *Geochemical heterogeneity within mid-ocean ridge lava flows: insights into eruption, emplacement and global variations in magma generation*. Retrieved from www.elsevier.com/locate/epsl

Sarda, P., & Graham, D. W. (1989). Mid-Ocean ridge popping rocks: implications for degassing at ridge crests. *Earth and Planetary Science Letters*, 268–289.

Schouten, H., Klitgord, K. D., & Whitehead, J. A. (1985). Segmentation of mid-ocean ridges. *Nature*, *317*(6034), 225–229. https://doi.org/10.1038/317225a0

Schwartz, D. M., Soule, S. A., Wanless, V. D., & Jones, M. R. (2018). Identification of

erosional terraces on seamounts: Implications for interisland connectivity and subsidence in the galápagos archipelago. *Frontiers in Earth Science*, *6*. https://doi.org/10.3389/feart.2018.00088

Singh, S. C., Crawford, W. C., Carton, H., Seher, T., Combier, V., Cannat, M., et al. (2006). Discovery of a magma chamber and faults beneath a Mid-Atlantic Ridge hydrothermal field. *Nature*, *442*(7106), 1029–1032. https://doi.org/10.1038/nature05105

Sinton, J. M., Smaglik, S. M., Mahoney, J. J., & Macdonald, K. C. (1991). Magmatic processes at superfast spreading mid-ocean ridges: glass compositional variations along the East Pacific Rise 13°-23°S. *Journal of Geophysical Research*, *96*(B4), 6133–6155. https://doi.org/10.1029/90JB02454

Sinton, John M., & Detrick, R. S. (1992). Mid-ocean ridge magma chambers. *Journal of Geophysical Research*, *97*(B1), 197. https://doi.org/10.1029/91JB02508

Sleep, N. H., & Biehler, S. (1970). Topography and tectonics at the intersections of fracture zones with central rifts. *Journal of Geophysical Research*, *75*(14), 2748–2752. https://doi.org/10.1029/jb075i014p02748

Smith, D. K., Cann, J. R., & Escartín, J. (2006). Widespread active detachment faulting and core complex formation near 13°N on the Mid-Atlantic Ridge. *Nature*, *442*(7101), 440–443. https://doi.org/10.1038/nature04950

Smith, D. K., Escartı, J., Schouten, H., & Cann, J. R. (2008). Fault rotation and core complex formation: Significant processes in seafloor formation at slow-spreading mid-ocean ridges (Mid-Atlantic Ridge, 13 ° –15 ° N). *Geochemistry, Geophysics, Geosystems*, (November 2007). https://doi.org/10.1029/2007GC001699

Tolstoy, M., Harding, A. J., & Orcutt, J. A. (1993). *Crustal Thickness on the Mid-Atlantic Ridge: Bull's Eye Gravity Anomalies and Focused Accretion*. *Reprint Series* (Vol. 262).

Wanless, V. D., & Behn, M. D. (2017). Spreading rate-dependent variations in crystallization along the global mid-ocean ridge system. *Geochemistry, Geophysics, Geosystems*, *18*(8), 3016–3033. https://doi.org/10.1002/2017GC006924

White, R., Detrick, R., Sinha, M., & Cormier, M. H. (1984). Anomalous seismic crustal structure of oceanic. *Geophys. J. R. Astr. Soc.*, *79*, 779–798.

Whitehead, J. A., Dick, H. J. B., & Schouten, H. (1984). A Mechanism for magmatic accretion under spreading centres. *Nature Publishing Group*, *312*(5991), 237–242. https://doi.org/10.1038/309126a0

APPENDIX A

Geochemical Data

Table A.1. Major Element Contents of the 14°N Segment. Collected on a Cameca SX Five Electron Microprobe at Boise State University.

Sample	Lon	Lat	SiO2	TiO2	Al2O3	FeO	MnO	MgO	CaO	Na2O	K2O	P2O5	TOTAL	K/Ti
4823-070	-45.0441475	14.0180948	51.21	1.55	15.37	9.05	0.17	7.09	11.48	2.70	0.67	0.24	99.54	0.43
4823-071	-45.043227	14.0181111	51.08	1.54	15.44	8.96	0.16	7.15	11.49	2.72	0.66	0.25	99.45	0.43
4823-072	-45.0412921	14.0177106	51.38	1.83	14.77	10.43	0.20	6.45	10.63	2.83	0.57	0.23	99.32	0.31
4823-073	-45.0406658	14.0177931	50.74	2.10	14.37	11.08	0.20	5.77	9.91	2.98	0.68	0.28	98.11	0.32
4823-074	-45.0390572	14.0175075	50.98	2.19	14.30	11.39	0.21	5.52	9.68	3.04	0.68	0.29	98.28	0.31
4823-075	-45.0383107	14.0172466	51.05	1.32	15.22	9.03	0.14	8.09	12.29	2.31	0.32	0.14	99.92	0.24
4823-076	-45.0373563	14.0172042	50.83	1.52	15.16	9.48	0.18	7.29	11.35	2.58	0.58	0.20	99.17	0.38
4823-077	-45.0362261	14.0171736	50.94	1.49	15.20	9.39	0.17	7.35	11.43	2.56	0.56	0.22	99.31	0.38
4823-078	-45.0355814	14.0206943	50.93	1.50	15.06	9.51	0.18	7.23	11.31	2.58	0.58	0.21	99.09	0.39
4823-079	-45.0355703	14.0207372	51.13	1.53	15.10	9.57	0.19	7.18	11.26	2.60	0.59	0.22	99.37	0.39
4823-080	-45.0352308	14.0213609	51.29	1.49	15.29	9.46	0.17	7.35	11.42	2.55	0.57	0.20	99.80	0.38
4823-081	-45.0357384	14.0246017	51.33	1.59	15.25	9.50	0.18	7.14	10.94	2.69	0.57	0.23	99.40	0.36
4823-083	-45.0372182	14.0276886	50.85	1.53	15.33	9.45	0.18	7.28	11.19	2.66	0.56	0.22	99.25	0.36
4823-084	-45.0375698	14.0284158	50.71	1.25	15.35	8.67	0.16	8.24	12.52	2.24	0.39	0.16	99.68	0.31
4823-085	-45.0362143	14.0293736	51.52	1.56	15.42	9.22	0.18	7.33	10.77	2.66	0.59	0.22	99.46	0.38
4823-086	-45.0346051	14.0303634	51.28	1.56	15.38	9.14	0.17	7.34	10.74	2.67	0.60	0.23	99.11	0.39
4823-087	-45.0345963	14.0303808	50.70	1.54	15.29	9.19	0.17	7.45	10.90	2.67	0.59	0.23	98.72	0.38
4823-088	-45.0331748	14.0313849	50.87	1.57	15.30	9.19	0.17	7.18	11.00	2.65	0.59	0.23	98.75	0.37
4824-089	-45.0364059	14.0781693	50.76	1.50	15.03	9.44	0.18	7.31	11.57	2.57	0.52	0.19	99.08	0.35
4824-090	-45.0357191	14.0784171	50.98	1.72	14.98	9.83	0.19	6.88	10.96	2.71	0.57	0.23	99.06	0.33
4824-091	-45.0349653	14.0786805	50.79	1.82	14.95	10.04	0.18	6.75	10.67	2.77	0.59	0.24	98.79	0.32
4824-092	-45.0345113	14.0786288	50.82	1.83	14.92	10.05	0.20	6.70	10.66	2.77	0.59	0.25	98.78	0.32
4824-093	-45.0331544	14.0787824	51.30	2.12	14.60	10.86	0.20	5.92	10.03	2.93	0.69	0.29	98.92	0.33
4824-094	-45.0301128	14.0788506	51.20	1.67	15.04	9.85	0.18	6.75	10.66	2.72	0.63	0.24	98.94	0.38
4824-095	-45.0286128	14.0789531	51.19	1.68	14.99	9.93	0.18	6.74	10.62	2.75	0.64	0.24	98.96	0.38
4824-096	-45.0244295	14.0783723	51.09	1.48	15.24	9.22	0.16	7.50	11.48	2.50	0.49	0.19	99.35	0.33
4824-097	-45.0232306	14.0783529	51.04	1.38	15.45	8.88	0.16	7.82	11.89	2.41	0.43	0.18	99.64	0.31
4824-098	-45.0232032	14.0783659	50.76	1.37	15.47	8.87	0.16	7.83	11.88	2.40	0.44	0.17	99.36	0.32
4824-099	-45.0218158	14.0798646	51.11	1.44	15.52	9.06	0.16	7.61	11.64	2.48	0.47	0.19	99.68	0.33
4824-100	-45.020438	14.0818821	52.23	1.95	14.47	11.06	0.21	5.65	9.89	3.03	0.64	0.25	99.36	0.33
4824-101	-45.019979	14.0864596	51.68	1.61	15.14	9.75	0.19	6.98	10.90	2.64	0.54	0.22	99.65	0.34
4824-102	-45.0199905	14.086554	51.43	1.59	15.19	9.70	0.18	6.88	10.77	2.73	0.56	0.21	99.23	0.35
4824-103	-45.0200595	14.0888079	51.62	1.73	15.03	9.87	0.18	6.50	10.26	2.84	0.66	0.25	98.93	0.38
4824-104	-45.0200595	14.0888079	51.54	1.72	15.10	9.82	0.18	6.51	10.33	2.82	0.65	0.25	98.92	0.38
4824-105	-45.0195163	14.0915476	51.64	1.49	15.18	9.69	0.17	7.20	11.25	2.60	0.46	0.17	99.85	0.31
4824-106	-45.0193537	14.0917082	51.12	1.49	15.20	9.62	0.17	7.21	11.25	2.61	0.46	0.18	99.31	0.31
4825-107	-45.0327441	14.0312128	51.50	1.39	15.51	8.93	0.17	7.93	11.63	2.46	0.46	0.17	100.16	0.33
4825-109	-45.0072074	14.0765052	51.09	1.75	14.54	10.73	0.19	6.27	10.41	2.84	0.58	0.21	98.62	0.33
4825-110	-45.0091839	14.0755764	50.92	1.55	15.29	9.27	0.18	7.33	11.36	2.61	0.56	0.22	99.29	0.36
4825-111	-45.0101069	14.0752435	51.16	1.57	15.40	9.32	0.17	7.31	11.30	2.61	0.56	0.22	99.63	0.36
4825-112	-45.010014	14.0752466	50.97	1.57	15.35	9.33	0.18	7.36	11.37	2.63	0.56	0.22	99.54	0.36
4825-113	-45.0112572	14.0767682	50.71	1.64	15.10	9.65	0.17	6.96	11.23	2.66	0.59	0.24	98.95	0.36
4825-114	-45.0112509	14.0768453	50.49	1.65	15.06	9.69	0.18	6.84	11.21	2.60	0.60	0.23	98.56	0.36
4825-115	-45.0104559	14.0780876	50.62	1.88	14.25	12.18	0.22	5.69	10.09	3.05	0.65	0.25	98.87	0.35
4825-116	-45.0132012	14.0778368	50.16	1.52	15.36	9.24	0.16	7.51	11.37	2.58	0.55	0.22	98.67	0.36
4825-117	-45.0141761	14.0783256	50.37	1.51	15.41	9.19	0.16	7.57	11.45	2.57	0.55	0.20	98.98	0.36
4825-118	-45.0177465	14.074167	51.41	1.36	15.54	8.73	0.16	7.70	11.80	2.53	0.54	0.20	99.98	0.40
4825-119	-45.0175551	14.074263	50.36	1.36	15.42	8.69	0.16	7.67	11.83	2.53	0.53	0.21	98.77	0.39
4825-120	-45.0175356	14.0742507	50.76	1.37	15.41	8.65	0.16	7.66	11.80	2.51	0.53	0.19	99.04	0.39
4825-121	-45.019922	14.0720849	50.43	1.16	15.53	8.33	0.16	8.25	12.49	2.31	0.38	0.15	99.18	0.33
4825-122	-45.0195836	14.0713223	51.16	1.54	15.10	9.31	0.18	7.13	11.20	2.64	0.54	0.23	99.03	0.35
4957-374	-45.016529	14.147546	49.40	1.15	16.13	7.86	0.14	8.20	13.19	2.31	0.54	0.16	99.08	0.47
4957-375	-45.014869	14.147625	49.79	1.20	16.11	8.06	0.14	7.91	13.27	2.37	0.56	0.17	99.60	0.46
4957-376	-45.011781	14.146746	52.50	2.27	14.35	11.10	0.19	4.99	9.56	3.28	0.77	0.28	99.30	0.34
4957-377	-45.008642	14.150259	52.32	2.15	14.64	10.55	0.18	5.39	9.87	3.04	0.73	0.26	99.13	0.34
4957-378	-45.008642	14.150259	52.29	2.16	14.55	10.53	0.18	5.42	9.92	3.14	0.73	0.27	99.18	0.34
4957-379	-45.003991	14.148174	52.38	2.19	14.42	10.99	0.19	5.23	9.65	3.24	0.76	0.26	99.30	0.34
4957-380	-44.998704	14.147463	50.34	1.50	15.42	8.76	0.15	7.24	11.70	2.61	0.63	0.23	98.59	0.42
4957-381	-44.9987	14.147459	50.37	1.51	15.43	8.76	0.15	7.16	11.68	2.62	0.64	0.23	98.56	0.42
4957-382	-44.997914	14.147333	50.21	1.51	15.32	8.71	0.16	7.25	11.64	2.61	0.62	0.22	98.24	0.41
4957-383	-44.992682	14.147005	50.12	1.17	15.95	9.08	0.15	8.04	11.69	2.42	0.31	0.13	99.07	0.26
4826-123	-45.0491101	13.8670581	49.93	1.72	14.76	9.85	0.18	6.77	10.96	2.56	0.63	0.25	97.61	0.36
4826-124	-45.0440479	13.8638805	50.74	1.70	15.27	9.16	0.17	6.90	10.96	2.62	0.68	0.26	98.45	0.40
4826-125	-45.0440865	13.8638789	50.13	1.70	15.28	9.12	0.17	6.89	11.02	2.69	0.69	0.25	97.93	0.40
4826-126	-45.0441444	13.8639107	50.35	1.69	15.30	9.21	0.15	6.91	11.04	2.69	0.68	0.26	98.30	0.40
4826-127	-45.0397742	13.8624852	50.29	1.56	14.83	9.80	0.19	6.80	10.96	2.71	0.58	0.22	97.94	0.37
4826-128	-45.0395255	13.8623779	50.73	1.64	14.90	9.82	0.17	6.71	10.80	2.74	0.60	0.22	98.35	0.37
4826-129	-45.0269162	13.8564324	49.01	1.12	15.51	8.50	0.16	8.67	12.96	2.14	0.41	0.16	98.64	0.36
4826-131	-45.0235104	13.8551055	48.93	1.18	15.60	8.56	0.16	8.66	12.81	2.19	0.44	0.17	98.70	0.37
4826-132	-45.0169875	13.8526266	50.06	1.35	15.29	9.17	0.18	8.33	11.25	2.44	0.46	0.19	98.72	0.34
4826-133	-45.0169802	13.8526455	50.86	1.34	15.29	9.19	0.17	8.39	11.20	2.43	0.46	0.19	99.51	0.34
4826-134	-45.0150096	13.8494942	49.60	1.28	15.45	9.03	0.17	8.47	11.36	2.37	0.42	0.18	98.34	0.32
4826-135	-45.0138797	13.8482061	49.56	1.37	15.34	9.15	0.18	8.13	11.16	2.46	0.46	0.20	98.02	0.33

Sample	Lon	Lat	SiO2	TiO2	Al2O3	FeO	MnO	MgO	CaO	Na2O	K2O	P2O5	TOTAL	K/Ti
4952-290	-45.0165853	13.9316482	50.31	0.96	15.09	9.25	0.16	8.20	13.43	2.21	0.27	0.11	100.00	0.28
4952-291	-45.0191031	13.927998	50.50	1.18	15.16	10.26	0.18	7.64	11.87	2.49	0.21	0.13	99.63	0.18
4952-292	-45.019115	13.9280684	50.38	1.17	15.20	10.24	0.17	7.76	11.81	2.49	0.20	0.12	99.54	0.17
4952-293	-45.0219054	13.9303969	49.52	0.92	16.25	9.90	0.17	8.64	12.02	2.18	0.20	0.10	99.91	0.22
4952-294	-45.0218638	13.9303831	49.86	0.93	16.31	9.98	0.18	8.41	12.25	2.26	0.21	0.09	100.48	0.22
4952-295	-45.0238798	13.9310915	51.94	1.95	14.39	10.68	0.18	5.65	10.35	3.17	0.68	0.26	99.24	0.35
4952-296	-45.025626	13.9301843	48.83	0.71	15.58	10.29	0.17	8.75	13.41	2.05	0.08	0.05	99.92	0.12
4952-297	-45.0257851	13.9300966	48.71	0.71	15.47	10.27	0.17	8.75	13.39	2.05	0.07	0.05	99.65	0.10
4952-298	-45.0317012	13.9307943	51.57	1.25	15.23	9.05	0.16	7.40	12.03	2.66	0.47	0.15	99.96	0.37
4952-299	-45.034035	13.9323748	51.24	1.39	15.23	9.23	0.17	7.28	12.42	2.58	0.55	0.19	100.28	0.39
4952-300	-45.034035	13.9323748	51.28	1.40	15.17	9.32	0.16	7.29	12.46	2.61	0.55	0.18	100.43	0.39
4952-301	-45.036972	13.9337641	50.71	1.42	15.06	9.24	0.16	7.22	12.35	2.61	0.55	0.19	99.51	0.39
4952-302	-45.0396119	13.9339067	52.06	1.31	14.96	9.64	0.17	6.90	12.01	2.83	0.57	0.18	100.63	0.44
4952-303	-45.0413066	13.9355549	51.01	1.69	14.70	10.00	0.17	6.51	11.24	2.83	0.62	0.21	98.98	0.36
4952-304	-45.0412994	13.9355749	50.97	1.64	14.79	9.75	0.17	6.67	11.35	2.80	0.60	0.21	98.96	0.36
4958-384	-45.052523	13.937784	50.76	1.10	14.49	10.28	0.18	7.35	12.71	2.44	0.31	0.12	99.75	0.28
4958-385	-45.052119	13.938057	50.83	1.22	14.59	10.76	0.18	6.78	12.28	2.62	0.36	0.14	99.77	0.30
4958-386	-45.051255	13.938542	50.59	1.19	14.43	10.53	0.18	7.02	12.35	2.51	0.34	0.13	99.27	0.29
4958-387	-45.049633	13.938914	48.60	0.97	15.98	9.36	0.15	8.12	12.99	2.28	0.26	0.11	98.83	0.27
4958-388	-45.04966	13.9389	48.44	0.96	15.97	9.30	0.15	8.12	12.92	2.27	0.26	0.11	98.49	0.27
4958-389	-45.048714	13.938858	48.25	0.98	15.54	9.31	0.15	7.97	12.89	2.30	0.27	0.11	97.77	0.27
4958-390	-45.047317	13.938577	48.22	0.96	15.62	9.28	0.16	8.15	12.87	2.24	0.26	0.11	97.85	0.27
4958-391	-45.04708	13.937461	48.19	0.96	15.54	9.33	0.16	8.07	12.89	2.27	0.26	0.11	97.79	0.28
4958-392	-45.048223	13.936816	48.52	1.02	15.28	9.55	0.16	7.88	12.99	2.30	0.28	0.12	98.10	0.27
4958-393	-45.046711	13.934119	50.34	1.26	14.74	10.27	0.18	7.00	12.13	2.49	0.35	0.14	98.90	0.28
4958-394	-45.045931	13.932405	51.38	1.67	14.68	11.11	0.20	6.14	10.92	3.03	0.58	0.22	99.94	0.35
4958-395	-45.047089	13.929882	51.21	1.72	14.36	11.19	0.19	5.96	10.78	3.02	0.60	0.22	99.26	0.35
4958-396	-45.048081	13.929032	51.15	1.67	14.49	10.92	0.19	6.10	10.86	3.00	0.59	0.21	99.20	0.35
4958-397	-45.051761	13.928293	49.47	1.02	15.24	10.13	0.18	7.91	12.66	2.35	0.25	0.12	99.32	0.25
4958-398	-45.054166	13.927263	50.09	1.26	15.05	10.36	0.19	7.39	12.33	2.53	0.35	0.15	99.70	0.28
4958-399	-45.054175	13.927254	50.23	1.26	15.01	10.44	0.18	7.41	12.30	2.56	0.36	0.15	99.89	0.28
4958-400	-45.05452	13.928107	50.85	1.20	15.26	10.50	0.19	7.52	12.36	2.49	0.33	0.15	100.85	0.28
4958-401	-45.0545	13.928731	50.27	1.30	14.95	10.43	0.18	7.31	12.17	2.58	0.37	0.16	99.73	0.28
4958-402	-45.054495	13.92877	49.82	1.19	15.16	10.36	0.19	7.49	12.38	2.44	0.33	0.15	99.49	0.28
4822-064	-44.9513625	13.8181739	53.58	1.21	15.38	9.78	0.15	8.27	9.74	2.51	0.08	0.07	100.77	0.07
4822-065	-44.9512978	13.8179426	52.98	1.21	15.34	9.74	0.16	8.28	9.71	2.51	0.09	0.07	100.08	0.07
4822-066	-44.9512975	13.8179458	52.90	1.21	15.29	9.81	0.16	8.29	9.76	2.50	0.08	0.08	100.07	0.06
4822-067	-44.949595	13.8163592	53.05	1.22	15.39	9.73	0.15	8.19	9.78	2.51	0.09	0.08	100.18	0.07
4948-222	-44.971954	13.809991	48.39	0.94	15.81	9.34	0.16	8.43	12.38	2.36	0.25	0.12	98.19	0.27
4948-223A	-44.970112	13.809991	49.11	0.95	16.35	9.69	0.16	8.65	12.51	2.20	0.25	0.11	99.98	0.26
4948-223B	-44.970112	13.809991	48.95	0.94	16.25	9.68	0.16	8.62	12.48	2.19	0.25	0.12	99.65	0.27
4948-234	-44.96672	13.809215	49.62	0.96	15.76	9.71	0.16	8.32	12.55	2.25	0.21	0.10	99.62	0.22
4948-235	-44.960626	13.814077	49.64	0.94	15.88	9.62	0.16	8.28	12.83	2.13	0.21	0.10	99.78	0.22
4950-255	-44.983375	13.810133	50.04	1.21	15.80	9.58	0.17	8.34	11.55	2.42	0.30	0.15	99.55	0.25
4950-256	-44.984606	13.809025	50.15	1.22	15.89	9.51	0.16	8.25	11.57	2.43	0.31	0.15	99.63	0.25
4950-257	-44.985651	13.807897	49.78	1.18	15.82	9.42	0.15	8.32	11.74	2.38	0.29	0.14	99.23	0.25
4950-258	-44.986052	13.808063	50.09	1.17	15.87	9.46	0.16	8.36	11.74	2.40	0.30	0.15	99.70	0.25
4950-259	-44.98938	13.808107	50.21	1.20	15.81	9.55	0.16	8.20	11.75	2.45	0.29	0.15	99.78	0.24
4950-260	-44.989362	13.808091	49.96	1.19	15.52	9.55	0.16	8.19	11.78	2.43	0.29	0.14	99.22	0.25
4950-261	-44.989367	13.808075	49.78	1.20	15.60	9.47	0.16	8.18	11.77	2.45	0.31	0.16	99.07	0.26
4950-262	-44.990838	13.809363	51.07	1.62	15.18	9.36	0.16	7.52	11.13	2.74	0.60	0.24	99.62	0.37
4950-263	-44.991073	13.810114	51.20	1.63	15.36	9.43	0.17	7.41	11.16	2.81	0.60	0.23	100.00	0.37
4950-264	-44.993713	13.812157	51.00	1.63	15.31	9.39	0.16	7.39	11.13	2.80	0.60	0.23	99.64	0.37
4950-265	-44.997569	13.815298	48.02	0.69	16.10	11.22	0.19	8.65	12.91	2.00	0.11	0.08	99.97	0.17
4950-268	-45.001298	13.817522	51.44	1.31	14.72	9.82	0.18	7.06	12.06	2.05	0.44	0.17	99.25	0.34
4950-269	-45.002753	13.818472	51.88	1.81	14.68	11.00	0.18	6.05	11.13	2.24	0.53	0.23	99.73	0.29
4959-403	-45.013709	13.81078	48.72	0.78	16.28	10.30	0.17	8.39	11.48	2.29	0.07	0.08	98.57	0.09
4959-404	-45.01372	13.810791	48.85	0.79	16.19	10.36	0.17	8.26	11.50	2.27	0.07	0.07	98.54	0.09
4959-405	-45.014577	13.811586	48.79	0.81	16.06	10.37	0.16	8.30	11.44	2.21	0.08	0.07	98.30	0.10
4959-406	-45.014563	13.811582	48.77	0.81	16.12	10.28	0.16	8.21	11.43	2.21	0.08	0.07	98.14	0.10
4959-407	-45.015937	13.812736	48.68	0.82	15.76	10.61	0.16	8.22	11.38	2.25	0.08	0.06	98.03	0.10
4959-410	-45.01962	13.812974	50.35	1.44	14.84	9.16	0.16	6.73	11.54	2.55	0.51	0.20	97.49	0.35
4959-411	-45.019697	13.812587	50.17	1.44	14.77	9.06	0.16	6.73	11.56	2.62	0.51	0.20	97.21	0.36
4959-412	-45.022588	13.814144	50.06	1.34	14.84	8.79	0.16	7.09	11.97	2.36	0.49	0.18	97.26	0.36
4959-413	-45.023281	13.814255	49.99	1.40	14.75	9.02	0.15	6.91	11.77	2.61	0.52	0.20	97.31	0.37
4959-414	-45.025599	13.814518	49.97	1.43	14.75	9.05	0.16	6.74	11.66	2.64	0.53	0.18	97.10	0.37
4959-415	-45.02832	13.810394	49.95	1.47	15.01	8.84	0.16	7.21	11.18	2.54	0.52	0.21	97.07	0.35
4959-416	-45.032045	13.809673	50.76	1.50	15.49	9.25	0.15	7.51	11.47	2.76	0.55	0.19	99.63	0.37
4959-417	-45.032141	13.809667	50.81	1.51	15.47	9.25	0.16	7.51	11.49	2.73	0.53	0.20	99.66	0.35
4959-418	-45.034782	13.809477	50.81	1.51	15.46	9.23	0.16	7.55	11.49	2.73	0.53	0.20	99.65	0.35
4959-419	-45.034776	13.80942	50.70	1.51	15.51	9.24	0.16	7.55	11.56	2.71	0.54	0.21	99.68	0.36
4959-420	-45.03861	13.810727	50.72	1.63	15.00	9.73	0.18	6.64	11.66	2.85	0.69	0.23	99.34	0.42
4959-421	-45.038732	13.811242	50.80	1.64	15.14	9.83	0.18	6.63	11.60	2.85	0.68	0.23	99.56	0.42
4818-001	-45.0066863	13.7741412	49.78	1.87	14.84	9.94	0.15	7.65	10.84	2.85	0.60	0.32	98.84	0.32
4818-002	-45.0074418	13.7742504	49.93	1.84	14.89	9.99	0.17	7.61	10.71	2.70	0.60	0.35	98.79	0.33
4818-003	-45.0107651	13.773684	50.52	1.83	14.95	10.01	0.19	7.30	10.78	2.73	0.61	0.34	99.26	0.33
4818-004	-45.012758	13.7748075	49.93	1.21	15.64	9.72	0.19	7.77	11.79	2.32	0.30	0.19	99.05	0.25
4818-005	-45.0132328	13.7749409	49.59	1.13	15.81	9.70	0.19	7.95	12.25	2.32	0.30	0.15	99.39	0.26
4818-006	-45.0131983	13.7748883	49.40	1.12	15.82	9.61	0.18	7.94	11.99	2.28	0.29	0.18	98.82	0.26
4818-007	-45.0141886	13.7751082	50.05	1.22	15.69	9.61	0.16	7.89	11.99	2.36	0.29	0.15	99.40	0.24
4818-008	-45.0170691	13.7751509	49.82	1.12	15.38	10.18	0.17	7.86	12.41	2.27	0.28	0.12	99.60	0.25
4818-009	-45.0178208	13.7756906	50.02	1.13	15.46	10.18	0.18	7.87	12.42	2.18	0.29	0.16	99.88	0.26
4818-010	-45.0168531	13.7761621	49.20	1.13	15.72	9.65	0.17	7.88	12.09	2.27	0.30	0.17	98.58	0.27
4818-011	-45.0254281	13.773806	50.33	1.56	14.89	10.44	0.19	6.52	11.30	2.70	0.55	0.25	98.74	0.35
4818-012	-45.0255495	13.7738979	50.85	1.58	14.79	10.47	0.17	6.49	11.42	2.67	0.55	0.21	99.20	0.35

Sample	Lon	Lat	SiO2	TiO2	Al2O3	FeO	MnO	MgO	CaO	Na2O	K2O	P2O5	TOTAL	K/Ti
4819-014	-45.0310803	13.7816705	50.80	1.56	14.96	10.29	0.19	6.55	11.45	2.68	0.55	0.27	99.29	0.35
4819-015	-45.0314511	13.7809299	50.91	1.61	14.85	10.43	0.20	6.37	11.24	2.69	0.58	0.30	99.18	0.36
4819-016	-45.0321314	13.7792199	49.64	1.47	14.93	10.28	0.19	6.67	11.44	2.58	0.52	0.23	97.96	0.35
4819-017	-45.0334829	13.77841	49.72	1.47	14.86	10.25	0.19	7.05	11.27	2.57	0.49	0.19	98.07	0.34
4819-018	-45.0346253	13.7780994	50.71	1.55	14.99	10.06	0.16	6.31	11.34	2.77	0.76	0.27	98.92	0.49
4819-019	-45.0347842	13.7778057	50.10	1.59	15.05	10.28	0.19	6.17	11.03	2.76	0.79	0.33	98.29	0.50
4819-020	-45.0357114	13.7774433	50.49	1.62	14.92	10.29	0.17	6.08	11.19	2.85	0.81	0.27	98.69	0.50
4819-021	-45.0359546	13.7771843	50.71	1.61	15.05	10.37	0.19	6.08	11.05	2.80	0.82	0.33	99.01	0.51
4819-022	-45.0384956	13.7781168	50.50	1.66	14.79	10.21	0.16	6.44	11.29	2.71	0.57	0.22	98.55	0.34
4819-023	-45.0385391	13.7781154	51.04	1.65	14.83	10.24	0.19	6.38	11.11	2.69	0.58	0.28	98.98	0.35
4819-024	-45.0404875	13.7788998	51.28	1.67	14.79	10.20	0.16	6.39	11.21	2.74	0.57	0.23	99.25	0.34
4819-025	-45.0437591	13.7792156	50.61	1.52	15.03	9.97	0.17	6.76	11.63	2.59	0.54	0.27	99.10	0.36
4819-026	-45.0468945	13.7773239	50.60	1.66	14.82	10.26	0.18	6.35	11.04	2.73	0.59	0.27	98.49	0.35
4819-027	-45.0490039	13.7762802	50.66	1.67	14.76	10.37	0.19	6.29	10.93	2.77	0.59	0.30	98.52	0.36
4819-028	-45.0489995	13.7761877	50.33	1.67	14.88	10.47	0.19	6.14	10.81	2.77	0.60	0.28	98.14	0.36
4819-029	-45.0498792	13.7755171	50.37	1.32	15.71	8.77	0.16	7.82	11.93	2.28	0.47	0.23	99.06	0.36
4819-030	-45.0525128	13.7739715	50.83	1.14	15.46	9.38	0.16	8.17	11.95	2.29	0.28	0.13	99.78	0.25
4819-031	-45.0534672	13.7739314	50.25	1.30	15.22	9.49	0.15	7.49	12.16	2.43	0.36	0.16	99.01	0.28
4820-032	-45.0134709	13.7670408	50.29	1.01	15.37	10.18	0.16	8.01	12.54	2.24	0.22	0.10	100.12	0.22
4820-033	-45.0134712	13.7670515	49.89	1.00	15.46	10.18	0.15	8.08	12.64	2.22	0.22	0.13	99.96	0.22
4820-034	-45.012419	13.7668898	49.24	1.04	15.24	10.25	0.16	7.87	12.62	2.27	0.24	0.11	99.04	0.23
4820-035	-45.0108479	13.7668553	50.15	1.86	14.89	10.01	0.15	7.44	10.84	2.78	0.61	0.29	98.99	0.33
4820-036	-45.0104128	13.766911	49.86	1.86	14.85	9.96	0.15	7.39	10.70	2.77	0.61	0.29	98.44	0.33
4820-037	-45.0081022	13.7675402	50.44	1.88	14.99	9.91	0.16	6.99	10.97	2.77	0.61	0.31	99.03	0.33
4820-038	-45.004984	13.7684652	50.05	1.80	15.07	9.81	0.18	7.49	11.08	2.72	0.63	0.32	99.14	0.35
4820-039	-45.0050632	13.768567	50.06	1.81	14.90	9.89	0.15	7.46	10.93	2.76	0.63	0.29	98.88	0.35
4820-040	-45.0040809	13.7692362	49.71	1.80	15.07	9.76	0.15	7.42	11.09	2.79	0.62	0.28	98.69	0.35
4820-041	-45.0025637	13.7695415	49.84	1.82	15.16	9.69	0.16	7.21	11.12	2.72	0.63	0.28	98.64	0.35
4820-042	-45.002495	13.769557	50.71	1.81	15.18	9.74	0.17	7.23	11.23	2.79	0.65	0.34	99.85	0.36
4820-043	-45.0007623	13.7698156	49.88	1.81	14.88	9.83	0.16	7.35	10.89	2.78	0.61	0.29	98.48	0.34
4820-044	-45.0001118	13.7695106	50.27	1.40	15.15	9.85	0.15	8.23	11.23	2.51	0.25	0.17	99.22	0.18
4820-045	-44.9982246	13.7687522	50.54	1.41	15.03	9.93	0.15	8.43	11.19	2.50	0.25	0.18	99.61	0.18
4820-046	-44.9972252	13.7688293	51.47	1.39	15.07	9.92	0.17	8.33	11.17	2.44	0.26	0.22	100.43	0.19
4820-047	-44.9981786	13.7709105	51.05	1.37	15.15	9.79	0.17	8.33	11.27	2.44	0.25	0.19	100.00	0.18
4821-048	-45.0119757	13.7816262	50.29	1.85	14.79	9.89	0.15	7.56	10.76	2.73	0.59	0.27	98.89	0.32
4821-049	-45.0119497	13.77962	49.97	1.84	14.93	9.99	0.18	7.61	10.81	2.69	0.60	0.33	98.94	0.32
4821-050	-45.0116683	13.776345	50.46	1.85	14.88	9.97	0.15	7.40	10.88	2.73	0.60	0.30	99.22	0.32
4821-051	-45.0114259	13.7751221	50.22	1.84	14.89	9.95	0.15	7.40	10.90	2.75	0.61	0.30	99.01	0.33
4821-053	-45.0110386	13.7738647	50.41	1.85	14.91	10.01	0.15	7.38	10.75	2.73	0.60	0.28	99.06	0.32
4821-054	-45.0110186	13.7738488	50.55	1.84	14.93	10.01	0.18	7.37	10.84	2.74	0.61	0.33	99.39	0.33
4821-055	-45.0104149	13.7735723	50.17	1.87	14.88	10.02	0.15	7.42	10.87	2.80	0.59	0.30	99.06	0.32
4821-056	-45.0104129	13.7736251	50.29	1.84	14.91	9.97	0.16	7.37	10.79	2.75	0.60	0.30	98.97	0.33
4821-057	-45.0090467	13.7737677	50.12	1.82	14.97	10.03	0.18	7.31	10.77	2.73	0.61	0.33	98.86	0.33
4821-058	-45.0090804	13.7737785	50.60	1.85	14.88	9.97	0.16	7.32	10.79	2.77	0.60	0.29	99.22	0.32
4821-059	-45.0089651	13.7710077	50.01	1.82	14.94	10.00	0.18	7.42	10.89	2.70	0.61	0.32	98.90	0.34
4942-136	-45.014412	13.761744	48.77	2.22	14.78	10.07	0.17	7.54	10.76	3.05	0.91	0.45	98.72	0.41
4942-138	-45.012322	13.760524	49.59	2.25	15.38	9.82	0.16	6.96	11.25	3.08	0.97	0.43	99.89	0.43
4942-139	-45.012199	13.763187	50.31	1.88	15.04	10.07	0.17	7.54	10.79	2.81	0.62	0.30	99.55	0.33
4942-140	-45.012641	13.763625	50.30	1.87	15.02	10.14	0.18	7.55	10.88	2.82	0.61	0.30	99.67	0.32
4942-141	-45.012626	13.763607	50.51	1.86	15.02	10.08	0.17	7.51	10.89	2.81	0.60	0.30	99.75	0.32
4942-142	-45.011375	13.763916	51.14	1.53	15.30	9.57	0.13	7.22	11.35	2.76	0.43	0.20	99.64	0.28
4942-143	-45.008304	13.76378	50.28	1.82	15.02	9.88	0.18	7.49	10.92	2.81	0.63	0.30	99.33	0.35
4942-144	-45.005976	13.762316	50.42	1.82	15.15	9.80	0.18	7.30	11.10	2.81	0.62	0.30	99.51	0.34
4942-145	-45.0047	13.762584	50.41	1.78	15.21	9.69	0.17	7.21	11.17	2.76	0.62	0.29	99.29	0.35
4942-146	-45.004738	13.762537	50.06	1.79	15.19	9.71	0.16	7.27	11.20	2.75	0.62	0.30	99.05	0.35
4942-147	-45.001829	13.764022	50.56	1.81	15.46	9.71	0.17	6.91	11.36	2.62	0.61	0.29	99.49	0.34
4942-148	-45.001871	13.764042	50.61	1.86	15.65	9.59	0.17	6.39	11.38	2.90	0.64	0.29	99.47	0.34
4943-149	-45.009509	13.780549	50.37	1.53	15.05	9.90	0.19	7.97	10.77	2.62	0.41	0.21	99.02	0.27
4943-150	-45.008748	13.779359	50.49	1.59	15.29	9.96	0.17	7.10	11.05	2.70	0.42	0.22	99.00	0.26
4943-151	-45.00781	13.780034	50.05	1.53	15.04	9.99	0.18	8.14	10.77	2.62	0.41	0.20	98.93	0.27
4943-152	-45.006841	13.778346	50.84	1.16	15.28	9.10	0.13	9.26	11.39	2.29	0.32	0.15	99.92	0.27
4943-153	-45.006847	13.778352	50.85	1.17	15.11	9.10	0.11	9.32	11.35	2.25	0.32	0.13	99.71	0.28
4943-154	-45.006811	13.778282	49.95	1.91	15.08	10.01	0.18	7.26	10.86	2.82	0.59	0.30	98.95	0.31
4943-155	-45.007034	13.777753	49.81	1.91	15.04	10.07	0.18	7.43	11.08	2.53	0.58	0.32	98.95	0.30
4943-156	-45.005002	13.775613	50.01	1.37	15.69	9.75	0.18	7.67	11.47	2.55	0.38	0.19	99.26	0.28
4943-157	-45.004066	13.773164	50.33	1.85	15.13	9.99	0.18	7.32	10.95	2.83	0.63	0.30	99.49	0.34
4943-158	-45.004068	13.773189	50.45	1.84	15.19	9.97	0.18	7.19	11.07	2.82	0.62	0.30	99.63	0.34
4943-159	-45.003955	13.773154	50.13	1.84	15.16	9.99	0.18	7.23	11.16	2.76	0.62	0.31	99.39	0.34
4944-160	-45.012487	13.78418	50.43	1.55	15.08	9.95	0.17	7.99	10.80	2.64	0.43	0.22	99.26	0.28
4944-161	-45.010327	13.78305	50.59	1.55	15.00	9.92	0.18	8.03	10.73	2.64	0.43	0.21	99.27	0.28
4944-162	-45.010346	13.783087	50.91	1.56	14.89	9.80	0.13	7.96	10.70	2.73	0.43	0.20	99.31	0.28
4944-163	-45.00843	13.783937	50.41	1.54	15.06	9.90	0.18	7.87	10.76	2.63	0.44	0.23	99.02	0.29
4944-164	-45.008534	13.783927	51.16	1.58	15.01	9.89	0.13	7.80	10.85	2.77	0.44	0.20	99.83	0.28
4944-165	-45.00636	13.781928	51.08	1.53	15.10	9.87	0.19	8.01	10.76	2.63	0.43	0.22	99.82	0.28
4944-166	-45.006343	13.781952	50.40	1.53	14.97	9.88	0.19	8.01	10.77	2.64	0.43	0.21	99.03	0.28
4944-167	-45.006351	13.781921	50.76	1.54	15.04	9.83	0.18	8.01	10.78	2.64	0.42	0.23	99.43	0.28
4944-168	-45.005332	13.78291	50.92	1.54	15.08	9.90	0.18	7.97	10.78	2.63	0.42	0.21	99.62	0.27
4944-169	-45.005362	13.78288	50.91	1.52	15.14	9.84	0.18	8.04	10.72	2.69	0.42	0.21	99.67	0.27
4944-171	-45.00436	13.782604	51.72	1.43	15.51	9.71	0.14	7.53	11.36	2.67	0.39	0.17	100.63	0.27
4944-172	-45.004367	13.782597	50.73	1.40	15.71	9.70	0.18	7.52	11.33	2.61	0.40	0.19	99.77	0.28
4944-173	-45.00247	13.783488	50.70	1.39	15.75	9.67	0.18	7.61	11.35	2.60	0.39	0.20	99.83	0.28
4944-174	-45.001216	13.78542	50.94	1.31	15.30	9.56	0.18	8.59	11.12	2.49	0.26	0.17	99.91	0.20
4944-175	-45.000222	13.787884	50.16	1.31	15.25	9.67	0.17	8.64	11.06	2.50	0.25	0.18	99.18	0.19
4944-176	-45.000973	13.789898	50.78	1.34	15.52	9.62	0.17	8.02	11.27	2.52	0.24	0.16	99.64	0.18
4944-177	-45.000839	13.7911	50.75	1.31	15.24	9.65	0.18	8.61	11.11	2.49	0.25	0.17	99.77	0.19

Sample	Lon	Lat	SiO2	TiO2	Al2O3	FeO	MnO	MgO	CaO	Na2O	K2O	P2O5	TOTAL	K/Ti
4945-178	-45.012555	13.756492	50.17	1.94	15.30	9.92	0.18	6.74	11.29	2.80	0.66	0.32	99.31	0.34
4945-179	-45.012635	13.754457	50.18	1.89	15.17	9.84	0.18	7.31	10.98	2.81	0.67	0.31	99.34	0.35
4945-180	-45.012623	13.754449	50.06	1.91	14.91	9.78	0.13	7.47	10.94	2.92	0.67	0.28	99.06	0.35
4945-181	-45.012622	13.754443	50.38	1.88	15.14	9.87	0.17	7.58	10.93	2.82	0.65	0.31	99.73	0.35
4945-182	-45.010408	13.754555	49.39	2.27	15.60	9.65	0.17	6.37	11.25	3.09	0.96	0.43	99.18	0.42
4945-183	-45.0087	13.754718	48.32	2.16	15.31	9.75	0.17	7.04	11.04	3.01	0.90	0.41	98.12	0.42
4945-184	-45.005212	13.756092	49.46	1.80	15.37	9.41	0.16	7.57	11.25	2.79	0.67	0.32	98.79	0.37
4945-187	-44.997126	13.760716	50.80	1.34	15.14	9.61	0.16	8.66	11.08	2.48	0.24	0.18	99.69	0.18
4945-188	-44.997125	13.760718	50.85	1.35	15.04	9.59	0.17	8.74	11.03	2.49	0.25	0.19	99.69	0.19
4945-189	-44.995896	13.762023	51.15	1.36	15.10	9.54	0.12	8.63	11.13	2.63	0.25	0.15	100.06	0.18
4945-190	-44.99581	13.764785	50.73	1.41	15.43	9.87	0.17	8.11	11.25	2.53	0.27	0.17	99.94	0.19
4945-191	-44.996901	13.766739	50.76	1.38	15.55	10.05	0.17	7.62	11.35	2.54	0.24	0.17	99.86	0.18
4945-192	-44.996897	13.766741	51.10	1.40	15.47	9.97	0.19	7.55	11.33	2.53	0.25	0.19	99.96	0.18
4945-193	-44.99655	13.767269	50.77	1.41	15.31	9.84	0.18	7.98	11.12	2.54	0.27	0.18	99.60	0.19
4945-194	-44.996552	13.767265	50.68	1.40	15.26	9.87	0.18	8.02	11.08	2.54	0.27	0.18	99.48	0.19
4945-195	-44.99655	13.767265	50.51	1.41	15.32	9.92	0.18	8.05	11.15	2.53	0.27	0.19	99.52	0.19
4946-197	-45.018687	13.749435	50.62	1.91	15.12	9.87	0.18	7.09	11.02	2.78	0.66	0.30	99.55	0.34
4946-198	-45.017191	13.748999	49.65	1.89	14.92	9.91	0.18	7.64	10.90	2.78	0.65	0.32	98.83	0.34
4946-199	-45.014615	13.74845	49.57	1.88	14.90	9.86	0.18	7.66	10.87	2.78	0.65	0.31	98.67	0.35
4946-200	-45.013611	13.748229	50.60	1.88	14.92	9.91	0.18	7.67	10.90	2.77	0.66	0.31	99.80	0.35
4946-201	-45.013621	13.748278	49.16	2.19	14.94	9.83	0.17	7.36	10.98	2.99	0.95	0.44	99.01	0.43
4946-202	-45.008339	13.750467	49.26	2.21	14.85	9.84	0.18	7.48	10.95	2.95	0.95	0.43	99.11	0.43
4946-203	-45.008353	13.750502	49.82	2.21	14.91	9.89	0.16	7.51	10.98	2.98	0.95	0.43	99.83	0.43
4946-204	-45.007185	13.750662	50.48	1.83	14.97	9.87	0.17	7.63	10.95	2.80	0.67	0.30	99.67	0.37
4946-205	-45.005169	13.750737	50.67	1.82	14.96	9.85	0.17	7.69	10.85	2.76	0.66	0.31	99.74	0.36
4947-206	-45.002689	13.751816	50.78	1.91	15.20	9.79	0.17	7.32	11.11	2.67	0.68	0.30	99.93	0.35
4947-206	-45.017756	13.742735	49.80	1.85	15.13	9.68	0.17	7.51	10.78	2.84	0.69	0.30	98.74	0.37
4947-207	-45.01692	13.742171	49.73	1.89	15.14	9.81	0.17	7.56	10.84	2.87	0.68	0.30	98.99	0.36
4947-208	-45.015873	13.74196	49.58	1.89	15.28	9.84	0.17	7.37	10.96	2.84	0.67	0.31	98.91	0.35
4947-209	-45.012342	13.740747	50.45	1.85	15.28	9.83	0.17	7.60	10.95	2.81	0.67	0.31	99.93	0.36
4947-209	-45.012342	13.740747	50.16	1.83	15.08	9.66	0.17	7.57	10.88	2.78	0.68	0.30	99.09	0.37
4947-210	-45.012347	13.740724	50.15	1.84	15.25	9.79	0.17	7.63	10.86	2.81	0.68	0.31	99.49	0.37
4947-211	-45.012357	13.740728	49.89	1.83	15.11	9.59	0.17	7.57	10.84	2.74	0.69	0.31	98.75	0.37
4947-213	-45.010754	13.741445	50.02	1.85	15.34	9.54	0.17	7.02	10.99	2.77	0.69	0.31	98.70	0.37
4947-214	-45.010737	13.741478	50.17	1.88	15.19	9.70	0.17	7.13	10.99	2.80	0.69	0.31	99.02	0.36
4947-215	-45.008893	13.742696	49.26	2.05	15.14	9.61	0.16	7.34	10.83	2.87	0.85	0.36	98.47	0.42
4947-215	-45.008893	13.742696	49.08	2.03	15.08	9.48	0.17	7.18	10.76	2.92	0.88	0.38	97.94	0.43
4947-216	-45.006916	13.742757	48.79	2.02	14.70	9.49	0.16	7.43	10.66	2.88	0.88	0.38	97.39	0.43
4947-217	-45.005812	13.742778	48.60	2.02	14.68	9.42	0.16	7.39	10.62	2.87	0.87	0.37	97.00	0.43
4947-218	-45.001125	13.74262	48.78	1.99	14.89	9.45	0.16	7.64	10.54	2.89	0.88	0.39	97.63	0.44
4947-219	-44.998741	13.745581	48.05	2.14	14.45	9.84	0.16	7.96	10.75	2.95	0.98	0.45	97.73	0.46
4949-240	-45.01559	13.728481	50.58	1.58	15.09	9.70	0.17	6.66	11.58	2.67	0.63	0.21	98.87	0.40
4949-241	-45.01513	13.728131	50.49	1.62	15.07	9.85	0.18	6.58	11.46	2.70	0.63	0.23	98.81	0.39
4949-242	-45.012901	13.728345	49.59	1.09	14.96	9.78	0.18	7.87	13.14	2.27	0.28	0.12	99.29	0.26
4949-243	-45.01088	13.727334	49.96	1.76	15.29	9.49	0.17	7.56	11.37	2.76	0.64	0.28	99.28	0.37
4949-244	-45.008204	13.728932	50.75	1.75	15.38	9.44	0.17	7.32	11.48	2.74	0.62	0.26	99.91	0.36
4949-245	-45.008273	13.728901	49.37	1.76	15.31	9.44	0.17	7.26	11.41	2.76	0.63	0.27	98.38	0.36
4949-246	-45.006767	13.729791	49.99	1.89	15.36	9.69	0.18	7.04	11.06	2.88	0.71	0.31	99.11	0.37
4949-247	-45.006738	13.72978	50.03	1.90	15.26	9.67	0.18	7.01	11.11	2.88	0.70	0.32	99.06	0.37
4949-248	-45.004749	13.726719	50.86	1.87	14.97	10.05	0.14	7.06	11.11	2.77	0.63	0.26	99.71	0.34
4949-249	-45.001001	13.726198	50.14	1.78	15.64	9.43	0.17	7.40	11.44	2.77	0.63	0.28	99.68	0.35
4949-250	-44.999429	13.726592	50.12	1.77	15.55	9.39	0.17	7.40	11.36	2.76	0.67	0.28	99.48	0.38
4949-251	-44.998963	13.726901	50.92	1.94	15.07	9.93	0.14	6.90	11.18	2.85	0.64	0.28	99.84	0.33
4949-252	-44.996452	13.725386	50.37	1.14	15.54	9.09	0.15	9.25	11.36	2.27	0.32	0.15	99.64	0.28
4949-253	-44.996419	13.724779	50.17	1.14	15.43	9.08	0.15	9.44	11.29	2.25	0.32	0.16	99.43	0.28
4949-254	-44.996417	13.724779	49.85	1.15	15.41	9.12	0.16	9.44	11.31	2.20	0.33	0.15	99.11	0.29
4951-272	-45.021726	13.74585	50.56	1.61	14.89	9.77	0.17	6.46	11.16	2.73	0.59	0.24	98.17	0.36
4951-273	-45.025384	13.747676	49.57	1.31	14.62	10.18	0.20	7.05	12.01	2.47	0.40	0.17	97.98	0.30
4951-274	-45.025394	13.74769	49.65	1.31	14.82	10.12	0.19	7.05	12.09	2.12	0.43	0.16	97.94	0.33
4951-275	-45.025484	13.750737	50.64	1.54	15.04	9.51	0.17	6.63	11.28	2.73	0.56	0.22	98.33	0.37
4951-277	-45.024616	13.753308	50.31	1.53	15.05	9.53	0.17	6.67	11.27	2.78	0.56	0.22	98.09	0.37
4951-278	-45.0246	13.753303	51.21	1.55	15.12	9.49	0.17	6.66	11.19	2.73	0.57	0.23	98.93	0.37
4951-279	-45.028426	13.75647	50.25	1.52	15.16	9.34	0.18	6.79	11.32	2.56	0.55	0.21	97.87	0.36
4951-280	-45.028352	13.757249	50.28	1.50	15.08	9.24	0.18	6.81	11.35	2.72	0.54	0.23	97.93	0.36
4951-281	-45.028825	13.75792	51.34	1.49	15.28	9.29	0.17	6.82	11.52	2.66	0.55	0.22	99.34	0.37
4951-282	-45.029501	13.758548	51.33	1.47	15.40	9.20	0.16	6.93	11.56	2.63	0.53	0.22	99.43	0.36
4951-283	-45.030586	13.758413	51.22	1.75	15.12	9.90	0.17	6.32	11.04	2.81	0.67	0.25	99.26	0.38
4951-284	-45.031766	13.758354	51.20	1.75	14.96	9.88	0.18	6.22	10.88	2.81	0.70	0.27	98.86	0.40
4951-285	-45.032419	13.760523	50.91	1.69	15.08	9.70	0.19	6.47	11.11	2.78	0.66	0.25	98.84	0.39
4951-286	-45.032143	13.761184	50.56	1.80	15.07	10.20	0.18	6.21	10.91	2.85	0.69	0.27	98.73	0.38
4951-287	-45.032575	13.762949	50.25	1.66	15.11	9.78	0.18	6.50	11.15	2.79	0.61	0.24	98.27	0.37
4951-288	-45.030102	13.765011	50.20	1.54	15.25	9.49	0.17	6.80	11.39	2.73	0.54	0.22	98.33	0.35
4951-289	-45.029353	13.765119	50.88	1.54	15.22	9.46	0.17	6.78	11.43	2.70	0.54	0.22	98.93	0.35
4956-351	-45.00892	13.770676	51.26	1.86	15.00	10.05	0.17	7.41	10.87	2.88	0.63	0.31	100.43	0.34
4956-352	-45.009026	13.770707	51.31	1.84	14.93	10.05	0.17	7.54	10.80	2.85	0.62	0.29	100.40	0.34
4956-353	-45.009029	13.770786	51.17	1.85	15.02	9.99	0.17	7.37	10.86	2.84	0.62	0.30	100.19	0.34
4956-354	-45.008978	13.771146	51.08	1.85	14.76	9.96	0.18	7.47	10.78	2.85	0.64	0.31	99.89	0.35
4956-355	-45.008961	13.771183	51.16	1.84	14.79	9.94	0.18	7.47	10.81	2.85	0.62	0.32	99.97	0.34
4956-356	-45.008856	13.771386	51.13	1.85	14.85	9.97	0.17	7.54	10.81	2.84	0.62	0.32	100.11	0.33
4956-357	-45.008969	13.771476	51.19	1.84	14.92	9.96	0.18	7.56	10.79	2.83	0.62	0.31	100.20	0.34
4956-359	-45.008969	13.771479	50.93	1.85	14.72	9.91	0.17	7.55	10.72	2.80	0.62	0.32	99.59	0.34
4956-360	-45.010124	13.771755	50.36	1.85	14.82	9.94	0.17	7.37	10.76	2.74	0.62	0.30	98.93	0.34
4956-361	-45.010125	13.771751	50.31	1.85	14.82	9.99	0.17	7.33	10.85	2.70	0.61	0.30	98.94	0.33
4956-362	-45.010697	13.771892	50.13	1.84	14.84	9.94	0.18	7.14	10.99	2.67	0.62	0.31	98.67	0.34
4956-363	-45.010759	13.77142	50.18	1.84	14.84	9.94	0.17	7.45	10.76	2.73	0.63	0.30	98.84	0.34
4956-364	-45.011019	13.769317	50.01	1.88	14.83	9.91	0.17	7.53	10.73	2.73	0.63	0.32	98.74	0.34
4956-365	-45.009706	13.768307	50.41	1.84	14.89	9.95	0.17	7.39	10.77	2.74	0.62	0.30	99.08	0.34
4956-366	-45.009699	13.76818	50.45	1.85	14.89	9.88	0.17	7.33	10.79	2.73	0.62	0.30	99.00	0.33
4956-367	-45.009772	13.767986	50.35	1.85	14.87	9.93	0.17	7.35	10.78	2.72	0.63	0.30	98.94	0.34
4956-368	-45.009721	13.767207	50.30	1.86	15.03	9.93	0.17	7.16	10.84	2.74	0.62	0.30	98.94	0.33
4956-369	-45.009563	13.766527	50.88	1.85	14.96	9.90	0.18	7.27	10.78	2.78	0.64	0.30	99.54	0.34
4956-370	-45.009615	13.766496	50.87	1.87	15.11	9.86	0.17	7.09	10.83	2.79	0.64	0.30	99.53	0.34
4956-371	-45.009618	13.766495	50.90	1.86	14.93	9.92	0.17	7.30	10.78	2.79	0.62	0.30	99.58	0.34
4956-372	-45.009764	13.766534	50.88	1.91	15.04	9.97	0.18	6.81	10.93	2.82	0.63	0.31	99.48	0.33
4956-373	-45.009882	13.766336	50.73	1.86	15.09	9.97	0.17	7.48	10.74	2.79	0.62	0.30	99.75	0.34

Sample	Lon	Lat	SiO2	TiO2	Al2O3	FeO	MnO	MgO	CaO	Na2O	K2O	P2O5	TOTAL	K/Ti
4953-305	-44.994025	13.719009	51.00	0.97	16.32	8.74	0.13	7.79	12.30	2.34	0.20	0.10	99.90	0.21
4953-306	-44.994057	13.719075	51.68	0.96	16.17	8.86	0.15	8.15	12.26	2.19	0.24	0.12	100.80	0.25
4953-307	-44.994044	13.719067	51.46	0.95	15.87	8.92	0.15	8.37	12.18	2.18	0.24	0.10	100.41	0.25
4953-308	-44.991917	13.716401	50.64	1.68	15.33	9.43	0.16	7.11	11.65	2.58	0.54	0.22	99.33	0.32
4953-309	-44.991939	13.71655	50.29	1.56	15.85	9.15	0.16	7.61	11.55	2.53	0.50	0.22	99.41	0.32
4953-310	-44.992901	13.713828	50.97	1.51	15.33	9.32	0.17	7.55	11.55	2.54	0.46	0.19	99.59	0.30
4953-311	-44.99287	13.709683	52.62	1.51	15.38	9.10	0.15	7.28	11.30	2.51	0.42	0.20	100.48	0.28
4953-312	-44.99231	13.706734	51.02	1.62	15.36	9.46	0.17	7.18	11.58	2.16	0.51	0.21	99.26	0.32
4953-313	-44.987193	13.7063	50.91	1.50	15.58	9.12	0.16	7.47	11.47	2.52	0.46	0.21	99.42	0.31
4953-315	-44.980391	13.704853	49.96	1.46	15.49	9.20	0.16	7.56	11.51	2.54	0.45	0.21	98.54	0.31
4953-316	-44.980386	13.704862	50.35	1.44	15.40	9.26	0.17	7.64	11.49	2.56	0.46	0.21	98.97	0.32
4953-317	-44.980362	13.704887	50.69	1.46	15.51	9.18	0.16	7.65	11.58	2.58	0.46	0.21	99.47	0.32
4953-318	-44.979285	13.703529	50.56	1.44	15.45	9.19	0.16	7.74	11.53	2.56	0.46	0.21	99.29	0.32
4953-319	-44.978482	13.70194	50.11	1.34	15.36	9.01	0.16	7.93	11.64	2.46	0.45	0.19	98.66	0.33
4953-320	-44.9787	13.7019	50.15	1.36	15.33	8.97	0.16	7.90	11.61	2.46	0.44	0.20	98.60	0.32
4954-321	-44.930529	13.607211	50.86	1.54	15.16	9.84	0.18	7.33	11.16	2.75	0.42	0.23	99.46	0.27
4954-322	-44.930612	13.607194	50.84	1.55	15.17	9.90	0.18	7.40	11.17	2.80	0.43	0.22	99.63	0.28
4954-323	-44.931107	13.606713	51.02	1.54	15.10	9.92	0.18	7.49	11.14	2.75	0.43	0.23	99.79	0.28
4954-324	-44.942828	13.612668	50.18	1.49	14.69	10.51	0.19	7.21	11.06	2.53	0.32	0.21	98.39	0.22
4954-325	-44.949517	13.614609	49.87	1.48	15.03	9.72	0.19	7.56	11.21	2.66	0.40	0.21	98.31	0.27
4954-326	-44.949517	13.614611	50.02	1.48	14.83	9.75	0.18	7.74	11.01	2.61	0.40	0.22	98.25	0.27
4954-327	-44.94972	13.614797	51.03	1.92	14.82	10.09	0.14	7.39	10.85	2.93	0.62	0.27	100.05	0.32
4954-328	-44.95105	13.616067	49.87	1.54	14.87	9.80	0.18	7.57	10.86	2.70	0.44	0.23	98.05	0.28
4954-329	-44.951373	13.616033	51.11	1.58	15.13	10.02	0.17	7.60	10.90	2.72	0.45	0.23	99.91	0.29
4954-330	-44.952831	13.616542	50.63	1.61	15.02	10.09	0.17	7.65	10.84	2.72	0.47	0.23	99.43	0.29
4954-331	-44.953233	13.618037	50.44	1.59	15.03	10.02	0.18	7.64	10.81	2.69	0.46	0.23	99.08	0.29
4954-332	-44.954899	13.619454	50.64	1.58	15.04	9.96	0.17	7.67	10.87	2.71	0.45	0.23	99.32	0.28
4954-333	-44.956909	13.621479	50.53	1.57	14.99	9.88	0.17	7.75	10.89	2.72	0.44	0.21	99.15	0.28
4954-334	-44.958525	13.626258	49.89	1.52	14.99	9.73	0.18	7.79	10.87	2.67	0.43	0.20	98.24	0.28
4954-335	-44.958435	13.628432	49.93	1.55	15.04	9.91	0.17	7.73	10.83	2.71	0.43	0.21	98.52	0.28
4955-337	-44.864469	13.58729	49.90	1.34	15.31	9.40	0.17	7.96	11.13	2.47	0.40	0.18	98.26	0.30
4955-338	-44.862662	13.587516	49.94	1.31	15.71	9.07	0.16	7.52	11.46	2.45	0.40	0.17	98.20	0.31
4955-339	-44.864104	13.5911	49.83	1.35	15.49	9.13	0.17	7.41	11.41	2.46	0.42	0.19	97.86	0.31
4955-340	-44.864104	13.591101	49.89	1.36	15.53	9.21	0.17	7.44	11.38	2.45	0.43	0.18	98.03	0.31
4955-341	-44.864661	13.592325	49.84	1.33	15.14	9.31	0.16	7.86	11.24	2.46	0.42	0.18	97.95	0.32
4955-342	-44.86434	13.595073	50.25	1.34	15.31	9.47	0.14	8.27	11.46	2.47	0.36	0.17	99.26	0.27
4955-343	-44.864354	13.595152	50.26	1.35	15.24	9.57	0.13	8.27	11.54	2.46	0.36	0.16	99.34	0.27
4955-344	-44.867582	13.596828	51.41	1.22	15.49	9.41	0.17	7.92	11.76	2.37	0.14	0.13	100.03	0.12
4955-345	-44.86758	13.596825	51.46	1.23	15.55	9.42	0.18	7.91	11.76	2.38	0.16	0.14	100.19	0.13
4955-346	-44.870105	13.598096	51.59	1.23	15.35	9.59	0.18	7.82	11.77	2.29	0.13	0.12	100.08	0.11
4955-347	-44.874527	13.600606	50.20	1.87	15.16	9.63	0.16	7.53	11.28	2.64	0.56	0.29	99.33	0.30
4955-348	-44.875785	13.600109	50.08	1.94	15.20	9.51	0.16	6.91	11.49	2.71	0.60	0.30	98.89	0.31
4955-349	-44.876679	13.600054	50.10	1.89	15.36	9.45	0.15	7.25	11.41	2.66	0.59	0.30	99.16	0.31
4955-350	-44.878051	13.600915	50.15	1.87	15.26	9.51	0.16	7.40	11.34	2.66	0.57	0.30	99.23	0.30

Table A.2 Trace Element Contents of the 14°N Segment. These data were measured on the LA-ICP-MS at Boise State University. Trace Element concentrations are given in ppm.

sample	Li	Sc	V	Cr	Co	Ni	Cu	Zn	Ga	Rb	Sr	Y	Zr	Nb	Cs	Ba	La	Ce	Pr	Nd	Sm	Eu	Tb	Gd	Dy	Ho	Er	Tm	Yb	Lu	Hf	Ta	Pb	Th	U
AL4823-071	4.20	36.17	228.66	120.17	36.66	55.84	81.05	70.32	14.99	14.64	283.84	22.03	124.32	23.40	0.14	171.34	13.06	28.51	3.72	15.87	3.63	1.27	0.89	4.04	3.92	0.79	2.13	0.32	1.94	0.29	2.82	1.47	0.90	1.41	0.46
AL4823-075	3.41	37.81	211.89	288.78	39.77	101.83	94.91	71.92	12.52	7.05	224.10	19.90	85.97	12.60	0.07	91.50	7.44	16.87	2.31	10.63	2.88	1.05	0.61	3.46	3.53	0.73	1.97	0.30	1.76	0.27	2.20	0.78	0.50	0.75	0.25
AL4823-079	4.82	38.59	251.70	159.98	39.71	62.52	79.27	78.03	13.90	13.90	224.10	19.90	85.97	12.60	0.07	91.50	7.44	16.87	2.31	10.63	2.88	1.05	0.61	3.46	3.53	0.73	1.97	0.30	1.76	0.27	2.20	0.78	0.50	0.75	0.25
AL4823-084	3.44	40.09	221.95	306.26	39.84	109.73	103.25	68.39	12.78	8.54	220.01	20.04	87.01	14.61	0.10	107.85	8.35	18.53	2.51	11.18	2.93	1.01	0.60	3.39	3.48	0.72	2.02	0.30	1.83	0.28	2.15	0.92	0.58	0.87	0.29
AL4823-088	5.02	37.12	249.03	197.29	38.10	80.17	68.43	77.62	15.43	14.19	253.73	25.16	132.29	23.19	0.15	164.22	12.78	28.48	3.61	16.13	3.92	1.32	0.76	4.38	4.30	0.90	2.45	0.38	2.27	0.35	3.01	1.45	0.81	1.38	0.44
AL4824-092	5.38	37.92	280.55	198.85	37.79	64.48	66.17	89.57	15.49	13.44	244.75	27.37	133.41	23.26	0.14	157.84	12.88	29.53	3.93	17.03	4.21	1.42	0.82	4.81	4.84	1.01	2.74	0.43	2.57	0.39	3.15	1.46	0.95	1.35	0.42
AL4824-096	4.49	37.60	244.65	209.37	39.15	62.35	80.67	78.73	15.36	13.74	257.05	22.81	109.87	19.82	0.12	166.75	11.04	24.73	3.35	14.37	3.59	1.28	0.70	4.15	4.04	0.83	2.24	0.34	2.04	0.31	2.60	1.22	0.86	1.15	0.36
AL4824-100	6.95	38.12	293.94	208.78	38.26	25.38	67.71	97.02	16.60	14.61	257.30	30.54	154.84	25.69	0.14	171.34	14.13	33.13	4.44	19.20	4.72	1.61	0.92	5.29	5.34	1.10	3.04	0.47	2.81	0.43	3.60	1.60	1.15	1.55	0.47
AL4824-104	5.81	37.24	254.02	189.51	35.97	57.75	63.70	85.43	16.18	16.16	233.87	29.61	147.55	26.03	0.16	176.76	14.46	31.98	4.19	18.09	4.49	1.46	0.89	5.14	5.15	1.08	2.99	0.46	2.69	0.43	3.52	1.64	1.11	1.47	0.53
AL4825-107	4.63	37.12	239.84	261.91	38.92	88.71	64.64	64.13	13.11	10.06	245.16	21.58	125.80	20.39	0.12	165.25	10.39	23.25	3.12	13.43	3.40	1.18	0.60	3.85	3.82	0.79	2.12	0.33	1.98	0.31	2.27	0.95	0.73	1.07	0.32
AL4825-112	5.40	36.49	246.25	209.04	40.44	79.60	65.39	92.71	14.54	13.04	251.50	24.43	121.19	21.75	0.13	156.40	12.65	28.32	3.71	15.99	3.90	1.35	0.72	4.57	4.33	0.89	2.46	0.38	2.27	0.35	2.91	1.34	1.43	1.35	0.41
AL4825-116	4.75	36.76	246.01	196.35	37.77	78.28	72.55	76.18	14.51	12.70	247.02	23.47	117.31	21.08	0.13	152.26	11.89	26.38	3.53	14.90	3.67	1.24	0.70	4.11	4.13	0.84	2.31	0.36	2.11	0.32	2.75	1.32	0.90	1.28	0.39
AL4825-119	4.78	37.87	226.99	208.78	39.03	79.14	74.79	65.25	14.03	12.65	245.64	22.06	110.55	21.04	0.13	150.66	11.49	25.42	3.38	14.48	3.48	1.20	0.67	4.01	3.90	0.80	2.15	0.35	2.05	0.32	2.70	1.30	0.90	1.28	0.38
AL4825-122	5.42	38.88	247.37	206.33	38.51	73.91	73.91	78.21	14.58	12.58	247.71	25.80	124.93	21.47	0.13	147.68	12.01	27.08	3.62	15.67	3.90	1.33	0.76	4.53	4.53	0.93	2.56	0.40	2.34	0.36	2.96	1.32	0.92	1.25	0.39
AL4957-379	6.15	35.82	296.85	83.50	37.77	36.57	51.66	95.79	21.42	15.29	287.20	30.15	244.59	28.67	0.18	197.44	17.17	37.31	4.81	21.08	5.18	1.78	0.93	5.75	5.42	1.10	3.08	0.45	2.73	0.42	3.78	1.32	1.06	1.77	0.52
AL4957-374	3.81	36.6	210	325	39.8	119	92	59	15.8	11.18	298	16.9	70.8	16.90	0.140	159.8	10.27	21.20	2.75	11.60	2.78	1.04	0.512	3.15	3.09	0.630	1.71	0.250	1.55	0.235	1.93	0.966	0.734	1.13	0.326
AL4957-376	6.57	36.6	306	98	38.6	36	53	98	19.7	14.75	285	30.4	160.5	28.54	0.180	189.7	17.51	37.40	4.93	21.26	5.21	1.77	0.925	5.72	5.52	1.117	3.07	0.454	2.83	0.391	3.88	1.655	1.141	1.80	0.551
AL4957-381	5.00	38.0	252	242	38.4	81	74	73	16.7	12.37	294	22.3	118.1	23.04	0.163	157.5	13.88	29.07	3.79	16.05	3.81	1.33	0.677	4.22	4.07	0.826	2.27	0.336	2.09	0.317	2.83	1.375	0.992	1.49	0.447
AL4825-116	4.75	36.76	246.01	196.35	37.77	78.28	72.55	76.18	14.51	12.70	247.02	23.47	117.31	21.08	0.13	152.26	11.89	26.38	3.53	14.90	3.67	1.24	0.70	4.11	4.13	0.84	2.31	0.36	2.11	0.32	2.75	1.32	0.90	1.28	0.39
AL4825-123	4.91	36.83	255.80	162.22	38.17	60.80	77.86	79.82	15.51	15.21	240.81	24.46	125.48	23.77	0.14	176.46	12.90	28.49	3.61	16.14	3.88	1.33	0.73	4.35	4.27	0.89	2.42	0.37	2.23	0.35	2.92	1.46	0.94	1.34	0.43
AL4825-124	4.91	35.39	245.47	208.47	35.45	66.12	67.26	74.99	15.54	15.90	258.98	24.35	134.14	26.69	0.15	183.57	14.26	31.30	4.12	17.25	4.11	1.38	0.75	4.47	4.31	0.88	2.45	0.37	2.18	0.33	3.12	1.63	0.97	1.58	0.49
AL4825-125	5.04	36.04	252.85	212.77	36.63	68.92	72.91	77.14	15.75	16.25	262.80	24.98	137.03	27.28	0.15	188.64	14.55	32.10	4.19	17.58	4.19	1.41	0.76	4.49	4.44	0.91	2.50	0.38	2.16	0.37	3.23	1.73	2.76	1.61	0.50
AL4826-126	5.11	36.34	249.70	178.08	37.08	75.10	68.15	77.63	15.85	16.10	267.27	25.01	135.71	26.94	0.16	188.98	14.56	31.83	4.13	17.41	4.20	1.41	0.76	4.55	4.35	0.91	2.47	0.38	2.17	0.35	3.18	1.72	0.98	1.58	0.48
AL4826-127	5.28	38.24	261.32	134.62	39.07	49.56	68.86	81.22	15.47	13.91	235.66	25.09	118.47	22.04	0.15	161.02	12.05	27.03	3.56	15.13	3.82	1.32	0.75	4.34	4.31	0.91	2.47	0.39	2.38	0.36	2.80	1.40	0.85	1.30	0.39
AL4826-128	5.57	38.48	267.40	139.41	38.95	52.21	70.28	83.80	15.91	14.52	242.73	26.29	125.90	23.48	0.14	167.38	12.70	28.32	3.75	16.15	3.99	1.38	0.80	4.60	4.62	0.95	2.60	0.41	2.50	0.38	3.01	1.47	0.87	1.35	0.41
AL4826-129	3.21	39.22	202.87	296.15	42.43	102.92	106.58	63.81	12.40	9.36	232.69	16.74	80.51	15.66	0.09	110.62	8.33	18.75	2.47	10.43	2.66	0.97	0.53	3.06	3.00	0.62	1.66	0.25	1.56	0.23	1.92	0.98	0.57	0.89	0.29
AL4826-131	3.35	38.65	204.75	286.21	42.01	100.45	103.56	63.81	12.40	9.36	232.69	16.74	80.51	15.66	0.09	110.62	8.33	18.75	2.47	10.43	2.66	1.01	0.55	3.18	3.15	0.65	1.74	0.26	1.58	0.24	2.03	1.06	0.58	0.94	0.31
AL4826-132	4.66	37.91	232.59	232.50	42.38	119.78	76.79	74.10	13.67	10.87	217.39	23.36	109.77	18.11	0.10	121.65	10.15	23.01	3.11	13.44	3.44	1.18	0.69	3.94	4.07	0.87	2.31	0.36	2.18	0.34	2.56	1.12	0.67	1.08	0.33
AL4826-133	4.60	37.80	229.70	231.67	42.32	116.31	77.51	73.25	13.67	10.88	215.23	23.19	109.13	18.10	0.10	120.52	10.16	22.87	3.07	13.49	3.40	1.17	0.69	3.96	4.01	0.85	2.32	0.37	2.24	0.33	2.59	1.11	0.67	1.07	0.34
AL4826-134	4.35	37.00	224.31	264.16	42.39	123.92	76.76	70.63	12.85	9.51	204.74	22.07	99.77	16.26	0.09	107.13	9.12	20.79	2.83	12.00	3.14	1.11	0.65	3.66	3.83	0.81	2.17	0.35	2.13	0.32	2.33	0.99	0.63	0.97	0.32
AL4826-135	4.65	37.79	229.50	235.92	42.05	120.16	76.21	73.65	13.46	10.62	211.06	22.97	107.64	17.95	0.09	116.74	9.94	22.74	3.02	13.11	3.34	1.18	0.69	3.85	4.01	0.84	2.31	0.37	2.20	0.33	2.53	1.11	0.98	1.07	0.34
AL4952-299	3.01	48.0	189	394	51.4	126	133	66	10.8	1.10	116	16.9	24.0	2.02	0.014	16.0	1.64	4.18	0.68	3.54	1.30	0.61	0.394	1.92	0.280	0.628	1.83	0.287	1.82	0.285	0.80	0.129	0.156	0.15	0.047
AL4952-303	5.61	38.3	277	135	40.6	62	83	71	15.7	10.45	238	19.9	86.8	1.31	0.132	140.3	11.17	23.68	3.11	13.21	3.22	1.14	0.590	3.61	3.62	0.740	2.04	0.304	1.91	0.287	2.11	0.002	0.764	1.19	0.354
AL4958-393	5.93	39.8	291	56	43.0	37	72	89	17.5	11.50	217	26.5	110.4	20.91	0.146	155.5	12.47	26.32	3.49	15.14	3.85	1.37	0.746	4.45	4.67	0.974	2.74	0.410	2.57	0.391	2.79	1.205	0.846	1.31	0.381
AL4822-064	3.15	25.32	204.20	288.42	45.33	200.02	91.19	87.70	11.26	1.60	162.49	17.20	57.33	3.67	0.02	23.63	2.39	6.35	1.07	5.78	2.20	0.90	0.54	2.97	3.12	0.63	1.62	0.25	1.42	0.21	1.68	0.24	0.20	0.19	0.07
AL4822-066	3.16	25.98	178.64	289.13	44.98	199.10	89.50	87.59	11.24	1.60	161.78	17.15	57.47	3.67	0.02	24.02	2.40	6.40	1.06	6.00	2.26	0.90	0.53	3.04	3.15	0.63	1.65	0.25	1.44	0.22	1.66	0.24	0.20	0.19	0.07
AL4948-232	2.92	37.94	119.02	551.38	47.03	145.52	119.54	67.38	11.95	3.88	146.18	17.18	47.94	7.46	0.05	55.14	4.71	10.48	1.46	6.72	1.96	0.79	0.46	2.62	2.98	0.462	1.75	0.27	1.72	0.26	1.83	0.44	0.33	0.46	0.13
AL4950-255	8.284	37.274	212.056	425.065	43.316	126.895	78.433	66.397	10.558	6.557	140.357	21.694	81.200	10.830	0.063	75.520	6.501	15.357	2.177	9.773	2.649	0.987	0.571	3.696	3.772	0.790	2.252	0.363	2.016	0.326	2.056	0.707	0.497	0.617	0.190
AL4950-256	6.617	37.885	221.101	442.195	45.474	123.826	79.098	67.443	10.972	6.879	148.156	22.401	84.781	11.264	0.069	79.899	7.023	16.570	2.297	10.294	2.831	1.013	0.600	3.854	3.883	0.820	2.308	0.372	2.153	0.345	2.089	0.730	0.668	0.656	0.217
AL4950-257	7.280	37.963	213.897	452.519	44.214	127.144	81.339	66.623	10.656	6.408	145.220	21.357	79.384	10.428	0.064	75.028	6.299	14.836	2.119	9.671	2.649	0.971	0.576	3.611	3.697	0.783	2.217	0.346	2.047	0.320	1.947	0.679	0.501	0.580	0.186
AL4950-258	5.262	40.050	224.944	479.738	46.363	133.613	84.180	70.142	11.334	6.753	154.658	22.721	84.650	11.047	0.067	78.810	6.622	15.865	2.236	10.110	2.780	1.006	0.599	3.677	3.902	0.809	2.332	0.366	2.190	0.351	2.068	0.683	0.509	0.625	0.182
AL4950-259	4.34	38.49	235.14	326.36	44.84	124.02	83.42	69.58	13.77	6.01	156.88	22.62	83.85	10.69	0.07	81.42	7.06	16.22	2.21	10.19	2.79	1.03	0.62	3.62	3.89	0.82	2.34	0.36	2.14	0.32	1.97	0.49	0.57	0.66	0.19
AL4950-260	3.804	39.22	223.423	462.961	45.145	122.502	85.013	69.820	11.289	6.781	152.602	22.502	85.083	10.905	0.065	83.785	6.883	15.827	2.233	10.080	2.760	1.004	0.582	3.785	3.926	0.801	2.392	0.364	2.151	0.342	2.087	0.715	0.529	0.651	0.209
AL4950-262	12.798	32.258	343.104	54.727	32.610	33.969	188.411	97.255	19.221	15.248	395.728	25.304	95.358	2.045	0.932	230.451	7.743	20.163	3.140	14.998	4.025	1.246	0.757	4.414	4.407	0.912	2.462	0.385	2.351	0.358	2.705	0.136	4.784	1.201	0.447
AL4950-263	10.181	34.835	280.168	395.117	38.302	106.962	67.741	74.012	14.121	12.901	224.652	23.372	122.950	21.902	0.130	147.820	12.099	27.037	3.607	15.626	3.876	1.272	0.735	4.383	4.179	0.883	2.406	0.367	2.139	0.327	2.837	1.371	0.805	1.275	0.357
AL4950-264	6.948	35.224	282.789	382.313	38.306	105.014	67.061	73.738	14.165	12.913	227.924	23.876	123.399	22.097	0.129	148.925	12.245	27.076	3.629	15.654	3.797	1.261	0.743	4.356	4.249	0.878	2.456	0.367	2.211	0.340	2.967	1.436	0.853	1.283	0.380
AL4959-403	9.589	31.983	126.299	403.215	41.754	132.083	98.845	56.545	7.271	1.302	94.311	14.203	27.133	2.433	0.015	16.835	1.661	4.226	0.638	3.219	1.178	0.559	0.312	2.145	2.447	0.505	1.449	0.240	1.401	0.224	0.779	0.151	0.147	0.130	0.047
AL4959-404	3.17	38.08	166.11	349.69	50.66	160.19	118.06	68.03	10.87	1.39	122.53	17.15	33.09	2.72	0.02	20.40	2.08	5.20	0.78	4.05	1.47	0.67	0.42	2.28	2.85	0.62	1.83	0.29	1.73	0.26	0.92	0.15	0.16	0.17	0.07
AL4959-410	10.586	31.476	334.012	53.675	31.770	32.988	178.207	95.282	18.583	14.959	385.557	24.641	92.829	1.981	0.896	221.214	7.511	19.681	3.037	14.469	3.898	1.216	0.736	4.375	4.283	0.871	2.415	0.377	2.307	0.361	2.581	0.130	4.677	1.129	0.441
AL4959-412	4.33	38.41	235.26	168.69	40.60	68.47	81.50	71.30	16.31	9.79	245.47	20.85	98.46	18.32	0.12	135.11	9.45	20.09	3.14	12.90	3.20	1.17	0.62	3.72	3.65	0.74	2.09	0.31	1.89	0.29	2.25	0.84	0.71	1.12	0.34
AL4959-415	11.069	36.669	218.357	199.132	37.356	56.833	75.815	70.715	13.166	10.935	218.280	21.424	100.217	18.683	0.111	130.874	10.287	22.655	3.068	13.177	3.250	1.180	0.641	3.773	3.897	0.796	2.173	0.335	1.937	0.310	2.458	1.143	0.720	1.055	0.345
AL4959-416	4.96	36.28	255.25	293.41	39.73	102.93	66.70	75.96	17.15	10.05	229.68	24.25	117.08	19.60	0.13	142.59	11.93	26.25	3.40	14.91	3.69	1.29	0.72	4.28	4.34	0.88	2.46	0.37	2.26	0.34	2.69	0.90	0.78	1.20	0.35
AL4948-233b	3.59	37.6	199	387	48.8	141	115	65	12.6	3.54	160	16.7	92.834	6.92	0.047	50.7	4.38	9.70	1.37	6.29	1.85	0.76	0.444	2.41	2.92	0.620	1.76	0.268	1.68	0.255	1.26	0.411	0.320	0.47	0.139
AL4948-233b	3.70	39.1	204	343	46.6	150	117	64	12.8	4.40	156	18.4	45.1	8.74	0.060	59.3	5.42	11.38	1.60	7.18	2.00	0.79	0.475	2.57	3.13	0.681	1.95	0.300	1.91	0.292	1.40	0.516	0.380	0.56	0.159
AL4959-414	3.31	26.0	151	95	24.7	39	48	45	9.9	5.86	156	13.3	53.4	11.35	0.077	79.4	7.12	14.55	1.98	8.57	2.12	0.75	0.397	2.41	2.41	0.495	1.37	0.203	1.26	0.189	1.51	0.663	0.463	0.75	0.212
AL4822-067	4.12	26.4	176	338	46.3	198	89	87	13.8	1.38	163	16.7	47.7	3.67	0.018	21.4	2.52	6.20	1.07	5.88	2.29	0.93	0.514	2.86	3.14	0.628	1.68	0.242	1.47	0.215	1.68	0.226	0.212	0.22	0.063
AL4959-413	4.79	38.3	246	170	39.0	66	78	73	15.6	9.35	245	20.5	96.2	18.47	0.125	123.6	10.98	23.64	3.06	13.22	3.31	1.18	0.614	3.70	3.72	0.768	2.10	0.315	1.66	0.291	2.35	1.072	0.754	1.14	0.347
AL4959-421	5.12	35.8	254	47	39.6	45	82	79	17.6	13.04	277	22.1	113.3	24.27	0.174	170.2	14.12	28.47	3.61	16.02	3.82	1.33	0.677	4.20	4.03	0.825	2.27	0.316	2.10	0.314	2.74	1.402	0.928	1.52	0.452
AL4822-065	4.23	26.5	178	357	46.0	203	90	87	13.8	1.50	163	16.9	48.0	3.90	0.020	22.7	2.67	6.46	1.10	6.03	2.30	0.94	0.514	2.87	3.16	0.639	1.69	0.247	1.49	0.219	1.69	0.293	0.257	0.23	0.069
AL4959-405	3.16	36.4	170	330	50.5	147	110	65	11.5	1.42	125	15.9	26.9	2.94	0.019	19.7	2.14	4.98	0.79	3.98	1.45	0.65	0.396	1.99	2.69	0.591	1.70	0.262	1.67	0.256	0.94	0.193	0.179	0.19	0.067
AL4950-260	4.80	38.8	243	330	47.3	124	81	70	13.9	5.58	166	21.7	67.1	10.43	0.071	72.0	6.84	14.98	2.17	9.91	2.80	1.02	0.594	3.36	3.80	0.810	2.28	0.349	2.17	0.327	2.02	0.730	0.541	0.67	0.199

sample	Li	Sc	V	Cr	Co	Ni	Cu	Zn	Ga	Rb	Sr	Y	Zr	Nb	Cs	Ba	La	Ce	Pr	Nd	Sm	Eu	Tb	Gd	Dy	Ho	Er	Tm	Yb	Lu	Hf	Ta	Pb	Th	U
AL4818-001	6.16	34.35	250.39	244.00	41.85	116.75	71.09	81.65	14.83	12.90	274.90	29.19	150.68	24.71	0.12	146.64	13.01	29.81	4.06	17.79	4.52	1.53	0.89	5.08	5.13	1.05	2.83	0.43	2.59	0.40	3.58	1.49	0.83	1.33	0.43
AL4818-002	6.33	34.98	254.61	248.10	43.75	135.67	71.50	85.54	14.88	13.21	275.45	29.83	153.94	24.86	0.13	149.69	13.24	30.08	4.17	18.18	4.61	1.57	0.92	5.33	5.23	1.09	2.91	0.45	2.74	0.42	3.68	1.53	0.83	1.35	0.44
AL4818-003	6.32	35.93	260.15	239.83	41.66	105.70	75.53	83.87	14.95	13.18	252.66	30.33	151.81	24.34	0.13	149.61	12.97	29.57	4.06	17.96	4.55	1.56	0.92	5.35	5.20	1.12	2.99	0.46	2.77	0.44	3.62	1.47	0.88	1.32	0.43
AL4818-004	4.71	39.32	224.42	291.28	42.74	103.83	91.43	65.04	11.28	6.66	159.20	22.31	82.29	11.48	0.07	79.02	6.61	15.52	2.18	9.86	2.74	1.02	0.62	3.64	3.80	0.83	2.28	0.35	2.15	0.35	2.15	0.71	0.50	0.66	0.21
AL4818-005	4.35	41.24	219.18	308.92	44.29	106.97	98.95	65.18	11.39	6.54	166.32	21.54	77.05	11.09	0.06	77.94	6.45	14.95	2.07	9.43	2.66	0.98	0.60	3.50	3.62	0.80	2.18	0.33	2.06	0.33	1.97	0.68	0.49	0.63	0.19
AL4818-006	4.17	39.34	205.54	331.30	41.17	102.99	96.98	65.00	10.05	6.21	163.56	20.22	74.20	10.94	0.07	72.53	6.17	14.12	2.01	8.85	2.46	0.91	0.55	3.04	3.37	0.72	1.98	0.33	1.88	0.31	1.82	0.53	0.42	0.59	0.18
AL4818-007	4.66	38.26	214.01	315.76	40.94	103.87	88.68	67.81	10.21	6.26	159.69	21.84	79.72	11.23	0.06	73.33	6.31	14.78	2.13	9.44	2.61	0.96	0.59	3.30	3.71	0.79	2.14	0.35	2.06	0.34	1.96	0.55	0.44	0.61	0.19
AL4818-008	3.93	43.06	197.59	352.01	43.76	102.71	110.38	64.80	9.81	6.02	160.64	20.01	66.86	10.43	0.07	70.12	5.74	13.21	1.85	8.06	2.32	0.86	0.54	2.94	3.33	0.71	1.95	0.33	1.91	0.31	1.66	0.51	0.38	0.55	0.17
AL4818-009	3.05	44.57	212.16	282.97	45.95	101.76	124.81	70.28	11.32	6.44	164.06	20.99	69.17	10.76	0.07	75.83	6.12	14.11	1.96	8.99	2.47	0.91	0.58	3.18	3.60	0.76	2.15	0.34	2.02	0.32	1.74	0.67	0.49	0.62	0.21
AL4818-010	4.55	42.87	228.76	320.05	45.62	104.91	105.66	66.66	11.76	6.82	171.64	21.85	79.41	11.53	0.07	82.02	6.74	15.61	2.17	9.95	2.74	1.02	0.62	3.60	3.71	0.80	2.22	0.34	2.11	0.35	2.11	0.72	0.55	0.67	0.21
AL4818-011	4.70	40.26	254.20	169.43	41.88	78.25	102.26	80.61	14.48	11.80	218.31	25.68	111.59	19.64	0.13	140.73	10.94	24.35	3.26	14.04	3.66	1.26	0.74	4.21	4.37	0.93	2.62	0.41	2.42	0.37	2.61	1.23	0.74	1.16	0.38
AL4818-012	5.42	41.19	265.66	132.97	41.75	64.66	92.17	79.05	14.77	12.69	217.35	26.95	117.40	20.68	0.13	150.46	11.53	25.92	3.41	15.04	3.75	1.32	0.80	4.55	4.61	0.98	2.68	0.40	2.53	0.41	2.86	1.26	0.81	1.21	0.36
AL4819-014	5.30	39.55	247.44	168.24	39.44	70.09	87.93	77.87	13.18	12.02	216.86	25.23	114.42	20.61	0.13	139.51	11.05	24.58	3.35	13.99	3.56	1.25	0.73	4.14	4.32	0.91	2.48	0.41	2.36	0.39	2.67	1.00	0.72	1.13	0.35
AL4819-015	5.31	39.82	252.99	141.19	38.95	62.04	90.52	79.72	13.30	12.53	220.67	25.84	118.23	21.00	0.13	145.49	11.44	25.63	3.50	14.58	3.73	1.27	0.75	4.26	4.49	0.94	2.53	0.42	2.41	0.39	2.75	1.04	0.72	1.18	0.36
AL4819-016	5.12	39.93	241.24	166.12	39.78	67.86	91.10	77.25	12.71	11.40	211.78	24.69	107.19	19.26	0.12	133.80	10.27	23.04	3.13	13.35	3.42	1.19	0.70	4.00	4.17	0.87	2.43	0.40	2.31	0.37	2.52	0.94	0.63	1.07	0.32
AL4819-017	5.10	39.86	245.43	169.12	40.01	64.23	87.39	77.92	13.02	11.72	217.39	25.28	109.69	19.70	0.12	137.63	10.60	23.67	3.23	13.43	3.49	1.23	0.71	4.04	4.29	0.90	2.47	0.41	2.32	0.38	2.56	0.97	0.65	1.08	0.33
AL4818-018	5.33	36.40	239.60	148.03	37.59	53.86	75.28	78.70	13.75	13.39	225.91	24.75	119.07	20.70	0.14	154.37	11.33	25.26	3.45	14.43	3.65	1.27	0.73	4.14	4.24	0.87	2.34	0.39	2.18	0.36	2.79	0.99	0.69	1.14	0.35
AL4819-019	4.22	33.09	199.44	35.11	37.96	44.18	76.67	74.01	14.16	16.46	228.07	22.47	127.19	27.34	0.16	176.92	14.11	29.41	3.66	15.38	3.41	1.26	0.64	3.71	4.00	0.92	2.21	0.33	1.91	0.29	2.75	1.30	1.10	1.60	0.54
AL4819-020	5.43	36.16	239.91	51.19	41.22	45.29	86.99	79.95	16.29	16.90	264.13	23.98	121.96	25.85	0.17	186.69	13.93	29.76	3.85	15.99	3.74	1.28	0.72	4.20	4.17	0.87	2.36	0.36	2.19	0.33	2.82	1.23	1.03	1.56	0.47
AL4819-021	5.27	36.15	236.44	75.23	41.70	53.95	95.55	80.54	16.16	16.77	261.63	23.62	122.95	25.69	0.17	184.72	14.06	29.83	3.86	16.14	3.76	1.31	0.72	4.20	4.20	0.86	2.33	0.36	2.20	0.32	2.92	1.25	1.04	1.53	0.48
AL4819-022	5.36	36.37	241.93	132.39	37.15	50.25	75.80	79.92	13.72	13.59	222.39	24.90	119.96	21.10	0.14	156.23	11.46	25.70	3.52	14.54	3.72	1.28	0.75	4.28	4.31	0.90	2.39	0.39	2.22	0.36	2.83	1.03	0.70	1.16	0.36
AL4819-023	5.27	36.59	235.49	47.99	41.32	44.49	92.72	80.36	16.22	17.01	265.85	23.53	121.68	25.99	0.17	188.07	14.04	30.01	3.85	16.13	3.68	1.29	0.71	4.19	4.15	0.86	2.32	0.36	2.16	0.32	2.80	1.26	1.08	1.56	0.49
AL4819-024	5.29	37.81	240.21	157.40	38.82	62.57	79.62	80.31	14.15	13.32	219.70	24.58	116.73	20.37	0.12	151.63	11.20	25.05	3.45	14.70	3.70	1.26	0.74	4.25	4.34	0.89	2.38	0.38	2.25	0.36	2.76	1.01	0.81	1.17	0.36
AL4819-025	5.02	39.43	244.34	153.66	40.13	56.03	86.94	79.44	14.82	12.96	224.57	23.95	109.68	19.69	0.12	151.85	11.08	24.50	3.26	14.22	3.56	1.25	0.72	4.14	4.25	0.88	2.37	0.36	2.20	0.32	2.66	0.95	0.78	1.12	0.35
AL4819-026	5.11	39.41	245.92	153.52	40.70	60.74	84.41	76.50	14.86	13.15	226.73	24.18	113.02	20.31	0.13	154.48	11.14	24.84	3.33	14.28	3.56	1.25	0.70	4.20	4.23	0.88	2.40	0.37	2.22	0.34	2.68	1.23	0.74	1.14	0.34
AL4819-027	5.37	39.06	252.87	140.11	39.97	56.83	84.09	84.39	15.51	14.03	228.49	25.85	120.49	21.02	0.14	161.27	11.84	26.26	3.50	15.35	3.85	1.35	0.78	4.45	4.57	0.96	2.57	0.39	2.37	0.36	2.90	1.02	0.87	1.23	0.39
AL4819-028	5.19	37.00	239.79	161.91	37.64	58.49	84.22	79.50	14.11	13.14	220.12	24.36	115.44	20.36	0.12	152.74	11.25	25.06	3.42	14.55	3.62	1.26	0.74	4.20	4.31	0.88	2.42	0.38	2.24	0.36	2.76	0.99	0.79	1.16	0.38
AL4819-029	4.49	36.13	227.77	317.66	39.19	110.73	77.33	64.32	12.93	10.12	201.99	20.20	97.06	17.07	0.10	119.17	9.52	21.36	2.86	12.53	3.08	1.07	0.65	3.58	3.54	0.75	2.07	0.30	1.88	0.30	2.42	1.03	0.64	0.95	0.29
AL4819-030	4.06	40.52	199.21	388.40	42.68	104.00	114.02	70.69	10.66	6.45	174.10	19.49	71.33	11.23	0.06	76.49	6.28	14.34	2.02	9.04	2.46	0.93	0.55	3.08	3.40	0.72	1.98	0.31	1.91	0.29	1.78	0.56	0.46	0.65	0.21
AL4819-031	4.38	39.56	210.51	344.87	40.13	88.89	108.22	71.93	11.41	8.02	191.13	20.79	86.54	14.20	0.06	92.98	7.83	17.60	2.47	10.84	2.83	1.02	0.60	3.42	3.65	0.76	2.09	0.34	2.01	0.32	2.11	0.71	0.55	0.83	0.25
AL4820-032	3.53	43.57	188.16	355.77	46.58	123.57	116.47	64.28	9.30	4.43	139.68	19.06	54.39	8.05	0.02	53.65	4.52	10.24	1.47	6.83	1.97	0.78	0.50	2.68	3.22	0.69	1.90	0.31	1.91	0.31	1.41	0.40	0.31	0.45	0.15
AL4820-033	4.25	41.35	204.06	330.72	44.25	113.36	103.02	69.94	10.66	6.77	171.36	21.90	81.41	12.69	0.04	78.67	6.91	15.60	2.19	9.85	2.69	0.99	0.60	3.33	3.75	0.80	2.22	0.36	2.12	0.34	2.00	0.63	0.43	0.71	0.23
AL4820-034	3.69	44.69	194.71	353.63	44.47	99.77	119.84	65.65	9.50	4.65	139.38	19.80	58.39	8.69	0.02	56.93	4.85	11.06	1.58	7.27	2.13	0.82	0.52	2.87	3.35	0.73	2.03	0.34	2.02	0.32	1.50	0.44	0.30	0.49	0.15
AL4820-035	6.09	35.56	241.72	265.39	40.25	111.13	73.11	86.43	13.85	12.72	247.77	28.78	145.92	24.05	0.09	141.06	12.76	28.83	4.01	17.35	4.33	1.45	0.87	4.98	5.10	1.04	2.88	0.45	2.66	0.42	3.42	1.17	0.74	1.31	0.43
AL4820-036	6.12	35.58	242.48	265.47	40.79	116.13	66.11	87.18	13.88	12.64	247.59	28.98	147.69	24.21	0.08	139.43	12.78	28.75	3.99	17.48	4.41	1.47	0.86	5.06	5.13	1.04	2.84	0.45	2.65	0.42	3.43	1.18	0.74	1.31	0.45
AL4820-037	6.26	38.02	251.95	261.84	42.34	122.17	67.77	89.09	14.66	13.19	259.04	29.59	147.74	24.16	0.13	145.61	12.92	29.64	4.08	17.55	4.44	1.50	0.88	5.14	5.16	1.05	2.90	0.46	2.70	0.41	3.53	1.18	0.83	1.35	0.44
AL4820-038	6.14	37.35	252.49	273.18	42.03	127.63	71.24	85.80	15.15	14.29	257.22	29.87	144.93	24.46	0.13	161.49	12.86	29.30	4.02	17.41	4.44	1.49	0.90	5.24	5.30	1.09	2.98	0.47	2.78	0.43	3.48	1.18	0.82	1.40	0.44
AL4820-039	6.39	37.16	259.26	263.03	41.71	116.76	68.51	90.72	15.28	14.62	256.55	31.12	148.44	24.98	0.14	163.49	13.31	30.02	4.13	17.81	4.57	1.51	0.92	5.37	5.48	1.12	3.10	0.48	2.93	0.44	3.62	1.22	0.88	1.42	0.44
AL4820-040	6.20	36.25	247.39	287.49	41.65	124.39	65.28	86.51	14.52	14.56	258.03	29.84	146.11	24.68	0.13	167.84	13.07	29.53	4.05	17.60	4.56	1.50	0.90	5.20	5.24	1.10	2.99	0.48	2.84	0.45	3.48	1.18	0.98	1.44	0.45
AL4820-041(	6.06	36.50	275.26	279.21	42.02	114.71	68.48	87.90	19.18	13.14	265.52	30.58	207.11	24.96	0.15	171.72	14.06	30.65	4.03	18.01	4.64	1.55	0.89	5.32	5.31	1.08	3.05	0.47	2.80	0.43	3.42	1.27	0.91	1.49	0.44
AL4820-041	6.14	37.32	257.78	285.23	40.85	107.62	72.39	87.85	15.72	14.70	268.91	30.27	146.53	24.79	0.14	168.67	13.13	29.58	4.00	17.47	4.48	1.49	0.91	5.26	5.32	1.09	2.99	0.46	2.80	0.42	3.53	1.18	0.96	1.42	0.45
AL4820-041E	6.32	36.36	272.63	281.28	40.30	103.02	68.51	86.89	19.36	13.31	283.59	31.23	215.98	24.85	0.16	176.50	14.25	31.03	4.04	17.81	4.51	1.56	0.90	5.40	5.42	1.12	3.08	0.47	2.79	0.43	3.46	1.18	0.88	1.52	0.53
AL4820-042	6.02	36.58	270.38	279.11	43.16	125.31	69.95	87.99	19.21	13.58	267.34	30.46	206.00	24.80	0.15	171.32	14.00	30.49	3.96	17.66	4.54	1.53	0.89	5.33	5.33	1.08	3.01	0.47	2.76	0.42	3.48	1.28	0.95	1.50	0.44
AL4820-042	6.09	36.69	249.55	287.46	41.47	117.76	70.43	86.19	15.10	14.51	260.72	29.88	143.26	24.67	0.13	163.29	12.99	29.27	4.00	17.45	4.49	1.49	0.89	5.21	5.30	1.08	2.96	0.46	2.76	0.43	3.46	1.19	0.80	1.39	0.44
AL4820-043	6.17	36.24	252.21	267.77	42.21	125.48	64.22	86.64	14.84	14.18	250.02	30.63	145.71	24.10	0.13	159.02	12.96	29.18	4.02	17.41	4.43	1.46	0.90	5.21	5.30	1.09	3.04	0.47	2.81	0.43	3.50	1.17	0.81	1.36	0.43
AL4820-044	4.46	25.41	247.95	348.27	45.49	167.52	71.63	76.35	10.64	4.34	122.00	19.48	95.36	10.68	0.04	59.37	4.91	13.45	1.79	8.59	2.39	0.86	0.58	3.24	3.38	0.73	2.02	0.30	1.88	0.31	2.46	0.64	0.52	0.41	0.18
AL4820-045	5.62	37.68	245.56	384.94	43.90	152.69	71.93	79.49	10.66	5.50	138.18	28.03	101.72	10.78	0.04	59.40	6.62	16.56	2.46	11.08	3.31	1.12	0.77	4.32	4.72	1.00	2.79	0.45	2.70	0.42	2.54	0.52	0.42	0.59	0.18
AL4820-046	5.72	37.83	244.47	388.12	44.60	157.89	73.63	80.31	10.52	5.46	137.52	28.15	101.31	10.76	0.03	58.69	6.63	16.47	2.41	10.93	3.21	1.13	0.77	4.23	4.75	0.98	2.80	0.45	2.72	0.42	2.52	0.52	0.39	0.59	0.18
AL4820-047	5.65	36.89	252.40	361.57	44.80	159.47	70.82	75.42	11.38	5.53	139.46	27.49	99.72	10.13	0.05	64.46	6.44	16.01	2.32	11.10	3.24	1.15	0.78	4.37	4.62	1.02	2.76	0.42	2.60	0.41	2.54	0.61	0.60	0.57	0.18
AL4821-048	6.09	35.96	252.72	247.21	41.88	117.82	64.57	82.05	14.77	12.35	268.12	29.05	144.10	23.62	0.12	141.81	12.35	28.31	3.91	17.13	4.38	1.49	0.86	5.11	5.05	1.04	2.86	0.44	2.61	0.41	3.42	1.42	0.85	1.29	0.42
AL4821-049	6.22	36.08	249.58	255.81	42.41	126.21	60.54	83.23	14.91	12.77	278.86	29.17	149.40	24.53	0.11	141.45	12.85	29.11	3.95	17.47	4.45	1.52	0.81	5.27	5.08	1.06	2.92	0.45	2.66	0.40	3.49	1.47	0.72	1.29	0.43
AL4821-050	6.41	35.96	259.70	242.78	41.96	109.41	61.52	82.44	14.88	13.29	261.03	30.62	151.89	24.53	0.13	148.37	13.09	29.99	4.12	18.19	4.64	1.53	0.90	5.36	5.39	1.11	3.00	0.47	2.81	0.44	3.64	1.48	0.85	1.34	0.44
AL4821-051	6.32	36.57	259.28	248.98	41.86	107.64	60.49	83.16	15.10	13.26	259.31	30.49	151.79	24.65	0.13	149.88	13.22	30.24	4.18	18.28	4.64	1.55	0.91	5.39	5.39	1.11	3.00	0.48	2.82	0.43	3.60	1.49	0.93	1.38	0.44
AL4821-053	6.52	36.35	259.40	245.21	42.69	117.13	59.08	82.54	14.90	13.24	260.78	30.24	151.99	24.41	0.13	149.18	13.10	29.86	4.10	17.91	4.61	1.54	0.87	5.38	5.32	1.11	3.04	0.46	2.81	0.43	3.58	1.47	0.79	1.36	0.44
AL4821-054	6.25	35.89	255.32	243.96	41.42	109.31	56.12	81.47	14.76	13.14	258.63	30.12	151.44	24.37	0.11	144.38	13.00	29.45	3.99	17.68	4.51	1.51	0.90	5.29	5.41	1.11	3.03	0.46	2.76	0.42	3.46	1.46	0.73	1.32	0.42
AL4821-055	6.46	36.53	258.96	243.93	41.77	108.50	56.62	89.52	15.15	13.24	262.26	30.73	151.76	24.49	0.12	147.36	13.09	29.99	4.08	18.01	4.55	1.52	0.85	5.39	5.40	1.11	3.09	0.47	2.78	0.44	3.62	1.49	0.79	1.34	0.43
AL4821-056	6.26	35.47	255.53	239.19	40.59	103.13	58.80	80.92	14.85	12.94	255.13	30.01	149.74	24.20	0.13	147.24	12.95	29.70	4.05	17.61	4.49	1.49	0.88	5.24	5.23	1.08	2.95	0.47	2.73	0.42	3.55	1.44	0.87	1.32	0.43
AL4821-057	6.34	36.33	261.18	246.72	41.89	109.89	61.98	82.47	14.98	13.24	261.84	30.37	151.32	24.38	0.13	148.27	13.08	29.92	4.14	18.25	4.59	1.51	0.91	5.36	5.32	1.09	3.01	0.48	2.77	0.43	3.55	1.47	0.86	1.34	0.43
AL4821-058	6.36	35.71	252.17	242.02	41.70	112.06	55.32	80.63	14.70	13.08	258.25	30.10	148.30	24.21	0.11	143.32	12.86	28.81	3.96	17.53	4.49	1.48	0.80	5.29	5.33	1.08	3.00	0.46	2.74	0.43	3.50	1.45	0.74	1.31	0.42
AL4821-059	6.31	35.73	256.43	247.80	41.89	113.42	56.86	85.36	15.02	13.24	263.56	30.26	153.22	24.80	0.12	146.70	13.18	29.75	4.08	18.08	4.60	1.52	0.83	5.27	5.41	1.10	3.01	0.47	2.78	0.43	3.60	1.49	0.77	1.36	0.44
AL4943-154	5.81	34.52	254.13	232.27	43.17	109.40	68.97	87.71	17.11	11.70	271.71	29.17	142.07	23.48	0.12	149.04	13.97	31.09	4.03	18.18	4.56	1.55	0.85	5.22	5.28	1.06	2.95	0.43	2.71	0.40	3.46	1.42	1.11	1.39	0.44
AL4943-155	6.08	34.78	255.54	265.19	42.95	115.91	67.94	87.47	17.27	11.80	275.61	29.28	143.68	23.85	0.13	149.74	14.11	31.09	4.06	18.36	4.69	1.54	0.86	5.27	5.27	1.06	2.94	0.44	2.71	0.41	3.52	1.46	0.86	1.41	0.44
AL4943-156	4.94	37.73	240.98	249.33	42.76	104.49	75.22	73.70	14.39	7.87	167.56	24.63	94.76	13.23	0.09	100.56	8.73	19.52	2.61	12.11	3.29	1.17	0.68	4.03	4.32	0.89	2.57	0.39	2.42	0.36	2.44	0.80	0.63	0.83	0.25
AL4943-157	6.32	36.38	269.19	233.07	41.07	104.39	64.20	86.78	17.81	13.01	250.84	30.65	140.26	23.68	0.15	167.23	13.97	30.51	3.97	17.93	4.64	1.54	0.89	5.35	5.54	1.11	3.18	0.47	2.91	0.44	3.51	1.44	0.88	1.44	0.43
AL4943-159	6.21	36.08	265.18	229.16	40.84	106.49	62.43	86.07	17.69	12.88	248.85	30.58	139.96	23.52	0.13	166.13	13.93	30.22	3.97	17.73	4.55	1.55	0.87	5.31	5.49	1.12	3.15	0.48	2.85	0.43	3.50	1.43	0.87	1.45	0.43
AL4945-187	5.08	35.97	243.06	580.00	44.52	165.87	73.44	80.05	12.96	4.77	132.04	26.33	93.17	9.89	0.05	63.13	6.86	16.18	2.24	10.94	3.28	1.14	0.71	4.17	4.65	0.95	2.69	0.41	2.61	0.39	2.47	0.62	0.52	0.61	0.19
AL4945-189	5.14	35.52	238.10	586.47	44.87	169.40	73.91	77.13	12.86	4.70	130.95	25.92	89.40	9.60	0.05	61.48	6.69	15.89	2.20	10.67	3.15	1.11	0.69	4.10	4.50	0.94	2.71	0.41	2.54	0.39	2.40	0.61	0.50	0.60	0.18
AL4945-194	5.42	37.15	255.49	511.90	44.33	145.90	73.73	79.83	13.14	5.17	133.43	28.07	97.51	10.30	0.06	66.12	7.23	17.08	2.34	11.42	3.35	1.16	0.73	4.25	4.82	1.00	2.86	0.44	2.73	0.41	2.54	0.64	0.51	0.63	0.19
AL4945-195	5.34	36.94	255.59	516.25	44.70	148.02	74.07	80.00	13.30	5.17	132.44	27.69	96.65	10.29	0.06	66.28	7.18	16.89	2.36	11.40	3.33	1.16	0.74	4.34	4.77	1.00	2.90	0.44	2.73	0.41	2.53	0.64	0.52	0.64	0.19
AL4945-198	5.70	34.87	256.80	241.94	42.07	115.05	64.59	86.42	17.79	13.20	280.67	29.50	141.86	24.78	0.15	170.08	14.63	31.83	4.12	18.47	4.64	1.57	0.87	5.25	5.30	1.06	3.02	0.45	2.72	0.42	3.53	1.54	0.89	1.49	0.46
AL4946-199	6.17	35.82	259.74	268.30	42.90	118.91	64.95	88.47	18.13	13.45	277.46	29.65	144.09	25.82	0.15	172.77	14.80	31.80	4.21	18.67	4.67	1.57	0.87	5.22	5.21	1.05	2.95	0.45	2.73	0.41	3.45	1.52	0.89	1.48	0.46
AL4946-200	6.10	35.68	257.19	267.90	43.01	123.57	66.50	95.69	17.93	13.42	278.95	29.47	143.00	25.85	0.14	173.56	14.83	32.00	4.21	18.82	4.72	1

sample	Li	Sc	V	Cr	Co	Ni	Cu	Zn	Ga	Rb	Sr	Y	Zr	Nb	Cs	Ba	La	Ce	Pr	Nd	Sm	Eu	Tb	Gd	Dy	Ho	Er	Tm	Yb	Lu	Hf	Ta	Pb	Th	U
AU955:128	4.98	37.37	254.16	205.19	38.37	65.90	75.89	79.99	17.92	11.28	248.75	24.15	117.28	21.16	0.14	152.22	12.61	27.26	3.47	15.27	3.74	1.33	0.72	4.33	4.27	0.86	2.38	0.35	2.17	0.32	2.64	0.97	0.80	1.24	0.38
AU955:305	3.63	34.25	211.50	404.86	42.93	128.05	102.05	66.11	12.28	4.37	152.29	16.74	58.82	7.99	0.05	58.23	5.17	11.78	1.62	7.41	2.14	0.80	0.46	2.72	2.92	0.60	1.71	0.26	1.51	0.24	1.44	0.37	0.36	0.48	0.14
AU955:308	4.56	33.70	221.75	322.61	40.01	102.62	83.87	78.28	14.67	9.74	257.70	23.15	133.58	19.74	0.12	127.75	10.51	22.75	3.01	13.57	3.63	1.31	0.70	4.35	4.16	0.82	2.26	0.34	1.97	0.30	2.73	0.91	0.61	1.07	0.35
AU955:309	4.34	33.13	218.25	314.18	41.53	113.39	81.35	77.59	14.69	9.71	256.33	22.79	111.59	19.07	0.11	125.89	10.36	22.45	2.92	13.37	3.61	1.26	0.69	4.16	4.05	0.80	2.20	0.33	1.92	0.29	2.63	0.99	0.59	1.04	0.32
AU955:312	4.63	34.06	226.51	296.85	39.36	93.00	85.50	76.93	15.91	8.67	227.54	22.80	109.08	16.92	0.10	113.37	9.51	20.84	2.77	12.71	3.51	1.27	0.70	4.14	4.11	0.83	2.26	0.34	2.00	0.30	2.55	0.89	0.59	0.95	0.32
AU955:313	4.32	34.51	104.25	374.98	40.96	104.90	86.70	74.38	14.90	8.05	214.85	22.26	98.65	15.55	0.09	105.89	8.92	19.54	2.66	12.41	3.39	1.22	0.68	4.06	4.06	0.80	2.19	0.33	2.04	0.30	2.53	0.89	0.62	0.88	0.27
AU955:315	5.13	37.09	261.73	239.94	39.91	99.64	70.14	75.33	15.76	8.94	190.98	24.92	110.78	16.26	0.11	114.79	10.14	22.33	2.99	13.45	3.55	1.19	0.72	4.16	4.24	0.90	2.35	0.38	2.35	0.36	2.60	0.85	0.69	1.02	0.30
AU955:306	3.98	35.7	220	383	42.9	124	100	66	13.0	4.27	162	16.6	49.8	7.78	0.054	56.1	5.08	11.48	1.62	7.42	2.11	0.81	0.458	2.60	2.93	0.620	1.71	0.259	1.60	0.244	1.47	0.462	0.383	0.51	0.148
AU955:310	4.86	35.3	234	299	40.0	99	81	75	15.3	8.01	221	22.6	99.6	15.74	0.100	104.9	9.18	19.97	2.75	12.40	3.40	1.22	0.670	3.94	4.10	0.836	2.27	0.334	2.08	0.311	2.54	0.894	0.610	0.95	0.296
AU955:311	5.80	36.4	263	285	42.8	132	68	82	15.4	7.92	191	26.1	111.6	15.99	0.103	98.3	10.00	21.57	3.06	13.72	3.73	1.27	0.739	4.32	4.63	0.970	2.73	0.412	2.55	0.385	2.80	0.933	0.696	1.01	0.295
AU955:316	5.62	36.2	259	286	42.7	135	69	80	15.2	7.67	189	25.5	109.8	15.44	0.098	95.1	9.71	20.93	2.98	13.41	3.64	1.24	0.722	4.21	4.56	0.946	2.66	0.402	2.50	0.379	2.74	0.901	0.688	0.99	0.289
AU955:317	5.39	38.1	260	283	41.8	106	74	75	15.1	7.57	186	24.3	98.3	13.77	0.096	94.8	8.76	18.96	2.72	12.29	3.35	1.17	0.680	3.92	4.32	0.901	2.53	0.384	2.39	0.364	2.45	0.800	0.651	0.97	0.264
AU955:318	5.70	36.4	261	288	42.8	133	69	81	15.3	7.73	191	25.9	111.2	15.59	0.102	95.8	9.76	21.14	3.01	13.55	3.65	1.25	0.731	4.29	4.59	0.956	2.69	0.408	2.51	0.381	2.75	0.903	0.699	0.99	0.293
AU955:316	5.44	35.8	254	283	41.6	130	68	80	15.0	7.53	186	25.3	100.0	15.25	0.099	93.6	9.61	20.68	2.93	13.16	3.53	1.22	0.715	4.19	4.50	0.941	2.63	0.393	2.47	0.375	2.69	0.888	0.662	0.95	0.289
AU955:317	5.20	35.7	251	393	44.6	153	73	76	13.5	4.21	144	24.5	90.0	9.03	0.054	53.9	6.15	14.05	2.12	10.04	2.96	1.07	0.664	3.72	4.26	0.901	2.56	0.388	2.44	0.366	2.29	0.529	0.474	0.34	0.168
AU955:318	5.60	36.3	261	272	41.6	122	69	83	15.4	7.99	190	26.0	111.22	16.15	0.105	99.0	10.10	21.74	3.05	13.74	3.65	1.25	0.735	4.29	4.64	0.965	2.69	0.406	2.54	0.384	2.76	0.939	0.890	0.93	0.301
AU955:319	5.59	36.3	262	283	42.0	127	68	81	15.3	7.97	190	25.8	111.6	16.11	0.102	98.7	10.10	21.64	3.05	13.64	3.60	1.25	0.733	4.30	4.60	0.962	2.67	0.400	2.53	0.382	2.78	0.942	0.681	0.93	0.300
AU955:321	5.41	37.85	270.56	229.60	40.05	98.60	64.72	76.73	14.13	8.70	181.65	27.35	115.70	16.22	0.10	107.29	9.75	22.18	2.96	13.49	3.68	1.24	0.75	4.38	4.67	0.94	2.72	0.41	2.58	0.38	2.86	0.74	0.65	0.93	0.28
AU955:322	5.78	38.89	279.58	236.42	42.40	101.29	66.66	83.63	15.65	8.92	188.25	28.10	144.53	16.20	0.10	112.35	10.14	22.70	3.06	14.11	3.77	1.30	0.76	4.55	4.84	0.99	2.84	0.42	2.68	0.39	2.74	0.74	0.69	0.98	0.29
AU955:323	5.72	38.24	260.29	236.36	42.01	101.73	66.67	82.33	15.33	8.67	184.79	27.84	117.47	16.15	0.10	110.99	9.94	22.53	3.03	13.89	3.79	1.29	0.77	4.54	4.79	1.00	2.84	0.42	2.65	0.40	2.78	0.80	0.68	0.97	0.28
AU955:324	7.04	40.17	265.77	172.17	44.16	87.84	66.53	90.35	14.50	6.76	134.25	32.32	110.35	12.28	0.07	82.64	8.47	19.88	2.82	13.27	3.89	1.33	0.87	4.99	5.49	1.15	3.33	0.51	3.18	0.48	2.92	0.71	0.64	0.78	0.22
AU955:326	5.43	37.66	266.91	234.80	42.97	113.46	66.58	80.67	14.05	8.56	160.22	26.51	112.83	15.71	0.10	105.46	9.43	21.42	2.86	12.89	3.57	1.25	0.73	4.36	4.53	0.92	2.65	0.40	2.54	0.36	2.55	0.74	0.63	0.92	0.27
AU955:327	5.85	37.92	279.44	232.07	42.41	108.17	65.78	84.83	13.69	9.23	193.42	28.19	149.76	17.03	0.11	114.96	10.50	23.78	3.19	14.53	3.90	1.32	0.77	4.64	4.92	1.01	2.91	0.42	2.67	0.40	2.90	0.80	0.71	1.03	0.31
AU955:328	5.87	37.91	278.79	233.85	42.62	107.70	64.59	82.80	13.67	9.05	191.73	28.33	123.05	16.92	0.10	114.33	10.47	23.44	3.17	14.52	3.91	1.33	0.78	4.58	4.95	1.01	2.86	0.43	2.71	0.41	2.86	0.83	0.71	1.03	0.30
AU955:329	5.60	37.80	273.52	226.80	41.96	105.81	65.23	82.10	14.41	9.12	187.25	27.94	120.73	16.93	0.10	111.16	10.13	23.15	3.03	13.99	3.91	1.30	0.78	4.60	4.80	0.97	2.81	0.43	2.68	0.39	2.82	0.79	0.70	1.01	0.30
AU955:330	5.83	37.54	276.68	226.53	42.19	108.35	65.13	83.94	13.66	9.06	190.71	27.98	139.60	16.99	0.10	114.75	10.54	23.49	3.18	14.41	3.90	1.32	0.78	4.60	4.91	1.00	2.94	0.43	2.65	0.40	2.86	0.83	0.80	1.03	0.30
AU955:331	5.89	38.04	282.53	233.62	42.62	108.43	65.77	84.03	13.77	9.20	193.30	28.48	151.17	17.26	0.10	115.82	10.61	23.83	3.20	14.70	3.97	1.33	0.77	4.70	4.95	1.01	2.89	0.43	2.71	0.41	2.91	0.79	0.71	1.05	0.30
AU955:332	5.77	37.88	278.69	232.96	42.17	109.09	65.45	83.91	13.42	9.08	190.03	28.06	130.55	16.71	0.10	113.22	10.22	23.18	3.11	14.26	3.86	1.31	0.77	4.64	4.93	1.00	2.87	0.43	2.74	0.40	2.84	0.80	0.70	1.01	0.31
AU955:333	5.62	38.22	273.32	229.50	42.39	107.02	65.38	81.87	14.35	9.05	186.44	27.89	121.25	16.88	0.10	110.24	10.17	23.22	3.06	14.09	3.88	1.29	0.78	4.61	4.92	0.97	2.86	0.42	2.67	0.39	2.77	0.79	0.72	1.01	0.29
AU955:334	5.79	37.95	274.48	248.78	43.12	113.41	66.75	83.24	13.45	8.85	189.40	27.86	132.44	16.38	0.10	112.45	10.15	23.04	3.08	14.19	3.80	1.30	0.76	4.56	4.78	0.99	2.80	0.42	2.65	0.39	2.83	0.76	0.69	0.98	0.29
AU955:335	5.56	37.88	267.11	228.90	42.04	133.37	82.91	80.71	14.04	8.74	185.32	27.52	117.14	16.35	0.10	106.79	9.82	22.58	2.99	13.62	3.75	1.28	0.76	4.52	4.78	0.97	2.79	0.42	2.69	0.39	2.72	0.76	0.68	0.95	0.28
AU955:337	5.13	38.19	257.53	328.66	43.40	132.64	71.89	76.80	13.64	8.33	170.62	26.14	107.50	14.48	0.10	101.28	9.07	20.42	2.72	12.64	3.38	1.18	0.72	4.15	4.51	0.91	2.62	0.39	2.47	0.37	2.43	0.65	0.66	0.86	0.26
AU955:325	5.76	37.8	274	246	43.3	114	68	81	15.5	8.07	191	26.3	104.5	15.17	0.098	104.3	9.43	20.94	2.91	13.15	3.58	1.26	0.732	4.22	4.64	0.970	2.71	0.408	2.54	0.384	2.66	0.876	0.719	0.97	0.282
AU955:344	6.06	40.3	263	306	42.3	112	76	75	13.1	2.50	113	27.2	70.2	5.07	0.038	32.2	4.11	10.39	1.68	8.54	2.84	1.04	0.695	3.67	4.62	0.994	2.82	0.457	2.75	0.419	2.13	0.371	0.390	0.35	0.101
AU955:345	6.13	41.8	264	369	41.4	101	81	81	12.9	2.12	103	27.8	71.5	4.39	0.024	27.4	3.67	9.68	1.57	8.07	2.78	1.03	0.704	3.68	4.72	1.022	2.89	0.447	2.83	0.425	2.11	0.264	0.347	0.31	0.093
AU955:348	5.52	31.1	246	255	36.4	79	72	83	16.8	10.14	266	25.2	128.9	22.32	0.115	142.0	13.39	28.15	3.70	16.08	4.17	1.45	0.780	4.74	4.70	0.938	2.51	0.368	2.23	0.330	3.23	1.223	0.802	1.37	0.408